NASA CONTRACTOR REPORT

NASA CR-1943

A MODEL FOR MULTIPLE-DROP-IMPACT EROSION OF BRITTLE SOLIDS

by O. G. Engel

Prepared by
GENERAL ELECTRIC COMPANY
Evendale, Ohio 45215
for Lewis Research Center

NATIONAL AERONAUTICS AND SPACE ADMINISTRATION • WASHINGTON, D. C. • NOVEMBER 1971

1. Report No.	2. Government Accession No.	3. Recipient's Catalog No.
NASA CR-1943		

4. Title and Subtitle	5. Report Date
A MODEL FOR MULTIPLE-DROP-IMPACT EROSION OF BRITTLE SOLIDS	November 1971
	6. Performing Organization Code
7. Author(s)	8. Performing Organization Report No.
O. G. Engel	GESP-610
9. Performing Organization Name and Address	10. Work Unit No.
General Electric Company, Evendale, Evendale, Ohio 45215	
	11. Contract or Grant No.
	NAS W-1481
12. Sponsoring Agency Name and Address	13. Type of Report and Period Covered
National Aeronautics and Space Administration Washington, D. C. 20546	Contractor Report
	14. Sponsoring Agency Code

15. Supplementary Notes

L 97p.
References: p78-9

16. Abstract

A statistical model for the multiple-drop-impact erosion of brittle solids is developed. An equation for calculating the rate of erosion is given. The development is not complete since two quantities that are needed to calculate the rate of erosion with use of the equation must be assessed from experimental data. A partial test of the equation shows that it gives results that are in good agreement with experimental observation.

I. Bibliography

17. Key Words (Suggested by Author(s))	18. Distribution Statement
Impingement, Erosion, Cavitation, Drop-impact, Metals, Iron, Nickel, Tantalum, Zinc, Udimet 700, Statistical models	Unclassified - unlimited

19. Security Classif. (of this report)	20. Security Classif. (of this page)	21. No. of Pages	22. Price*
Unclassified	Unclassified	109	$3.00

* For sale by the National Technical Information Service, Springfield, Virginia 22151

FOREWORD

The work described in this report was supported by the National Aeronautics and Space Administration under NASA contract NAS W-1481. The work was monitored by Mr. Stanley G. Young of the NASA Lewis Research Center Materials and Structures Division.

Micrographs from which the grain size of the metals was determined were contributed by Mr. E. E. Hoffman of General Electric Company, Evendale, Ohio. A number of important contributions to the mathematical development of the statistical model were made by Dr. J. K. Casey, Computations Operation, General Electric Company, Evendale, Ohio. His active interest and ready assistance were of the greatest possible value in completing the work described. The computer program was developed in the basic language by Mr. Lars H. Sjodahl of General Electric Company, Evendale, Ohio. It was converted to double precision Fortran IV by Mr. M. A. Cummings, Manager, Mathematical Applications, General Electric Company, Evendale, Ohio.

Helpful suggestions were made by Dr. George Irwin of Lehigh University, Bethlehem, Pennsylvania, Mr. W. J. Trapp of the Air Force Materials Laboratory, Wright-Patterson Air Force Base, Ohio, Dr. H. C. Rogers of General Electric Research Laboratory, Schenectady, New York, and Dr. G. J. Hahn of General Electric Information Sciences Laboratory, Schenectady, New York.

TABLE OF CONTENTS

TABLE OF CONTENTS (Cont'd)

LIST OF ILLUSTRATIONS

LIST OF ILLUSTRATIONS (Cont'd)

LIST OF TABLES

SUMMARY

A statistical model of drop-impact erosion rate has been developed in terms of occurrences at the site of a typical cell. The model is restricted to brittle materials whose strength and/or energy-absorbing capability is small in comparison with the energy delivered by each drop impact. Consideration of the characteristic mode of failure of solids under single-drop impact (formation of a circular crack) leads to the result that, if each impact produces fracture of the solid struck, it is impossible to remove one fragment from each cell in an array of cells without removing a layer of material that is many fragments thick.

The effect of changing angle of attack as surface roughness increases with test time is reflected in the number of impacts required to remove an eroded fragment; the required number of impacts includes non-crack-forming impacts which result only in work-hardening if the solid under test is a metal.

An expression for the rate of fragment ejection has been developed by summing the binomial probability for x hits in n trials between limits imposed by a counting rule. The counting rule is a function of relative impact velocity, drop mass, strength of the solid, angle of attack of the impinging drops, work-hardening capacity of a metal, and accumulated subsurface damage. The volume of a typical fragment has been found to vary as the third power of the impact velocity if the eroded fragment is a tetrahedron and as the fourth power of the impact velocity if the eroded fragment is a prism. This velocity dependence is reflected in the rate of volume loss.

A partial test of the rate equations has been performed using drop-impact volume-loss data for five selected metals. The agreement between theoretical and experimental volume loss is acceptable when the theoretical loss is obtained with eroded fragments of equal (average) size. The agreement is substantially improved when fragments of increasing volume are considered.

Correlation has been found between the 0.2 percent offset yield strength and the number of impacts required to remove an eroded fragment.

Correlation has also been found between the ultimate tensile strength and both the volume of an eroded layer and the percentage change in layer volume.

The statistical model is not completely developed since two quantities that are needed to calculate the rate of erosion with use of the equation that is given must be assessed from experimental data.

For impact velocities of 1000 ft/sec or less, materials having strengths comparable to that of aged Udimet 700 alloy are beyond the limits of applicability of the statistical model in its present state of development.

A MODEL FOR MULTIPLE-DROP-IMPACT EROSION OF BRITTLE SOLIDS

I. INTRODUCTION

When liquid drops or jets impinge against the planar surface of a solid, high pressures and high fluid-flow velocities are produced. If impingement is continuous, even the strongest materials eventually fail. Cavitation damage is similar to drop-impact damage. Naude and Ellis[1][a] observed that a high-speed jet forms during the collapse of a cavitation bubble. This observation has provided a basis for understanding the similarities that exist.

Eventual development of a theoretical expression for the rate of drop-impact and cavitation erosion is important for several reasons. From an applied standpoint, such an expression would make it possible to assess the probable weight loss from an eroding part over an arbitrary time in service. It would also provide a basis for rating the resistance of materials to this form of attack. In addition, the very process of developing and testing such an expression should produce valuable insights into the mechanism of the erosion process.

The average rates at which cavitation and drop-impact erosion progress have been assessed from experimental weight-loss data for a number of metals by several groups of investigators. Thiruvengadam and co-workers[2] plotted an average rate against total test time. They found curves with the following features: a period during which essentially no weight loss is observed (incubation period), a period characterized by a rapid increase in erosion rate (accumulation period), a maximum rate, a decrease in rate (attenuation period), and a steady-state rate. Some variations of these features have been observed by other investigators. Hammitt, Robinson, Siebert, and Aydinmakine[3] found two and even three maxima in some but not all of their plots.

---

[a] Numbers in parentheses refer to literature references at the end of this report.

Heymann[4] discussed time dependence of erosion rate in terms of lifetimes of layers of cells which were described by statistical distribution functions; numerical results were obtained by assuming that no damage is done to underlayer material until it has emerged to the surface. Mok,[5] on the basis of the fact that damage to underlayer material does occur if stresses within this material exceed a critical value, produced a treatment of erosion rate based on cumulative fatigue damage; his treatment does not give the initial or final features of experimentally determined curves.[2]

Hammitt, Huang, Kling, Mitchell and Solomon[6] developed a treatment of erosion rate based on the energy-flux concept of Hoff, Langbein, and Rieger[7]; numerical results were obtained by excluding materials of high erosion resistance such as the tool steels and highly resistant alloys including the family of Stellites.

It was suggested[8] that a treatment of erosion rate based on lifetimes of individual cells might prove to be informative because it would lead to consideration of successive states or conditions that exist as erosion attack progresses. As a first approach to such a model of erosion rate, a simple but physically unreal case was considered.[8]

Lifetimes of the members of an assembly of cells can be treated statistically by considering the lifetime of a cell in the original surface layer and the lifetimes of successive underlayer cells below it through the thickness of the test specimen.[1] In the first development of this cellular model (see Section II), the erosion process is idealized by assuming that all of the eroded fragments have equal (average) volume. The attractive feature of this simplifying assumption is that it makes it possible to calculate rate of erosion, to calculate accumulated volume loss from this rate, and to compare the calculated volume loss with that obtained experimentally. However, it has been reported by Gould[9] that the size of eroded fragments increases with lapse of test time. A second development of the cellular model (see Section IV) takes the feature of increasing eroded fragment size into account.

---

[1] I am indebted to Dr. Wayne Nelson, Information Sciences Laboratory, General Electric Company, Schenectady, New York, for the suggestion that the cellular model can be developed in terms of a typical cell.

II. STATISTICAL MODEL BASED ON ERODED FRAGMENTS OF EQUAL VOLUME

Development of an equation for volume rate of erosion, in E of this section, is preceded by a consideration of major factors that affect this rate, in A through D of this section.

A. Strength of the Solid Under Test

The characteristic appearance of surface roughness that develops as drop-impact erosion progresses is different for materials of different strength and different ability to accept energy elastically. The extreme cases are: (A) materials whose ability to accept energy without fracture is small in comparison with the impact energy delivered by each liquid-drop blow, and (B) materials whose ability to accept energy without fracture is large in comparison with the impact energy delivered by each liquid-drop blow. For any given material, the classification is relative; it may be either in Class (A) or in Class (B) depending on the impact velocity and drop mass used in testing it.

The surface of a brittle material of Class (A) is uniformly eroded. For a material in this class, it appears that long-term drop-impact erosion may involve movement of an eroded surface layer through the thickness of the test specimen (see Figure 1,A). A Class (B) material will start to fail at weak spots; these spots may be grains with an unfavorable orientation or points where several grains meet as was suggested by Von Schwarz and Mantel.[10] When eroded fragments are ejected from the weak spots, residual crack ends remain. Residual crack ends are able to grow in length as more drop impacts occur with the result that eroded fragments will continue to be ejected from the weak spots. Pits eventually form at the sites of the weak spots and deepen until they pierce the test plate (see Figure 1,B).

The model of erosion rate in drop impact and cavitation developed in this report is directed to materials of Class (A). This means that each impact does some damage to the solid struck (work-hardening or fracture).

B. Geometry of Fracture

Baker, Jolliffe, and Pearson[11] have observed that, for corresponding positions on curves of mass loss against mass of impinging water, surface coarseness increases with drop size and distance between adjacent erosion peaks is proportional to and of the same order as the drop diameter. It

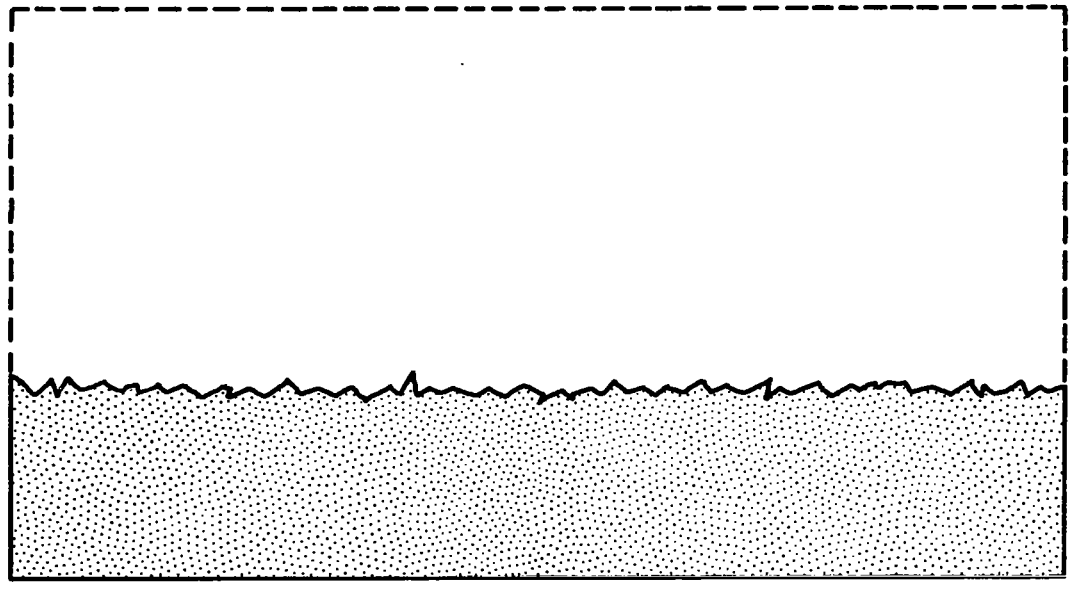

A. Brittle Material of Low Strength

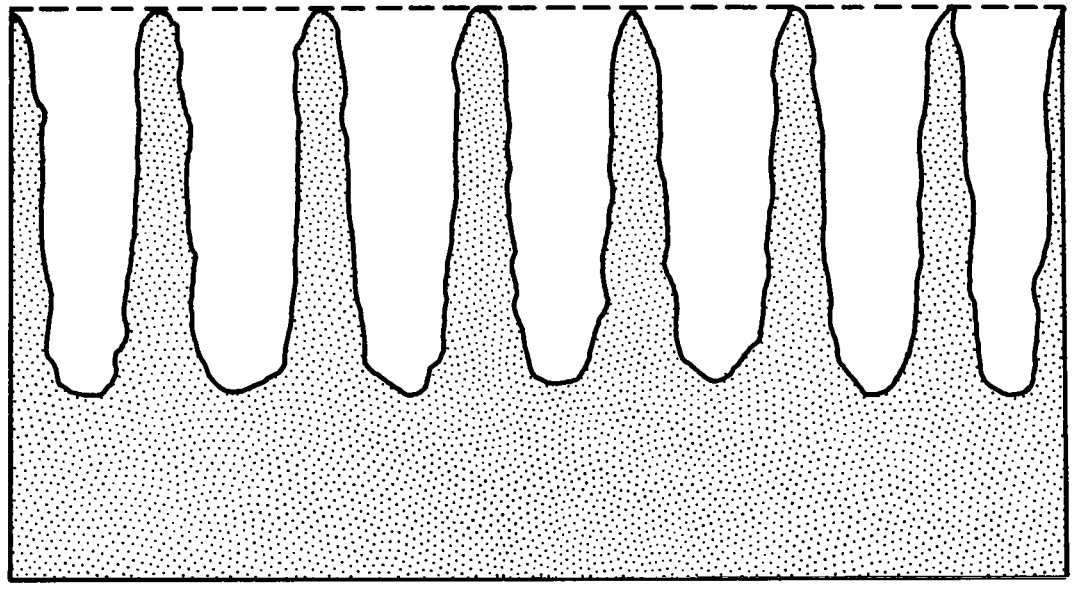

B. Brittle Material of High Strength

Figure 1. Progress of Erosion on Two Brittle Materials of Widely Different Strengths.

has also been observed[12] that the fracture pattern produced by drop impact is a circle or polygon of cracks depending on whether the solid material is isotropic or anisotropic; distance across this fracture pattern is roughly equivalent to the radius of the drop that impinged. Figure 2 shows such a circle of cracks in hot-pressed alumina.

The geometry of fracture appears to be dictated by the way in which an impinging drop produces stresses in tension and shear in a solid. When a liquid drop impinges normally against a planar solid, the impact pressure exists over a circular area. By analogy with the impact of a solid sphere, radial tensile stresses around the compressed area must be imposed and released during the impact. If the tensile strength of a brittle solid is exceeded by these radial tensile stresses, a single drop impact will produce not just one crack but all the cracks that comprise the circular (or polygonal) fracture pattern. In order to develop a cellular model of drop-impact erosion rate, it is necessary to assess the number of cells that will receive cracks during a single impact because the circular fraction pattern passes through them.

1. Number of Cracks per Impact Produced in σ-Cells

Let drops, all of which have the same radius, r, impinge at normal incidence over an area A of a test specimen and let the area A consist of an array of cells all of which have the same area, σ. Designating the number of cells in area A with the symbol η,

$$\eta = A/\sigma. \tag{1}$$

Let the array of σ-cells be represented by a matrix of closest packed circles; let the cell diameter be d. See Figure 3. Let the fracture pattern be a circle having radius r/2 and let the circle of fracture be inscribed on the matrix of σ-cells. A certain number of σ-cells is cut by the inscribed circle of fracture; this number is designated by the symbol η'.

Three circles of fracture with radii 1d, 2d, and 3d, respectively, have been inscribed on the matrix of σ-cells shown in Figure 3. At the bottom of Figure 3 the count of σ-cells cut by the inscribed circles of fracture is tabulated along with corresponding numbers obtained by dividing the circumference of the circle of fracture by the cell

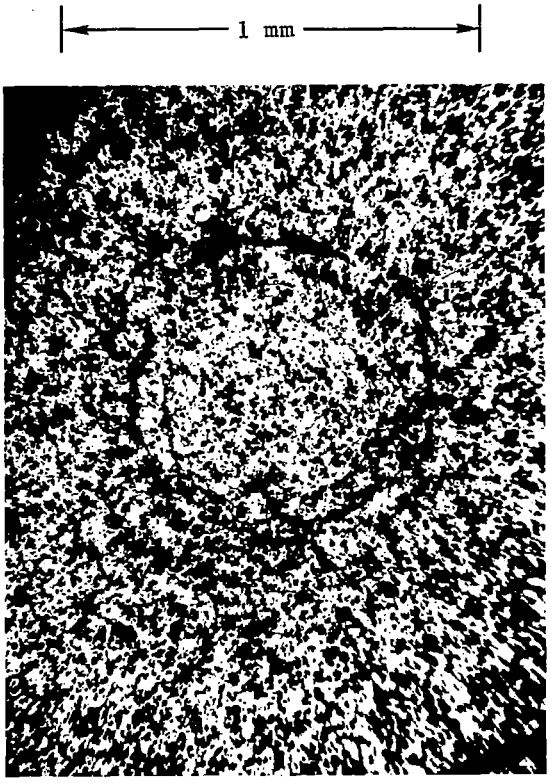

(a) Projectile plate: hot-pressed alumina; target: 2-mm mercury drop; impact velocity: 1403 ft per sec.

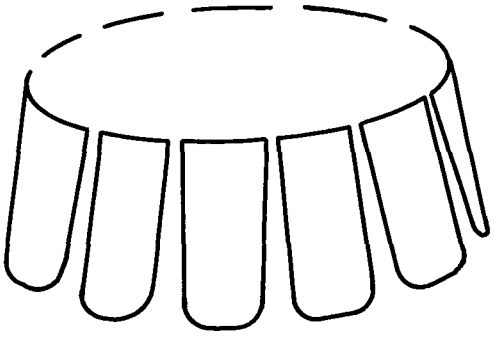

(b) Schematic Drawing of Subsurface Damage

Figure 2. Damage Mark Produced on Leading Face of Specimen of a Brittle Material as a Result of Collision with a Liquid Drop. View (a) is Reproduced from Reference [12].

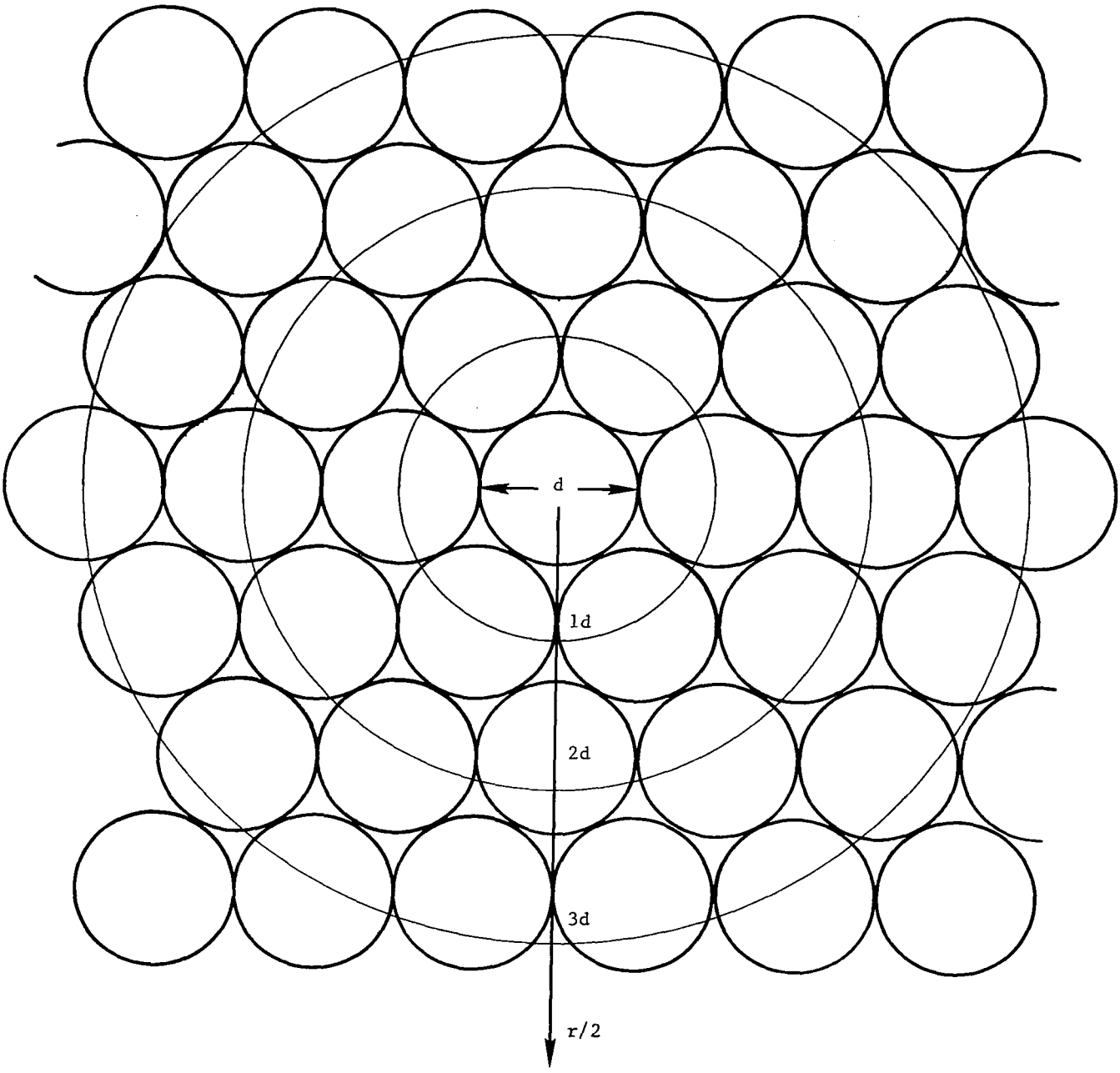

Radius of Circular Crack, r/2	Number of σ-Cells Cut	
	Actual Count	πr/d
d/2	0	3.1
d	6	6.3
2d	12	12.6
3d	18	18.8

Figure 3. Estimate of Number of σ-Cells Cut by the Circular Fracture Pattern.

diameter, d. It can be seen that the extent of agreement that exists is adequate to justify the relation

$$\eta' = \pi r/d \tag{2}$$

as an estimate of the number of cells that develop cracks when a single drop impact occurs.

In the cellular treatment of erosion rate that follows, an eroded fragment is identified with a single σ-cell and the diameter, d, of a σ-cell is taken to be the same as the distance across an eroded fragment.

2. Cracks Produced in a Typical Cell

In the special case illustrated in Figure 4, the center of impact occurred at the center of σ-cell W^*. This is also the center of the circle of fracture which contains V^* σ-cells. Let σ-cell W^* be regarded as a typical cell. If the centers of three drops that impinge against the circle of fracture shown in Figure 4 fall in three of the σ-cells A^* through V^*, the three circles of cracks formed as a consequence of these impacts will cut the typical cell W^*. In Figure 4 the σ-cells struck have been taken to be A^*, I^*, and P^*; the center of impact in each of these σ-cells is indicated with a solid circle. Each of the circles of fracture generated by these impacts will also cut through a total of V^* σ-cells; for each of these three impacts, the typical cell W^* will be only one of the V^* σ-cells cut.

The probability of hits in the typical cell W^* is statistically the same as the probability of hits in any of the σ-cells in the array including σ-cell W^* and σ-cells A^* through V^*. Physically, the probability of hits in σ-cells A^* through V^* determines the probability of cracks in σ-cell W^* whereas the probability of hits in σ-cell W^* determines the probability of compression in this cell. Because these probabilities are identical, the probability of hits in σ-cell W^* determines not only the probability of compression in σ-cell W^* but also the probability of crack formation in σ-cell W^*. In short, the probability of crack formation in σ-cell W^* is a function of hits in σ-cell W^* but the cracks that form in σ-cell W^* are not caused by hits that occur in σ-cell W^*.

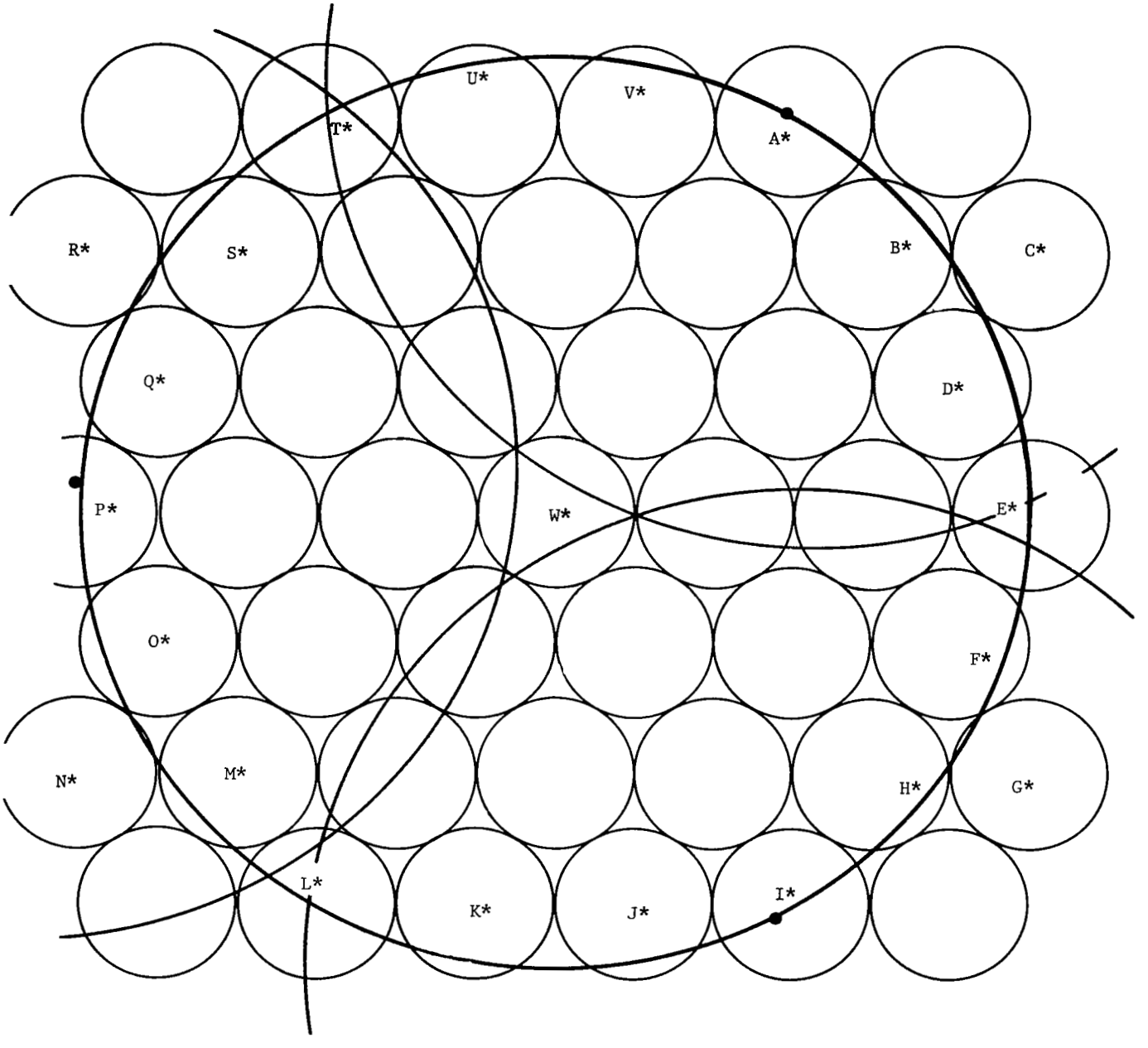

Figure 4. Schematic View of Macrocell Consisting of V* σ-Cells Surrounding σ-Cell W*. ($\eta' = V^*$)

3. Fragments Ejected from a Typical Cell Site

Reasoning based on the preceding considerations leads to the number of cracks produced in a typical cell site when each of the σ-cells in an array of such cells has received one or any other arbitrary number of impacts. Let the condition on the rain of drops be that it is a random rain in which the probability of impacts is uniform. For the purpose of the argument developed in this section only, let the further restriction be imposed that the distribution of impacts is uniform not in the usual sense that each cell has an equal probability of being hit but that each cell is actually hit the same number of times.

The number of σ-cells in the circle of fracture is η'. If each drop impact produces η' cracks, and if the specified type of rain progresses until one impact has occurred in each of the η cells in the impingement area A, then the total number of cracks formed is $\eta\eta'$ and the number of cracks formed per σ-cell is η'. Similarly, if the rain progresses until two impacts have occurred in each of the η cells, then a total of $2\eta\eta'$ cracks, or $2\eta'$ cracks per cell, have been formed. And if the rain progresses until three impacts have occurred in each of the η cells, then a total of $3\eta\eta'$ cracks, or $3\eta'$ cracks per cell, have been formed.

The number of cracks formed is an integral multiple of the product $\eta\eta'$. A rigorous proof of this statement has not yet been developed but the following intuitive argument indicates that it is correct. Because it is impossible to deliver a fractional part of an impact in each of the η cells, the only way that a fractional part of η' cracks could be formed per cell is that some cells would receive more impacts than others. This would require a nonuniform distribution of impacts which would violate the restrictive condition that the random rain has a uniform distribution of impacts.

Let it be required provisionally that N_o cracks must form in a σ-cell before an eroded fragment will be ejected and let the rain progress until each of the η cells in the impingement area A has received N_o impacts. Let one of the η cells be selected as a typical cell. This cell is surrounded by η' cells in the circle of cracking. If each cell in the array has received N_o impacts, then each of the η' cells in the

circle of cracking around the typical cell has received N_o impacts and each of these impacts has produced one crack in the typical cell. If all of the cells in the array have received N_o impacts, the typical cell has received N_o impacts and, in addition, the typical cell has received N_o η' cracks. Because it was specified provisionally that the formation of N_o cracks in a cell results in the ejection of a fragment, the site of the typical cell must eject η' fragments. Because there are η cells in the impingement area A, the total number of fragments ejected from all of the cell sites will be $\eta\eta'$.

Because of the geometry of liquid-drop-impact fracture, it is not possible for each cell in an array of cells to lose one and only one fragment. It is possible for each cell to lose η' or some integral multiple of η' fragments. Although the argument that excludes all but integral multiples of the product $\eta\eta'$ is so far supported only by an intuitive proof, it is confirmed a posteriori by experimental evidence (See Section III.I). Because of the geometry of liquid-drop-impact fracture, it is not possible to remove one fragment from each of the σ-cells in an array of σ-cells without simultaneously removing a layer of material from the test specimen; the layer removed consists of $\eta\eta'$ fragments.

C. Angle of Attack

For impacts that occur at angles smaller than 90 degrees, the amount of energy that is delivered to the material of the test specimen by each drop blow is reduced. Erosion investigators have compensated for this effect by considering only the normal component of the impact velocity. The normal component of the impact velocity, V is V sin θ, where θ is the angle of attack measured from the surface of the test specimen.

In terms of the normal component of the impact velocity, the energy delivered by impinging drops is $\frac{1}{2}$ M $(V \sin \theta)^2$ where M is the mass of a drop. If impingement occurs at normal incidence against the original surface of the test specimen, the energy delivered per impact is $\frac{1}{2}$ MV^2 because the sine of 90 degrees is unity. Let us identify this energy per impact with the formation of cracks of a given length in a particular solid.

After the first layer of $\eta\eta'$ fragments has been removed from the original, polished surface of a test specimen, a rough surface of underlayer material is exposed; the drops now impinge against this rough surface. Without the guidance of specific information, let it be assumed that on the average the angle of attack has been reduced to 45 degrees. Then the energy delivered per impact will be halved because the sine of 45 degrees is $\sqrt{2}/2$. If the energy delivered per impact is halved, and if the fractional part of the impact energy invested in crack formation remains the same, the surface area of the cracks that form must also be halved.

This suggests that twice as many crack-producing impacts may be required to circumscribe a fragment when the angle of attack is 45 degrees than were required when the angle of attack was 90 degrees. In Section II.3, the number of impacts required to circumscribe a fragment with impingement occurring at normal incidence was provisionally taken to be N_o. If the number of impacts required to circumscribe a fragment when the angle of attack is 45 degrees is N_1, then, on the basis of the preceding reasoning, $N_1 \simeq 2N_o$.

After the loss of the second layer of fragments is an accomplished fact, the angle that the exposed underlayer material presents to the impinging drops may or may not change again for a given material. If angle of attack is the only factor affecting the number of crack-producing impacts required to circumscribe a fragment at this stage of the erosion process, recourse to experimental data (See Section III) suggests that the angle of attack must be reduced to about 30 degrees. At this angle of attack, the energy delivered per impact will only be one fourth as much as it was when the drops impinged at normal incidence because the sine of 30 degrees is 1/2. The surface area of the cracks produced at this angle of attack will only be one fourth as large as it was when impingement occurred at normal incidence and, if the fractional part of the impact energy invested in crack formation remains the same, four times as many impacts should be required to circumscribe the fragments of the third layer of material to be removed from the test specimen as were required in the case of the first layer. If the number of impacts required to circumscribe a fragment when the angle of attack is 30 degrees is N_2, then, on the basis of the preceding reasoning, $N_2 \simeq 4N_o$.

The number of impacts required to circumscribe a fragment after a given number of impacts has already been sustained may be represented by the sequence

$$N_i = N_o, N_1, N_2 \ldots \quad (3)$$

which is hereafter referred to as the counting rule. The evaluations of N_o, N_1, and N_2 that were made in the preceding paragraphs are based on the premise that angle of attack governs the magnitude of successive counting-rule numbers and that angle of attack is progressively reduced. However, angle of attack is only one of a number of variables which determine the magnitudes of the counting-rule numbers.

D. Work-Hardening of Metals

Only a brittle metal, whose fracture strength is exceeded when it sustains an impact at an arbitrary velocity will develop a crack as the result of this impact. Most metals are ductile and must be work-hardened to the point of embrittlement before a crack will form. A question that needs to be answered is: How many superposed liquid drop impacts are required to work-harden a given metal to the point of embrittlement? The smallest possible number would be just one and, although it is not conclusive, the following empirical evidence suggests that one impact at a high velocity may be adequate for some metals.

Knoop microhardness numbers taken through the thickness of an alclad aluminum alloy specimen subjected to waterdrop impacts at the Cornell Aeronautical Laboratory, Buffalo, New York, shifted from a maximum of 74 at the eroded surface to an asymptotic value of 55, which was the characteristic hardness of the metal.[13] Although the test velocity was not specified, it was very likely 805 km/hr (500 mi/hr) because this velocity was commonly used in performing tests with use of the rotor and artificial rain facility at this laboratory at the time that the specimen was tested.

The ratio of maximum hardness produced by the rain impacts to asymptotic hardness of the metal is 74/55 or 1.34. Two conclusions can be drawn from this information: first, multiple waterdrop impacts at the specified velocity were able to produce a 34 percent increase in the hardness of the specimen, and, secondly, because the specimen was severely

eroded, a 34 percent increase in hardness can be associated with a sufficient embrittlement of the alclad aluminum alloy specimen material to permit crack formation in it.

Knoop microhardness numbers were also taken around a single crater produced in 1100-0 aluminum by the impact of a steel sphere at a velocity of 626 km/hr (389 mi/hr).[14] The average ratio of maximum hardness to asymptotic hardness for measurements taken below the crater and from the edge of the crater near the surface was found to be 1.54. This means that a 54 percent increase in hardness was produced by a single steel-sphere impact. This is in excess of the 34 percent increase in hardness required for sufficient embrittlement of the metal to permit drop-impact erosion of an alclad aluminum alloy specimen to progress.

Craters produced in 1100-0 aluminum by single waterdrop impacts at velocities above 1000 ft/sec were also studied[15] but, regrettably, Knoop microhardness numbers in the metal around these craters were not taken and the tested specimens are no longer available. Consequently, it is not known if a single waterdrop impact at these high velocities is able to produce work-hardening to the point of embrittlement of metals such as 1100-0 aluminum.

On the basis of the preceding evidence, it can be assumed that, for the high velocities being used in applications where drop-impact erosion occurs, it is possible that one waterdrop impact may work-harden a metal which has properties comparable to those of 1100-0 aluminum to a sufficient degree that a crack can form in it when a second impact occurs at the same point. If this assumption is made, then, for tetrahedral fragments, the minimum value that N_o, the first number of the counting rule, can have is four; this is one more than the minimum number of three cracks required to circumscribe a tetrahedral fragment. The numbers of the counting rule, N_i, must include both the impacts that are required for embrittlement of the metal of the test specimen and the crack-forming impacts required to circumscribe a piece of the solid and release it as an eroded fragment.

E. Equation for Rate of Volume Loss

Rate of volume loss, R, expressed in volume loss per impact is

R = (volume of material lost)/(number of impacts sustained).

If the volumes of eroded fragments are all equal, that is, if the average volume of an eroded fragment is used,

$$R = \frac{\text{(number of fragments ejected)(average volume per fragment)}}{\text{(number of impacts sustained)}}$$

The quotient of number of fragments ejected divided by the number of impacts sustained is the rate of fragment ejection, J. Designating the average volume of the typical ejected fragment with the symbol v, the rate of volume loss, R, is given by the product

$$R = Jv \ . \tag{4}$$

To evaluate R, it is necessary to obtain expressions for J and v.

1. Rate of Fragment Ejection, J

Ejection rate, J, is determined both by a statistical function, $P(x,n)$ and by a counting rule, N_i. The statistical function gives the probability that some number of impacts, x, will occur on the cell area, σ, when n impacts have occurred on the impingement area A. The counting rule, N_i, dictates the number of impacts required to eject a fragment from the cell area, σ, after some number of fragments (including zero) have already been ejected from this particular area.

a. Function $P(x,n)$

The function $P(x,n)$ is uniquely given by binomial probabilities if the rain of drops is random. If events are strictly independent in the sense that the probability of occurrence of one event does not affect the probability of occurrence of a succeeding event, their occurrence is described by the well known binomial distribution function. The impacts of the drops of a random rain are independent in this sense; the fact that a given site has been hit by one drop does not affect the probability that it will or will not be hit by a succeeding drop. Consequently, the impacts of a truly random rain against the individual cells in an array of cells can be exactly described by binomial probabilities.

The binomial probability, $P(x,n)$, for x impacts on a cell area, σ, when n impacts have occurred on impingement area A is given by

$$P(x,n) = \left[(n)!/(x)!\ (n-x)!\right]\ p^x\ (1-p)^{n-x} \tag{5}$$

where p is the probability of a hit on cell area, σ. If the random rain of drops is uniform, the probability, p, of a hit against any one of the cells having area σ is given by

$$p = \sigma/A \quad . \tag{6}$$

b. Counting Rule

The magnitude of the counting-rule numbers is determined by a number of variables. For a brittle material, the counting rule is primarily a function of relative impact velocity, V, drop mass, M, angle of attack, θ, and the energy per unit volume that the solid is able to accept without fracture through the condition that the energy delivered by a single drop impact, which is given by $\frac{1}{2} M (V \sin \theta)^2$, must exceed the energy per unit volume that the solid can accept before fracture will result. Clearly, for impacts against a given brittle solid, the magnitude of the counting-rule numbers will be reduced as impact velocity, drop mass, and angle of attack are increased. For a given impact velocity, drop mass, and angle of attack, the magnitude of the counting-rule numbers will be increased as brittle materials of progressively higher strength are considered.

A ductile metal must be work-hardened to the point of embrittlement before cracks will form in it. The counting-rule numbers for a ductile metal include both the impacts required to embrittle it and the impacts that are required to circumscribe a fragment with cracks. The magnitude of the counting-rule numbers will be larger as the number of impacts required to work-harden the metal under test is increased but this required number will depend upon the impact velocity, drop mass, and angle of attack.

The magnitude of the counting-rule numbers is also affected by conditions that develop as erosion progresses. The counting-rule numbers increase in magnitude if dissipation of impact energy occurs as a result of drop liquid that remains trapped in the surface roughness. The magnitude of the counting-rule numbers is decreased by the presence of residual crack ends and subsurface damage in underlayer material because the presence of crack ends and subsurface damage constitute a partial loosening of sections of the solid which will eventually break away as eroded fragments.

c. Function F(x,n)

The number of fragments ejected from the area A, F(x,n), is found by summing the probability, P(x,n) between the limits imposed by the counting rule, that is,

$$F(x,n) = \eta\eta' \sum_{x = N_o}^{N_o + N_1 - 1} P(x,n) + 2\eta\eta' \sum_{x = N_o + N_1}^{N_o + N_1 + N_2 - 1} P(x,n) + 3\eta\eta' \sum_{x = N_o + N_1 + N_2}^{N_o + N_1 + N_2 + N_3 - 1} P(x,n) + \text{etc...} \qquad (7)$$

where P(x,n) is given by Equation 5, and the probability of a hit, p, is given by Equation 6. For the necessity of the factor $\eta\eta'$, see Section II.B.3.

The function F(x,n), when plotted against x or n, is a step function because of the limits on the sums which are imposed by the counting rule. Let us consider the first term of the function F(x,n). The summation does not start with x = 0, but with $x = N_o$. No fragment can be ejected until at least N_o impacts have been received on the area, σ, of the typical cell; these impacts are received at normal incidence (or at some initially prescribed angle of incidence).

After these N_o impacts have been received at normal incidence, the ejection of the first layer of fragments becomes an accomplished fact. This is signified in Figure 5 by the abrupt rise from zero fragments to $\eta\eta'$ fragments after N_o impacts have been received on the cell area, σ. This abrupt rise is the first riser of the staircase plot of Figure 5. At this point a second period of quiescence occurs at impacts from N_o to $N_o + N_1 - 1$ are received on the cell area, σ. This period of quiescence constitutes the first tread in the staircase plot of Figure 5.

After the loss of $\eta\eta'$ fragments is an accomplished fact, the exposed underlayer surface of the cell area, σ, is no longer planar; the impingement angle is now reduced below 90 degrees. If it is reduced to an average value of 45 degrees, the energy delivered per impact is reduced by a factor of two and, on the basis of the reasoning presented

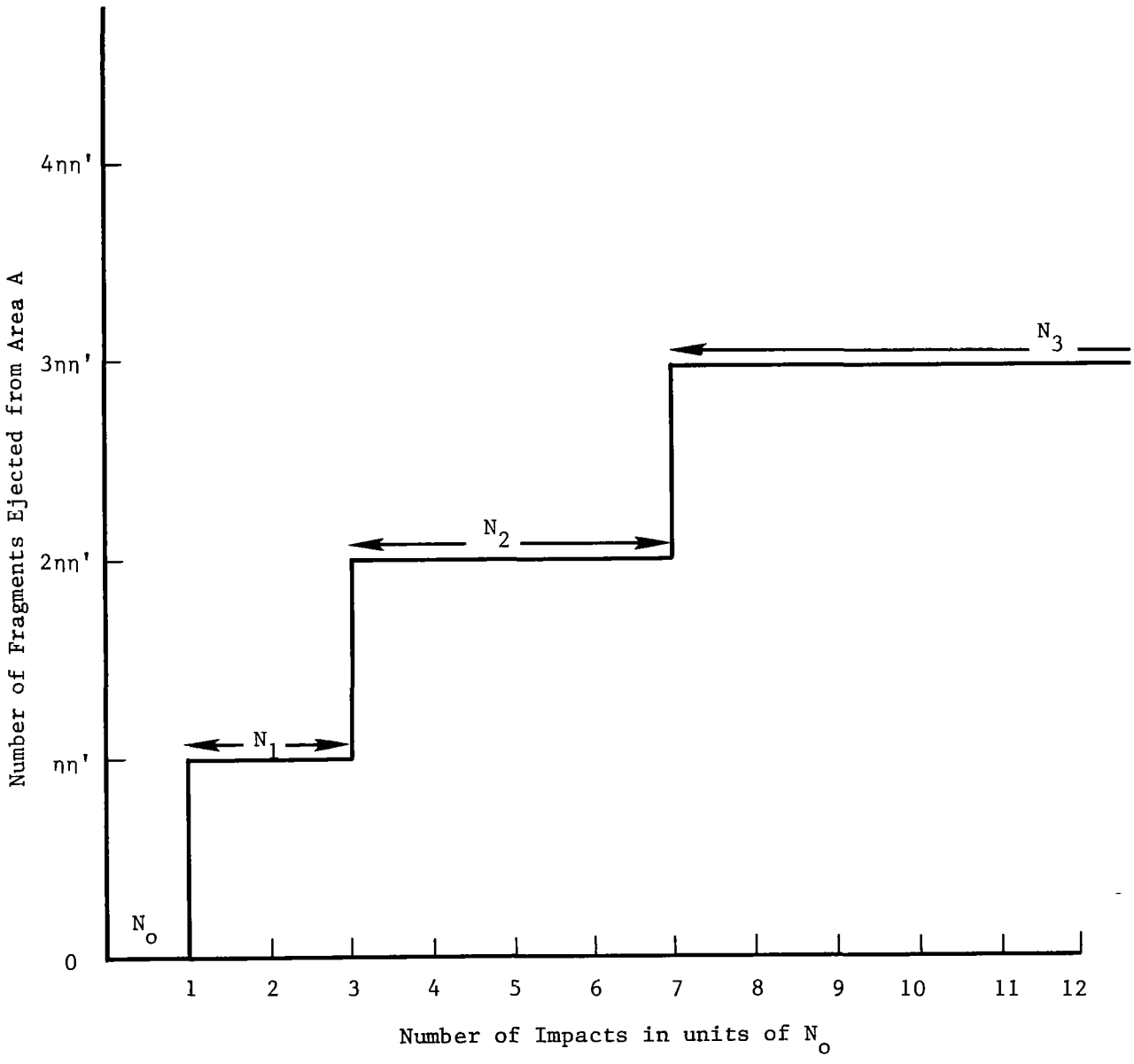

Figure 5. Schematic Representation of the Effect of the Counting Rule on the Ejection of Fragments.

in Section II.C, $N_1 \cong 2N_o$. During the period of quiescence represented by the first tread in the staircase plot of Figure 5, impacts are being received at an average angle of attack of 45 degrees.

We are now ready to consider the second term of the function $F(x,n)$. After N_o impacts have been received on area σ at an angle of 90 degrees and N_1 impacts have been received at the average impingement angle of 45 degrees, the ejection of the second layer of fragments from the area A becomes an accomplished fact. This is indicated by the second riser of the staircase plot of Figure 5. At this point a third period of quiescence sets in as the impacts from $N_o + N_1$ to $N_o + N_1 + N_2 - 1$ are received on the cell area, σ. This period of quiescence constitutes the second tread of the staircase plot of Figure 5.

After the loss of the second layer of fragments is an accomplished fact, empirical evidence (See Section III) suggests that the angle of attack is reduced to a value of about 30 degrees and that the counting-rule number N_2 is $4N_o$. During the period of quiescence represented by the second tread in the staircase plot of Figure 5, impacts are being received at an angle of attack of about 30 degrees or with a reduced energy that is equivalent to an effective angle of attack of 30 degrees.

We are now ready to consider the third term of the function $F(x,n)$. After N_o impacts have been received on area σ at an angle of 90 degrees, N_1 impacts have been received at an average impingement angle of 45 degrees, and N_2 impacts have been received at an effective impingement angle of 30 degrees, the ejection of the third layer of fragments from the area A becomes an accomplished fact. This is indicated by the third riser in the staircase plot of Figure 5. At this point a fourth period of quiescence sets in as impacts from $N_o + N_1 + N_2$ to $N_o + N_1 + N_2 + N_3 - 1$ are received on the cell area, σ. This period of quiescence constitutes the third tread of the staircase plot of Figure 5.

Whether or not the steps of the staircase plot shown in Figure 5 will be sharply delineated is determined by the magnitude of the probability of a hit, p, in conjunction with the magnitude of the counting-rule numbers, N_i. For a probability, p, of a given size, there is a threshold size range for the counting-rule numbers for which the probability distribution can be contained on a single tread of the counting-rule

staircase. If the size range of the counting-rule numbers is equal to or greater than this threshold size, the counting-rule steps will be sharply delineated in the plot of fragments lost against number of impacts sustained.

If the size range of the counting-rule numbers is smaller than the threshold size, the probability distribution will extend over more than one tread of the counting-rule staircase. For this condition, the counting-rule steps will appear only as oscillations in a plot of fragments lost versus number of impacts sustained. If the size range of the counting-rule numbers is so small that the probability distribution extends over many treads of the counting-rule staircase, the step nature of the counting rule will not be apparent at all in a plot of fragments lost against number of impacts sustained.

The magnitude of the number of impacts sustained, n, also has an effect on the sharpness with which the counting-rule staircase is reflected in the plot of fragments lost against number of impacts sustained. This follows because the probability distribution spreads as the number of impacts, n, is increased. For values of n that are large enough to permit the spread-out probability distribution to occupy more than one tread of the counting-rule staircase, the steps of the counting-rule staircase will appear only as oscillations in a plot of fragments lost against number of impacts sustained; for still larger values of n, the steps of the counting-rule staircase will not appear at all in such a plot. On the basis of these considerations, a plot of fragments lost against number of impacts sustained may exhibit a step structure for small values of n and be without this structure for large values of n.

d. Ejection Rate, Volume Rate, Accumulated Volume Loss

The average rate of fragment ejection over an interval from n_1 to n_2 impacts against area A is given by

$$J = (F_2 - F_1) / (n_2 - n_1) \ . \qquad (8)$$

To make the ejection rate, J, as instantaneous as possible, the quantity $(n_2 - n_1)$ should be made as small as feasible. From Equation 4, the average rate of volume loss, R, for each interval of n is Jv where v is

the volume of the average ejected fragment (See Section II.E.2) and J is the average rate of fragment ejection.

The accumulated volume loss can be calculated from the rate of volume loss. The increment of volume loss, Q, for each interval of n is the product of the rate of volume loss multiplied by the difference in n, that is,

$$Q = R\,\Delta n \quad . \tag{9}$$

The accumulated volume loss, L, up to any value of n is the sum of the values of Q up to the specified value of n, that is,

$$L = \sum_{i=1}^{n} Q_i \quad . \tag{10}$$

To calculate the rate of volume loss and the accumulated volume loss, it is necessary to have an expression for v, the volume of an ejected fragment.

2. Volume of an Ejected Fragment

Radial tensile stresses produced by the localized impact pressure and radial flow of drop liquid are the means by which an impinging drop damages a solid.[12,16] It is reasonable to expect that the rate at which drop-impact erosion progresses is a function of the variables which determine the magnitudes of these quantities. The variables in question are the relative impact velocity and the size and mass of the drops that impinge. The effect of these variables on the ejection rate, J, was discussed in the preceding section. Because relative impact velocity and drop mass control the energy delivered per impact, and because the energy delivered per impact governs the size of the surface area of the cracks that form, the relative impact velocity and drop mass must also determine the volume, v, of an eroded fragment.

a. Nature of the Typical Cell

The initial form of the cellular model[8] was directed to a homogeneous material that had uniform bond strength. Such a material is ideal; it has no preferred directions for crack propagation and no points

of special weakness. The closest approach to an ideal material of this kind is a single crystal of high quality. However, even single crystals contain defects. The majority of crystals are built up of micromosaic units that are 10^{-4} to 10^{-5} cm in linear dimensions.[17,18] These units are mutually disoriented by angles of the order of seconds or minutes of arc.[17]

The boundaries separating the slightly disoriented crystalline blocks have been considered to be the more stable ensembles into which dislocations have grouped themselves as the result of thermal treatment of a deformed crystal.[19] Bragg[20] and Burgers[21] were the first to suggest that the mosaic blocks are units whose bounding surfaces are dislocation walls. X-ray and optical investigations have revealed that, in addition to the very small micromosaic units, single crystals also contain larger macromosaic units which differ slightly in orientation and have dimensions of the order of 0.1 to 1 mm and larger.

The material in dislocation walls around mosaic units may be associated with the crack initiation and crack propagation that are thought to result in drop-impact erosion. In addition, the material in such walls is clearly in a higher energy state than material within the mosaic units themselves and, therefore, is more soluble. Chemical attack has never been eliminated as a drop-impact-erosion mechanism; under impact conditions, even water is a corrosive liquid (See Appendix A). In the light of these considerations, it seems reasonable to suppose that the typical cell, which becomes an eroded fragment, could be identified with the mosaic units of crystalline materials either on the basis of a crack-formation mechanism of erosion, a chemical attack mechanism of erosion, or a combination of these mechanisms.

b. Sizes of Typical Eroded Fragments

The question of the size of cavitation-eroded fragments has been explored by Brandenberger and DeHaller[22], Hoff and Langbein[23], and Gould[9]. In general, it was found that most of the eroded fragments have a size very close to that of a micromosaic unit, that is, 10^{-4} cm, but fragments up to 500 times this size were reported.

If an eroded fragment is identified with a σ-cell, this evidence suggests that it may be possible to associate the micromosaic unit with

the typical cell of smallest possible size. That is, the micromosaic unit size may constitute the lower limit of the possible size range for σ-cells.

It is noteworthy that cavitation-eroded fragments would be expected to be smaller than drop-impact-eroded fragments because the diameter of the jet formed during the collapse of a cavitation bubble is small in comparison with the drop diameters encountered in most drop-impact-erosion applications. Also, in this connection, it was observed by DeHaller[24] that cavitation erosion has a finer texture than drop-impact erosion.

Tentatively, it might be expected that a natural upper limit of ejected fragment size may be the grain size of a metal that is under test because A.S.T.M. grain sizes from 7 to 0 are, respectively, 30 to 360 times the 1-micron micromosaic unit size. However, under certain circumstances, some eroded fragments may consist of clusters of grains and grain fragments.

If eroded fragments produced in room-temperature tests are found to be in the size range of the grains of the test metal, this may provide evidence that chemical attack is playing a role in the mechanism of failure. Grain boundaries vary in composition from the material within the grains and are attacked in a corrosive environment. Water, under impact conditions, can become a corrosive liquid (See Appendix A).

Gould[9] has stated that the number of large eroded particles increases with increasing depth of erosion or with elapsed test time. If cell size is identified with eroded-particle size, this suggests that, for a calculation of erosion rate that extends over a considerable period of time, the typical cell increases in size. The consequences of an increase in cell size in terms of a statistical model of erosion rate are pointed out briefly in Section IV.

c. Shapes of Typical Eroded Fragments

The pyramid having the smallest number of sides in a tetrahedron. In terms of the initial cellular model of erosion rate[8], the eroded fragment produced by the least number of hits is a tetrahedral piece of the solid which has been cut loose by the intersection of three cracks.

Baker, Jolliffe, and Pearson[11] have reported evidence of subsurface cracks formed during drop-impact test. If subsurface cracks exist, then prismatic fragments or platelets can be cut loose by the intersection of three or more cracks that originate at the surface and extend down to the subsurface crack lying parallel to the surface.

An electron micrograph[2] of cavitation-eroded fragments from 12 percent chromium stainless steel is shown in Figure 6. This micrograph reveals fragments of many different sizes and shapes with a minimum face diameter of about one micron. The most predominant two-dimensional shape appears to be a polygon of at least five sides. As seen in two dimensions, some of the fragments are polygons of so many sides that they appear to be circular.

d. Volume of a Tetrahedral Fragment

The pyramid having the smallest number of sides is a tetrahedron. Let the typical fragment be a tetrahedron circumscribed by three semielliptic cracks AB, BC, and CA (See Figure 7) that have originated at the surface and have run down into the solid and intersected at point D. For simplicity, let the typical fragment be a regular tetrahedron with equal side length. The area of the triangular base, ABC, of side length b is $b^2\sqrt{3}/4$. The altitude h of a regular tetrahedron[25] is given by $b\sqrt{2/3}$ and the volume is 1/3 the product of the base multiplied by the altitude. Associating the edge length b with the minimal or critical tetrahedral fragment having volume, v_c,

$$v_c = b^3\sqrt{2}/12 \quad . \tag{11}$$

If the edge length b of the minimal tetrahedron is associated with the 1-micron edge length of a micromosaic unit, then $v_c = 0.118 \times 10^{-12}$ cm^3.

The area of one of the intersecting semielliptic cracks that form the tetrahedron ABCD in Figure 7 is $\pi h'b/2$ where h' is also the slant height of the tetrahedron. Because the slant height of a regular tetrahedron is given[25] by $b\sqrt{3}/2$, the area of the semielliptic crack

[2]This micrograph was obtained by Dr. G. Gould, General Electric Company, Materials and Processes Laboratory, Schenectady, New York.

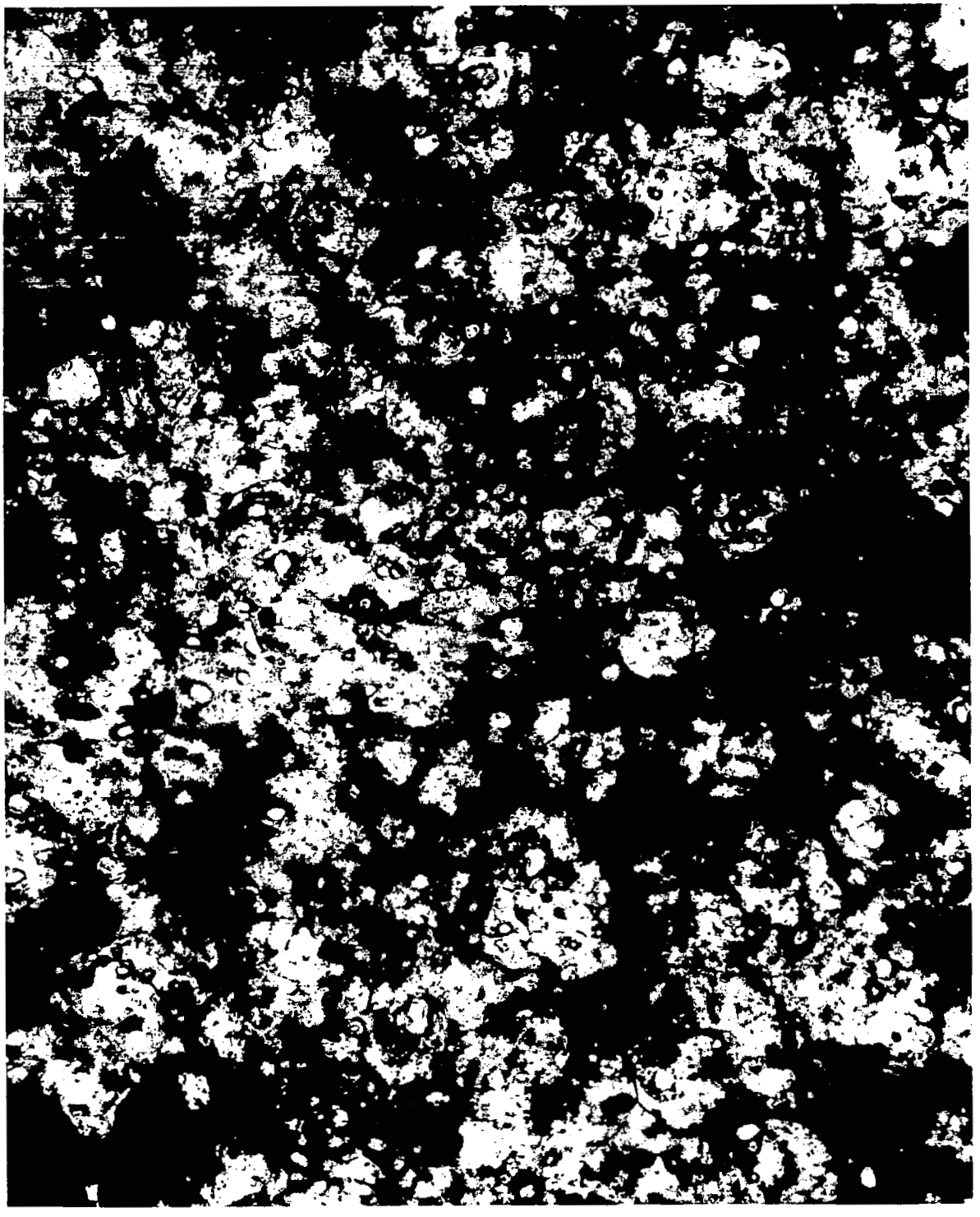

Figure 6. Electron Micrograph of Eroded Fragments of 12 Percent Chromium Stainless Steel (Photo by Dr. G. Gould).

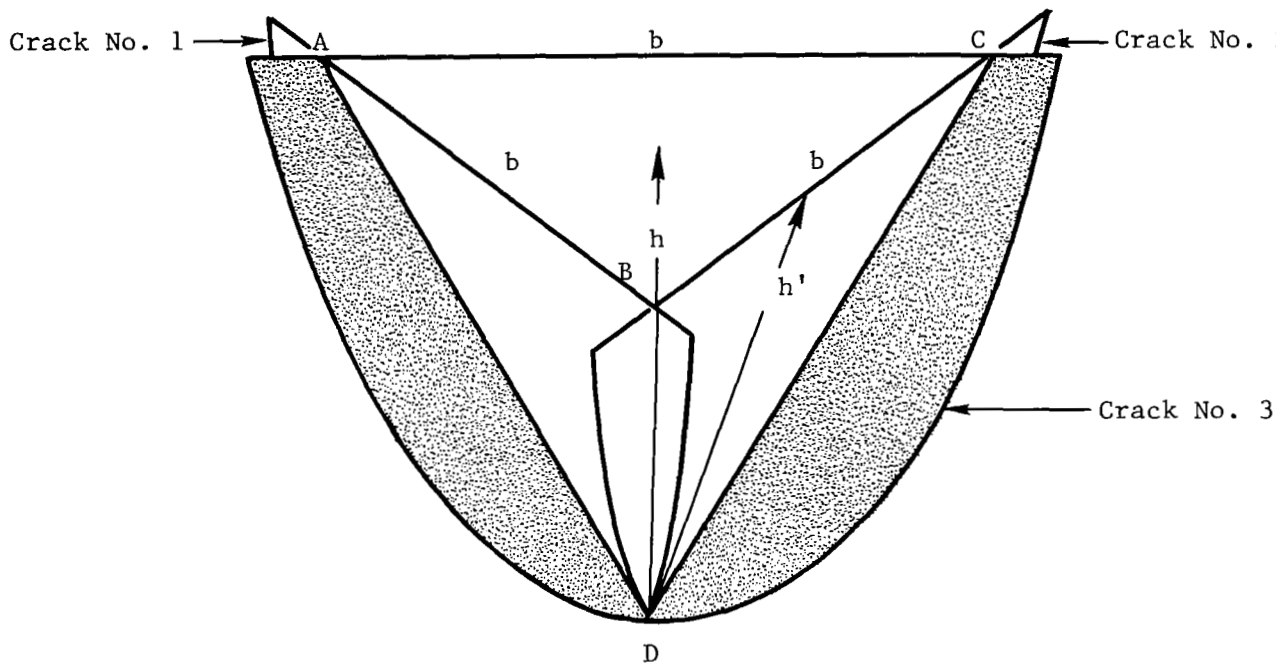

h = altitude of tetrahedron = b $\sqrt{2/3}$

h' = semi-axis of ellipse and slant height of tetrahedron = b $\sqrt{3}$ /2

Figure 7. Schematic Drawing of a Tetrahedral Fragment Formed by the Intersection of Three Semi-Elliptic Cracks.

is $\pi b^2\sqrt{3}/4$. For crack formation in a specific material, if the part of the impact energy that is invested in crack formation is doubled, the area of each of the intersecting semielliptic cracks will be doubled because the surface energy of a crack is the product of the area of the crack multiplied by the surface tension of the solid. To double the area of each of the semielliptic cracks, the original edge length b must increase to $\sqrt{2}$ (b).

Let E be the part of the impact energy that is invested in crack formation and let E_c be the critical threshold energy needed to form a crack. By analogy with the case in which the area of the semielliptic cracks is doubled, if the part of the impact energy that is invested in crack formation is increased E/E_c times, the area of the semielliptic cracks is given by $(\sqrt{E/E_c}(b)^2\ \pi\sqrt{3}/4$ and the original edge length b must increase to $\sqrt{E/E_c}$ b.

The volume of the tetrahedron cut out by the three larger-sized cracks will then be $(\sqrt{E/E_c}(b)^3\sqrt{2}/12$. If the edge length b is associated with the minimal unit of crack length for cracks extending from the surface, defined by the critical energy E_c or critical velocity V_c at which a crack is just able to form in the work-hardened state of a metal under drop-impact test, then the volume of a typical fragment formed at an impact energy associated with the crack formation energy E, or impact velocity which corresponds to the crack formation energy E, is proportional to $(E/E_c)^{3/2}$ or to $(V/V_c)^3$ times the volume of the minimal tetrahedral fragment associated with the energy E_c or with the velocity V_c.

For a specific material, the volume of the tetrahedral fragment, v_t, formed at an impact energy associated with the crack formation energy E or at a corresponding impact velocity is

$$v_t = kv_c\ (V/V_c)^3 \qquad (12)$$

where k is a proportionality constant and v_c is given by Equation 11. Associating the edge length b of the minimal tetrahedral fragment with the edge length of a 1-micron micromosaic unit, and using Equation 11 for the volume of the minimal tetrahedral fragment,

$$v_t = k\ (0.118 \times 10^{-12})\ (V/V_c)^3\ . \qquad (13)$$

It seems reasonable to expect that the constant k is a function of the drop mass, M, as well as of material properties such as the strength, S, and the elastic modulus, Y, of the solid being tested; this constant must, therefore, be different for different materials, drop sizes, and drop-liquid densities. A quantity that might reasonably be expected to enter into the expression for the constant k is the tensile force needed to open a crack.

The Griffith force[26] tending to pull a crack open is given by

$$(2TY/\pi c)^{1/2} \qquad \text{for plane stress}$$

and

$$(2TY/[\pi c(1 - \nu^2)])^{1/2} \qquad \text{for plane strain}$$

where T is surface tension, Y is Young's modulus, c is half the length of the crack, and ν is Poisson's ratio. Because the dimensions of force are $g.cm/sec^2$ and because the dimensions of surface tension are g/sec^2, a dimensionless factor would be obtained if the force tending to pull a crack open were to be divided into the product of surface tension multiplied by the drop diameter.

It seems unlikely that the thermodynamic surface tension should be used for T in the Griffith equation because the formation and propagation of a crack involves more than the creation of new surface. What should be used is the surface energy measured in a fracture process; for ductile materials such a measurement will be difficult to make. This surface energy can be obtained from the strain energy release rate (Irwin G-factor) which is proportional to the square of the yield strength divided by Young's modulus. For the case of plane stress, if T is taken to be proportional to S_y^2/Y, where S_y is the 0.2 percent offset yield strength of the solid, the Griffith force tending to pull a crack open would reduce to a constant times the quotient of yield strength divided by the square root of the half-length of the crack.

If Equation 12 or Equation 13 is substituted into Equation 4, it is seen that the volume rate of erosion for a specific material depends on the third power of the impact velocity for the case that the typical eroded fragment is a tetrahedron. The slant height of a regular pyramid of any number of sides is given by $[a^2 - (b/2)^2]^{1/2}$ where a and b are

the edge lengths of a triangular face. For the case that a = gb where g is a numerical coefficient, the slant height is $b(4g^2 - 1)^{1/2}/2$. Because the slant height of a regular pyramid of any number of sides is given by the same power of the edge length b as the slant height of a regular tetrahedron, it appears that the same velocity dependence of the rate of erosion should be obtained for pyramidal fragments of any number of sides as is obtained for tetrahedral fragments.

e. Volume of a Prismatic Fragment

The existence of subsurface cracks in eroded specimens was reported by Baker, Jolliffe, and Pearson[11]; however, the number of such cracks appeared to be restricted. If subsurface cracks that run parallel to the impacted surface are produced either as a result of subsurface shear stresses or by the growth of cracks from the side walls of existing craters, then cracks that run down from the surface may intersect the subsurface cracks to form eroded fragments that are prisms.

The potential energy invested in a crack of fixed depth is proportional to the length of the crack. Assuming that the fraction, E, of the impact energy that is used in crack formation remains constant as the impact energy is increased and that the depth of penetration of a crack extending downward from the surface is fixed by a subsurface crack running parallel to the surface, then, if the impact energy is doubled, the length of the crack which extends downward from the surface to the subsurface crack should also be doubled.

Let the typical fragment be a triangular prism circumscribed by three cracks, a, b, and c, and let it have an altitude or thickness determined by a pre-existing subsurface crack (See Figure 8, upper view). The area of the triangular upper and lower base, ABC, is given by $[s\ (s - a)(s - b)(s - c)]^{1/2}$ where $s = (a + b + c)/2$. If the impact energy is doubled, then the side lengths a, b, and c, will be doubled and the area of the upper and lower base will be increased by a factor of 2^2 or 4 times.

Similarly, for the case that the fragment is a polyhedron of four sides (See Figure 8, lower view) also having altitude or thickness determined by a pre-existing subsurface crack, if the impact energy is doubled then the lengths of the sides a, b, c, and d are doubled and

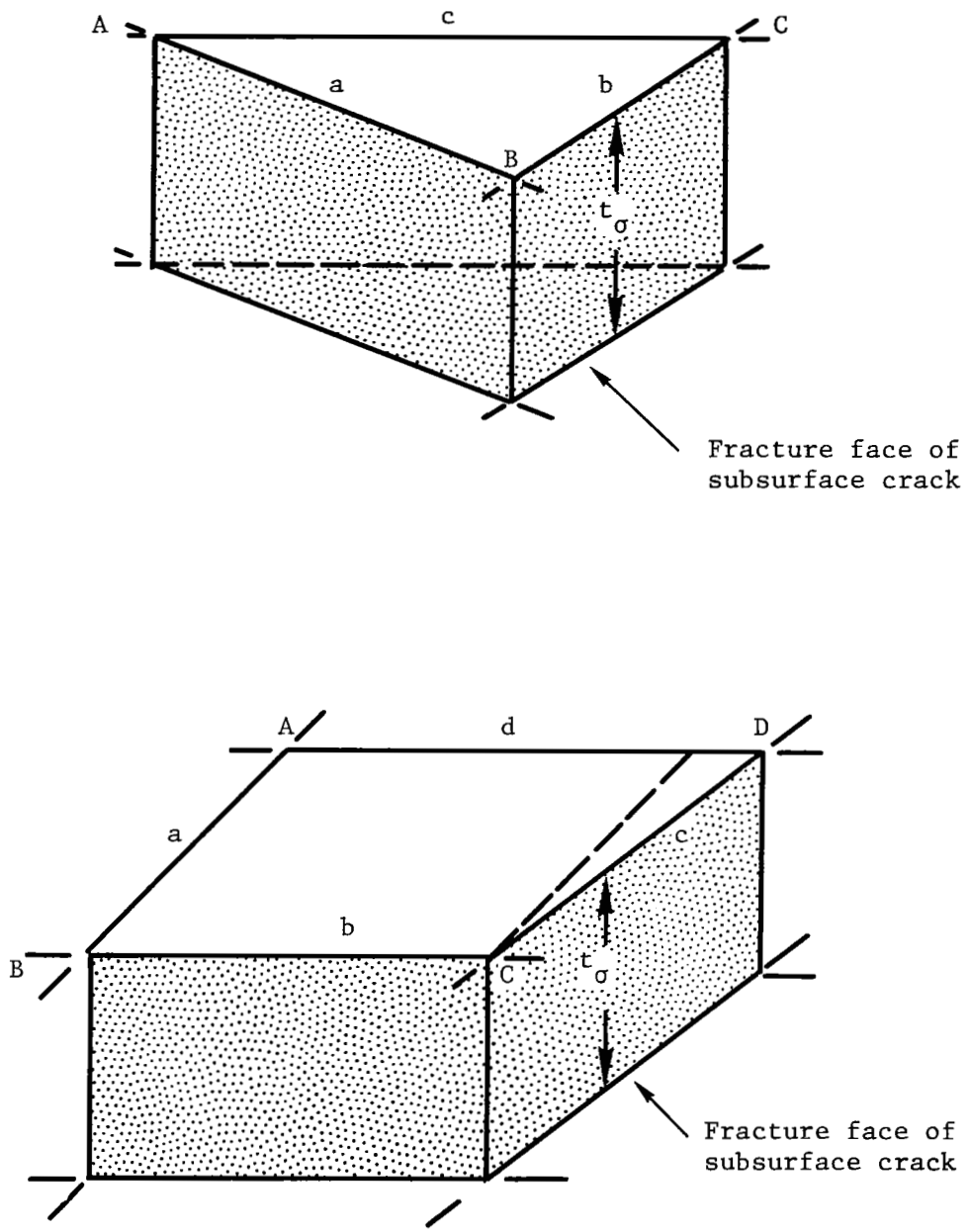

Figure 8. Schematic Drawings of Prismatic Fragments Whose Thickness is Determined by a Pre-Existing Subsurface Crack.

the area circumscribed by the four cracks is increased by a factor of 2^2 or 4 times. In general, if the impact energy is increased z-fold, the area circumscribed by the cracks that result is increased z^2 times.

If a minimal unit of crack length extending from the surface to the subsurface crack is defined by the critical energy, E_c, or critical velocity, V_c, at which such a crack is just able to form, then the surface area of a typical fragment formed at an energy, E, or at a velocity V, is proportional to $(E/E_c)^2$ or to $(V/V_c)^4$ times the minimal area associated with the energy, E_c, or with the velocity, V_c. The minimal area is the area of a fragment of the smallest possible size. This minimal area is designated as A_c.

In view of the preceding considerations, it appears that the volume of a prismatic eroded fragment, v_p, should be proportional to $(A_c)(t_\sigma)(V/V_c)^4$ where t_σ is the depth of the subsurface crack below the surface, that is

$$v_p = k'A_c t_\sigma (V/V_c)^4 \quad , \tag{14}$$

where k' is a proportionality constant which is a function of drop mass and material properties. If Equation 14 is substituted into Equation 4, it appears that the volume rate of erosion for a specific material depends on the fourth power of the impact velocity for the case that the eroded fragments are prismatic. Because the area of all regular polygons is a function of the square of the edge length and because the areas of irregular polygons can be expressed as the sums of the areas of regular polygons, it appears that the same velocity dependence of the rate of erosion should be obtained for prismatic fragments of all sizes and shapes.

III. PARTIAL TEST OF THE EQUATIONS

Equations 4, 7, 13, and 14 are not ready for independent test because they contain quantities that cannot yet be evaluated from theoretical considerations alone. They can be given a partial test by assessing the values of the needed quantities with recourse to experimental data. It was anticipated that partial test of these equations would in itself provide valuable information.

Both drop-impact and cavitation weight-loss data were collected under very carefully controlled conditions for the purpose of testing equations. The test specimens were of zinc, iron, tantalum, nickel, Udimet 700 in the solutioned state and Udimet 700 in the aged state. These metals represent the face-centered-cubic, body-centered-cubic, and hexagonal lattice-packing types. Information on the work-hardening characteristics, tensile stress-strain characteristics, impact behavior, and minimum velocity required to dent by impact of a steel sphere was obtained for these metals in an earlier study.[14] The specimens of these metals that were used for drop-impact and cavitation erosion tests were from the same heat and were in the same heat-treatment state as the impact specimens used in the earlier study.[14]

The experimental values of weight loss for these metals were determined after arbitrary periods of waterdrop impingement on a rotating-arm device.[3] All of the tests were performed at a relative impact velocity of 1000 ft/sec with 0.0866-cm-diameter drops. With the apparatus that was used,[28] both the impingement velocity and the drop diameter could be held constant with a high degree of precision. With the exception of Udimet 700, which was found to require long periods of test before erosion loss occurred, a separate test specimen was used for each data point. This eliminated changes in the impingement area, A, which occur as a consequence of removal and replacement of a test specimen in order to determine weight loss.

The drops impinged within a more or less circular area having a radius equal to the drop diameter. The reported rate at which the drops impinged was 161.5 per second. The reported data for the tests performed were test time, initial weight of specimen, and final weight of specimen. For a detailed description of the test apparatus, a discussion of procedures used in carrying out the tests, and a tabulation of the raw data, see Appendix B.

Weight loss during each time of exposure to drop impingement was found by subtracting the weight of the specimen after exposure from its

[3]The tests, which were obtained from the University of Minnesota, were carried out under the direction of Mr. John A. Almo; Mr. Michael McKay carried out most of the test runs.

weight before exposure. Weight loss was divided by the density of the metal to convert it to volume loss. Test duration times were multiplied by the rate at which the drops impinged to convert them to numbers of drop impacts sustained. The resulting data for the six metals are given in Table 1.

It was not possible to include a test of the equations with use of the cavitation data, which were collected independently by Mr. Stanley G. Young at the NASA Lewis Research Center, Cleveland, Ohio, in the present study. This test and whatever correlation may be found between the drop-impact and cavitation erosion data that were collected will be presented in a later study.

A. Relationships Needed to Test Equations 4 and 7

In the development of the statistical treatment, it was assumed that the typical cell in the array of cells has the size of an eroded fragment and that the diameter, d, of a σ-cell is equal to the distance across an eroded fragment. From Equation 6, taking the area of a σ-cell in the direction of impingement to be circular,

$$p = d^2\pi/4A$$

from which

$$d = (4A\ p/\pi)^{1/2} \quad . \tag{15}$$

Let it now be assumed that the number of impacts required to work-harden a piece of the solid, circumscribe it with cracks, and release it as an eroded fragment is proportional to the size of the fragment. The number of impacts required to release a fragment from the original surface of the test specimen at the start of a test is N_o. Then N_o is proportional to d. By trial, it appears from recourse to the experimental data that the proportionality constant is the reciprocal of the edge length of a micromosaic unit or about 10^4 cm^{-1}. This leads to the relationship,

$$N_o = 10^4 d \tag{16}$$

which states that the number of impacts required to release a fragment is equal to the diameter of the fragment expressed in microns.

TABLE 1

EXPERIMENTAL VOLUME LOSS DATA FOR THE SIX SELECTED METALS

ZINC		NICKEL		IRON		TANTALUM		UDIMET 700 Sol'n.		UDIMET 700 Aged	
Number of Impacts 10^3 Impacts	Volume Loss 10^{-4} cc	Number of Impacts 10^4 Impacts	Volume Loss 10^{-4} cc	Number of Impacts 10^5 Impacts	Volume Loss 10^{-4} cc	Number of Impacts 10^5 Impacts	Volume Loss 10^{-4} cc	Number of Impacts 10^6 Impacts	Volume Loss 10^{-4} cc	Number of Impacts 10^6 Impacts	Volume Loss 10^{-4} cc
2.42	0.70	0.236	1.01	0.388	1.77	0.563	0.00	1.464	3.03	1.454	0.37
2.46	0.42	0.491	0.22	0.775	3.04	0.969	2.77	1.755	7.82	2.038	6.06
4.84	1.40	0.581	1.46	0.969	6.10	1.292	3.25	2.046	9.21	2.328	9.72
4.87	1.54	1.000	2.69	1.132	6.99	1.948	5.96	2.627	12.50	2.910	13.38
9.69	2.80	1.455	1.46	1.295	7.24	2.422	4.64	3.208	14.39	3.491	16.41
9.74	2.24	2.426	3.48	1.551	6.98	3.230	8.37	4.371	18.30	4.072	18.93
12.23	5.75	4.882	7.07	1.950	7.24	3.908	12.53	5.419	23.61	4.654	21.46
14.54	5.60	9.693	12.8	2.326	9.52	5.249	15.54	6.687	29.16	5.235	23.23
14.54	5.74	14.535	16.62	3.101	11.68	7.751	17.29	8.011	33.45	5.814	25.00
19.38	6.30	19.383	15.61	4.652	15.74	9.690	19.04	9.303	34.97?	6.977	28.91
19.44	6.02	24.225	22.12	6.202	18.41	11.144	29.70?		hole	8.140	30.68
21.93	15.42	29.070	19.43	8.075	26.42	11.306	21.45			9.302	33.08
24.23	15.70	33.918	23.14	9.690	27.94	15.504	25.42?			10.465	35.35?
24.63	15.42	38.76	23.14				hole				hole
29.07	16.54	43.62	30.55?								
29.07	17.38										
29.51	25.51?										
31.51	22.01										
33.92	21.02										
34.00	26.49										
36.34	30.56										
36.35	29.72										
38.76	35.04										
38.79	34.90										
41.18	34.34										
41.52	32.52?										
	hole										

Substituting Equation 15 into Equation 16,

$$N_o = 1.12838 \times 10^4 \, (Ap)^{1/2} \, . \qquad (17)$$

For the experimental data that were collected, A = 0.0235606 cm^2. For these data only,

$$N_o = 1732 \, p^{1/2} \qquad (R1)$$

and

$$p = (N_o/1732)^2 . \qquad (R2)$$

The numbers given to these equations indicate that they are restricted in application to an impingement area of 0.0235606 cm^2.

The number of cells of area σ in an array that extends over area A is given by Equation 1. If a rain of n impacts occurs over area A, then the average number of impacts against a typical σ-cell in the array is the quotient $n\sigma/A$. With use of Equation 6, the average number of impacts that occur against the typical cell when a rain of n impacts occurs over area A is just p n where p is the probability of a hit against the cell.

A layer of $\eta\eta'$ fragments will be released from the area A when the number of impacts that occur at a typical cell site is N_o or when the average number of impacts is p n_o and n_o is a specific number of impacts that occur over area A. Remembering this fact, and multiplying Equation R2 by n_o,

$$pn_o = N_o^2 \, n_o/(1732)^2 = N_o .$$

From the second equality,

$$n_o = (1732)^2/N_o = 2999824/N_o . \qquad (R3)$$

B. Test of the Equations with Experimental Drop-Impact Volume-Loss Data for Iron

The drop-impact volume-loss data that were collected for iron are particularly well suited for test of the equations because a large number of data points happened to be collected over the range of impacts in which the maximum rate of volume loss occurred. These experimental volume-loss data for iron are plotted against number of impacts sustained in Figure 9.

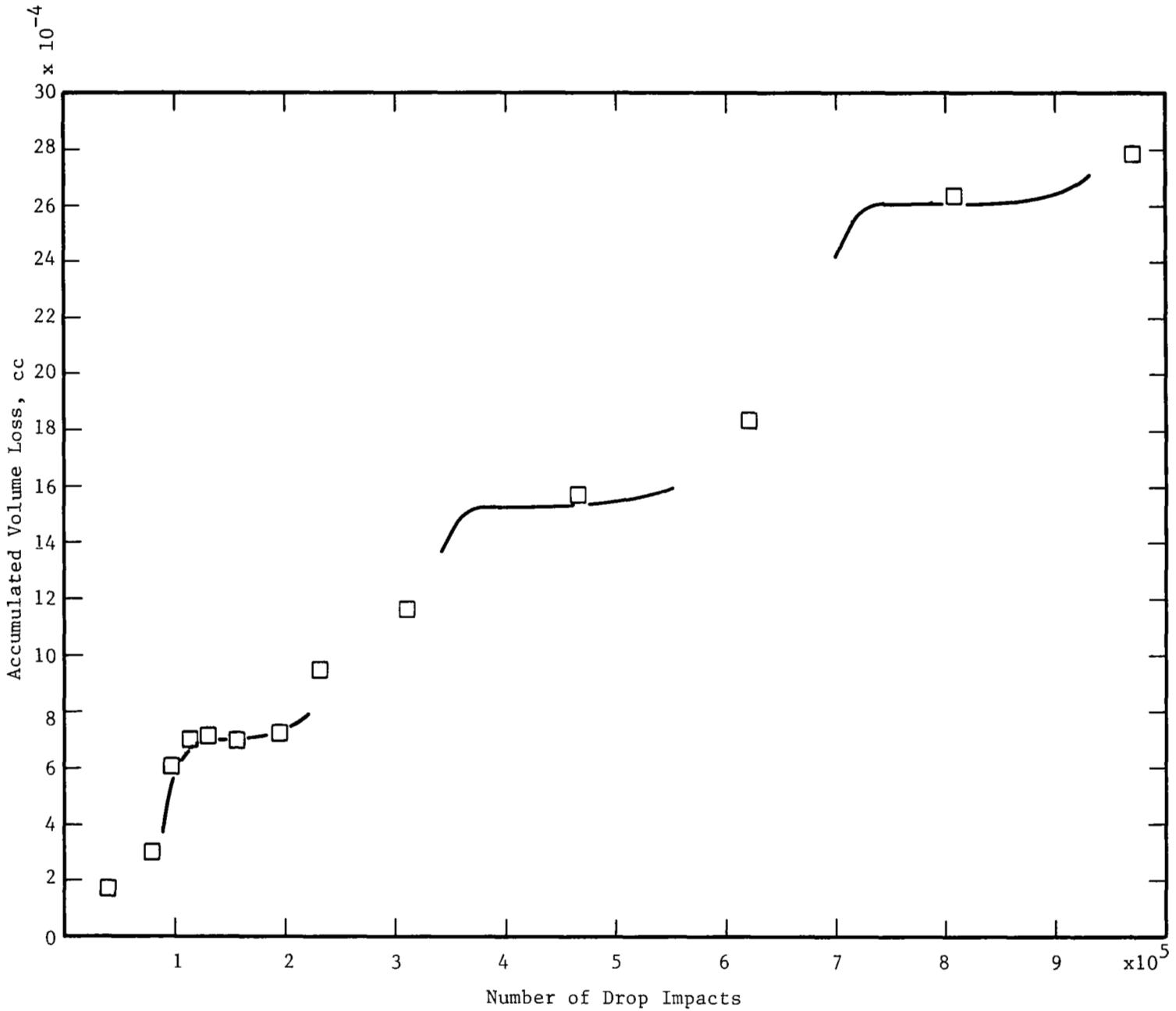

Figure 9. Experimental Accumulated-Volume-Loss Data for Iron. Three Knees in the Data are Indicated.

1. Expected Form of the Rate-of-Volume-Loss Curve

The maximum rate of volume loss occurs at the number of impacts for which the first sharp rise in accumulated volume loss takes place. In Figure 9, it can be seen by inspection that this first sharp rise in accumulated volume loss takes place somewhere between 0.9 and 1 x 10^5 impacts. Further inspection of Figure 9 indicates that two other sharp rises in accumulated volume loss also occur. These rises, which are located at about 2.75 x 10^5 and 6.5 x 10^5 impacts, respectively, are associated with peaks in the rate of volume loss that are lower than the first peak; the first peak is the maximum rate of volume loss.

The peaks in the rate of volume loss plotted against impacts sustained are separated by regions in which essentially no volume loss occurs. Three of such flat plateaus have been roughly indicated in Figure 9. The rate of volume loss on such a plateau is zero. From inspection alone, it can be concluded that the rate of volume loss for iron plotted against number of impacts sustained will have the form indicated schematically in Figure 10.

For a further discussion of features of rate curves see Section III.G.

2. Sample Calculation of Rate-of-Volume-Loss and Accumulated-Volume-Loss Curves

The theoretical work has not yet been carried far enough to provide an expression for the first number of the counting rule, N_o, or for the number of impacts, n_o, that must occur against an area, A, of a given material before the first sharp rise in accumulated volume loss takes place. It is necessary to have recourse to the experimental data to obtain the number of impacts, n_o. On the basis of the experimental data, 0.95 x 10^5 can be accepted as a probable value of the impacts that are required to reach the first sharp rise in accumulated volume loss for iron. Substituting this value of n_o into Equation R3, the value of N_o is found to be 32. Substituting this value of N_o into Equation R2, the probability of a hit, p, is found to be 3.4135 x 10^{-4}. For iron, with N_o equal to 32, the counting rule numbers, N_i, can be expected to pass through the values N_1 = 64 and N_2 = 128 as the angle at which the drops impinge changes from normal incidence to an effective angle of 30 degrees (See Section II.C).

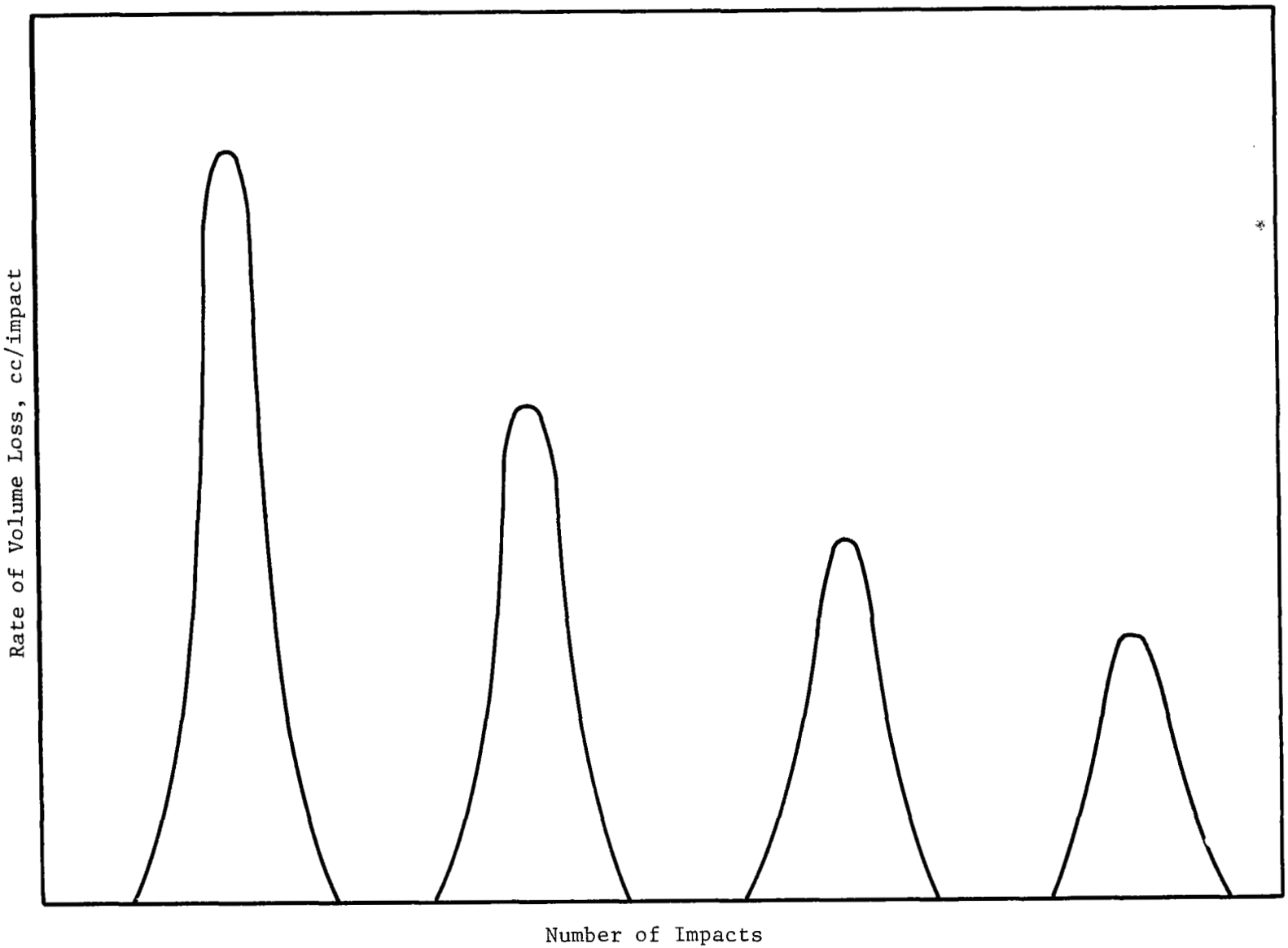

Figure 10. Schematic Representation of the Expected Form of the Rate-of-Volume-Loss Curve for Iron on the Basis of Inspection of the Accumulated-Volume-Loss Data.

The input data for iron to be used in the computer program (See Appendix C-B) for Equation 7 are: $p = 3.4135 \times 10^{-4}$, $N_o = 32$, $N_1 = 64$, and $N_2 = 128$. Because it was desired to calculate the rate of erosion for iron, a printout of the accumulated number of ejected layers of fragments was required and the condition $R_1 = R_2 = R_3 = 1$ was imposed (See Appendix C-B). The computer printout of layers of fragments ejected is given in the second column of Table 2.

From Equation 16 and the value of 32 for N_o, the diameter, d, of an eroded iron fragment is 0.0032 cm or 32 microns. This is about half the average grain size of the iron metal used, which was found to be 63 microns using the Heyn intercept method (ASTM Designation E112-63). Assuming that the area of a typical σ-cell in iron is the area of a circle having the diameter d = 0.0032 cm, the area, σ, of the typical cell or eroded fragment for iron is 8.0425×10^{-6} cm^2. Remembering that the impingement area, A, for the drop-impact tests performed is 0.0235606 cm^2, the number of σ-cells, η, for iron from Equation 1 is 2929.51. For the 0.0866-cm-diameter drops that were used, η' for iron from Equation 2 is 42.5098, and the product $\eta\eta'$ is 124532. The fragments ejected from area A when each σ-cell in this area has received some integral number of impacts is the product of $\eta\eta'$ times the number of layers ejected. The fragments ejected from area A are listed in column three of Table 2 and the values of average ejection rate, J, found with use of Equation 8 are given in column four.

The volume of a tetrahedral fragment is 0.11785 times the cube of the edge length. If the value d = 0.0032 cm is used for the edge length, the volume of a tetrahedral fragment for iron is 3.8617×10^{-9} cm^3. In order to make the first knee of the theoretical volume-loss-versus-impacts-sustained curve occur at the same value of accumulated volume loss as the first knee formed by the experimental data points, it was found by trial that the volume of the typical fragment for iron is 1.5 times this tetrahedral volume. This suggests that the ejected fragments may not all be tetrahedra. It is noteworthy that an eroded fragment volume larger than the tetrahedral volume is reasonable because some of the eroded fragments may be prisms; an eroded fragment volume smaller than the tetrahedral volume could not be justified. With use of the factor 1.5, the volume of an average iron fragment is given by the

TABLE 2

SUMMARY OF DATA FOR THE CALCULATED CURVES FOR IRON

Impacts n	Layers Ejected --	Fragments Ejected From Area A --	Ejection Rate J frgs/impact	Volume Rate R cc/impact	Volume Increment Q cc	Accumulated Volume Loss, L cc
0.25×10^5	0.0000	0	0.00000	0.00000	0.0000	0.0000
0.50×10^5	0.0008	99	0.00025	0.00143×10^{-9}	0.0001×10^{-4}	0.0001×10^{-4}
0.60×10^5	0.0110	1374	0.1275	0.7387×10^{-9}	0.0739×10^{-4}	0.0740×10^{-4}
0.70×10^5	0.0648	8071	0.6697	3.879×10^{-9}	0.3879×10^{-4}	0.4619×10^{-4}
0.75×10^5	0.1236	15398	1.465	8.488×10^{-9}	0.4244×10^{-4}	0.8863×10^{-4}
0.80×10^5	0.2078	25872	1.780	10.31×10^{-9}	0.5156×10^{-4}	1.402×10^{-4}
0.89×10^5	0.4082	50836	2.774	16.07×10^{-9}	1.446×10^{-4}	2.848×10^{-4}
0.90×10^5	0.4325	53864	3.028	17.54×10^{-9}	0.1754×10^{-4}	3.023×10^{-4}
0.91×10^5	0.4569	56901	3.037	17.59×10^{-9}	0.1759×10^{-4}	3.199×10^{-4}
0.92×10^5	0.4813	59936	3.035	17.58×10^{-9}	0.1758×10^{-4}	3.375×10^{-4}
0.93×10^5	0.5056	62958	3.022	17.51×10^{-9}	0.1751×10^{-4}	3.550×10^{-4}
0.94×10^5	0.5296	65956	2.998	17.37×10^{-9}	0.1737×10^{-4}	3.724×10^{-4}
0.95×10^5	0.5534	68919	2.963	17.16×10^{-9}	0.1716×10^{-4}	3.896×10^{-4}
0.96×10^5	0.5769	71838	2.919	16.91×10^{-9}	0.1691×10^{-4}	4.065×10^{-4}
0.97×10^5	0.5999	74704	2.866	16.60×10^{-9}	0.1660×10^{-4}	4.231×10^{-4}
0.98×10^5	0.6224	77508	2.804	16.24×10^{-9}	0.1624×10^{-4}	4.393×10^{-4}
0.99×10^5	0.6444	80242	2.734	15.84×10^{-9}	0.1584×10^{-4}	4.551×10^{-4}
1.00×10^5	0.6657	82901	2.659	15.40×10^{-9}	0.1540×10^{-4}	4.705×10^{-4}
1.10×10^5	0.8383	104399	2.150	12.45×10^{-9}	1.245×10^{-4}	5.951×10^{-4}
1.20×10^5	0.9351	116445	1.205	6.978×10^{-9}	0.6978×10^{-4}	6.649×10^{-4}
1.25×10^5	0.9614	119727	0.6564	3.802×10^{-9}	0.1901×10^{-4}	6.839×10^{-4}
1.50×10^5	0.9984	124328	0.1840	1.066×10^{-9}	0.2665×10^{-4}	7.105×10^{-4}
1.75×10^5	1.000	124529	0.00804	0.04657×10^{-9}	0.0116×10^{-4}	7.117×10^{-4}
2.00×10^5	1.001	124642	0.00452	0.02618×10^{-9}	0.0065×10^{-4}	7.123×10^{-4}
2.25×10^5	1.019	126907	0.09060	0.5248×10^{-9}	0.1312×10^{-4}	7.254×10^{-4}
2.50×10^5	1.136	141503	0.5838	3.382×10^{-9}	0.8455×10^{-4}	8.100×10^{-4}
2.75×10^5	1.427	177668	1.447	8.380×10^{-9}	2.095×10^{-4}	10.19×10^{-4}
2.78×10^5	1.468	182871	1.734	10.05×10^{-9}	0.3014×10^{-4}	10.50×10^{-4}
2.80×10^5	1.496	186346	1.738	10.06×10^{-9}	0.2013×10^{-4}	10.70×10^{-4}
2.85×10^5	1.565	194937	1.718	9.953×10^{-9}	0.4976×10^{-4}	11.20×10^{-4}
2.90×10^5	1.632	203192	1.651	9.564×10^{-9}	0.4782×10^{-4}	11.67×10^{-4}
2.95×10^5	1.694	210899	1.541	8.929×10^{-9}	0.4464×10^{-4}	12.12×10^{-4}
3.00×10^5	1.750	217898	1.400	8.108×10^{-9}	0.4054×10^{-4}	12.53×10^{-4}

TABLE 2 (Continued)

SUMMARY OF DATA FOR THE CALCULATED CURVES FOR IRON

Impacts n	Layers Ejected --	Fragments Ejected From Area A --	Ejection Rate J frgs/impact	Volume Rate R cc/impact	Volume Increment Q cc	Accumulated Volume Loss, L cc
3.05×10^5	1.799	224087	1.238	7.170×10^{-9}	0.3585×10^{-4}	12.88×10^{-4}
3.10×10^5	1.842	229419	1.066	6.177×10^{-9}	0.3089×10^{-4}	13.19×10^{-4}
3.15×10^5	1.878	233899	0.8960	5.190×10^{-9}	0.2595×10^{-4}	13.45×10^{-4}
3.25×10^5	1.931	240515	0.6616	3.832×10^{-9}	0.3832×10^{-4}	13.84×10^{-4}
3.50×10^5	1.988	247572	0.2823	1.635×10^{-9}	0.4088×10^{-4}	14.24×10^{-4}
3.75×10^5	1.999	248892	0.05280	0.3058×10^{-9}	0.0765×10^{-4}	14.32×10^{-4}
4.00×10^5	2.000	249050	0.00632	0.0366×10^{-9}	0.0092×10^{-4}	14.33×10^{-4}
4.25×10^5	2.000	249063	0.00052	0.0030×10^{-9}	0.0008×10^{-4}	14.33×10^{-4}
4.50×10^5	2.000	249063	0.00000	0.0000×10^{-9}	0.0000×10^{-4}	14.33×10^{-4}
4.75×10^5	2.000	249064	0.00004	0.0002×10^{-9}	0.0001×10^{-4}	14.33×10^{-4}
5.00×10^5	2.000	249070	0.00024	0.0014×10^{-9}	0.0003×10^{-4}	14.33×10^{-4}
5.25×10^5	2.001	249150	0.00320	0.0185×10^{-9}	0.0046×10^{-4}	14.34×10^{-4}
5.50×10^5	2.006	249744	0.02376	0.1376×10^{-9}	0.0344×10^{-4}	14.37×10^{-4}
5.75×10^5	2.028	252537	0.1117	0.6471×10^{-9}	0.1618×10^{-4}	14.53×10^{-4}
6.00×10^5	2.097	261149	0.3445	1.995×10^{-9}	0.4989×10^{-4}	15.03×10^{-4}
6.25×10^5	2.242	279142	0.7197	4.169×10^{-9}	1.042×10^{-4}	16.07×10^{-4}
6.30×10^5	2.280	283889	0.9494	5.499×10^{-9}	0.2750×10^{-4}	16.35×10^{-4}
6.40×10^5	2.363	294256	1.037	6.005×10^{-9}	0.6005×10^{-4}	16.95×10^{-4}
6.50×10^5	2.452	305382	1.113	6.445×10^{-9}	0.6445×10^{-4}	17.59×10^{-4}
6.60×10^5	2.543	316703	1.132	6.558×10^{-9}	0.6558×10^{-4}	18.25×10^{-4}
6.70×10^5	2.631	327641	1.094	6.336×10^{-9}	0.6336×10^{-4}	18.88×10^{-4}
6.75×10^5	2.672	332803	1.032	5.980×10^{-9}	0.2990×10^{-4}	19.18×10^{-4}
6.80×10^5	2.712	337690	0.9774	5.662×10^{-9}	0.2831×10^{-4}	19.46×10^{-4}
6.90×10^5	2.782	346484	0.8794	5.094×10^{-9}	0.5094×10^{-4}	19.97×10^{-4}
7.00×10^5	2.841	353822	0.7338	4.251×10^{-9}	0.4251×10^{-4}	20.40×10^{-4}
7.25×10^5	2.938	365893	0.4828	2.797×10^{-9}	0.6992×10^{-4}	21.10×10^{-4}
7.50×10^5	2.981	371184	0.2116	1.226×10^{-9}	0.3065×10^{-4}	21.40×10^{-4}
7.75×10^5	2.995	372986	0.07208	0.4175×10^{-9}	0.1044×10^{-4}	21.51×10^{-4}
8.00×10^5	2.999	373470	0.01936	0.1121×10^{-9}	0.0280×10^{-4}	21.54×10^{-4}
8.25×10^5	3.000	373578	0.00432	0.0250×10^{-9}	0.0063×10^{-4}	21.54×10^{-4}
8.50×10^5	3.000	373622	0.00176	0.0102×10^{-9}	0.0025×10^{-4}	21.55×10^{-4}
8.75×10^5	3.001	373773	0.00604	0.0350×10^{-9}	0.0087×10^{-4}	21.55×10^{-4}
9.00×10^5	3.007	374416	0.02572	0.1490×10^{-9}	0.0372×10^{-4}	21.59×10^{-4}
9.25×10^5	3.024	376529	0.08452	0.4896×10^{-9}	0.1224×10^{-4}	21.71×10^{-4}
9.50×10^5	3.067	381909	0.2152	1.247×10^{-9}	0.3116×10^{-4}	22.03×10^{-4}
9.75×10^5	3.153	392638	0.4292	2.486×10^{-9}	0.6215×10^{-4}	22.65×10^{-4}
10.00×10^5	3.289	409609	0.6788	3.932×10^{-9}	0.9831×10^{-4}	23.63×10^{-4}

product of 0.18856 times the cube of the edge length. Remembering that the volume of a cube is unity times the cube of the edge length, and that the volume of a tetrahedron is 0.11785 times the cube of the edge length, it appears that the eroded iron fragments are largely tetrahedral.

The rates of volume loss for iron found with use of Equation 4 and with the volume of an eroded fragment, v, equal to 1.5 times the volume of tetrahedron with an edge length of 0.0032 cm are given in column five of Table 2. The accumulated volume losses can be back-calculated from the rates of volume loss to provide a check of the curve of rate-of-volume-loss plotted against number of impacts sustained. The increments of volume loss, Q, calculated with use of Equation 9 are given in column six of Table 2. The accumulated volume losses calculated with use of Equation 10 are given in column seven.

Both the rate of volume loss and the accumulated volume loss found from Equation 7 with use of the computer program are shown in Figure 11 along with the experimental data points. Because the calculated rate of volume loss is an average value for an interval of impacts, Δn, the calculated values of rate of volume loss are plotted at the midpoints of the intervals. Expressed in time, the interval lengths are from 6 to 155 sec. It can be seen from Figure 11 that the theoretical volume loss back-calculated from the theoretical rate of volume loss is in good agreement with the experimental data points up to 7×10^5 impacts; for larger numbers of impacts sustained, the calculated curve falls below the data points. This appears to be the result of the fact that the eroded fragment size is increasing (See Section II.E.2.b) whereas the theoretical curves have been calculated for eroded fragments of equal size. Use of Equation 7 to calculate the accumulated volume loss curve for fragments of increasing size is discussed in Section IV.

C. Test of the Equations with Experimental Drop-Impact Volume-Loss Data for Nickel

By inspection of the experimental data, the first sharp rise in accumulated volume loss for nickel was taken to occur at n_o = 30,000 impacts. From Equation R3, the value of N_o is 99.9941 and from Equation R2 the probability, p, of a hit against the typical cell is 0.00333314.

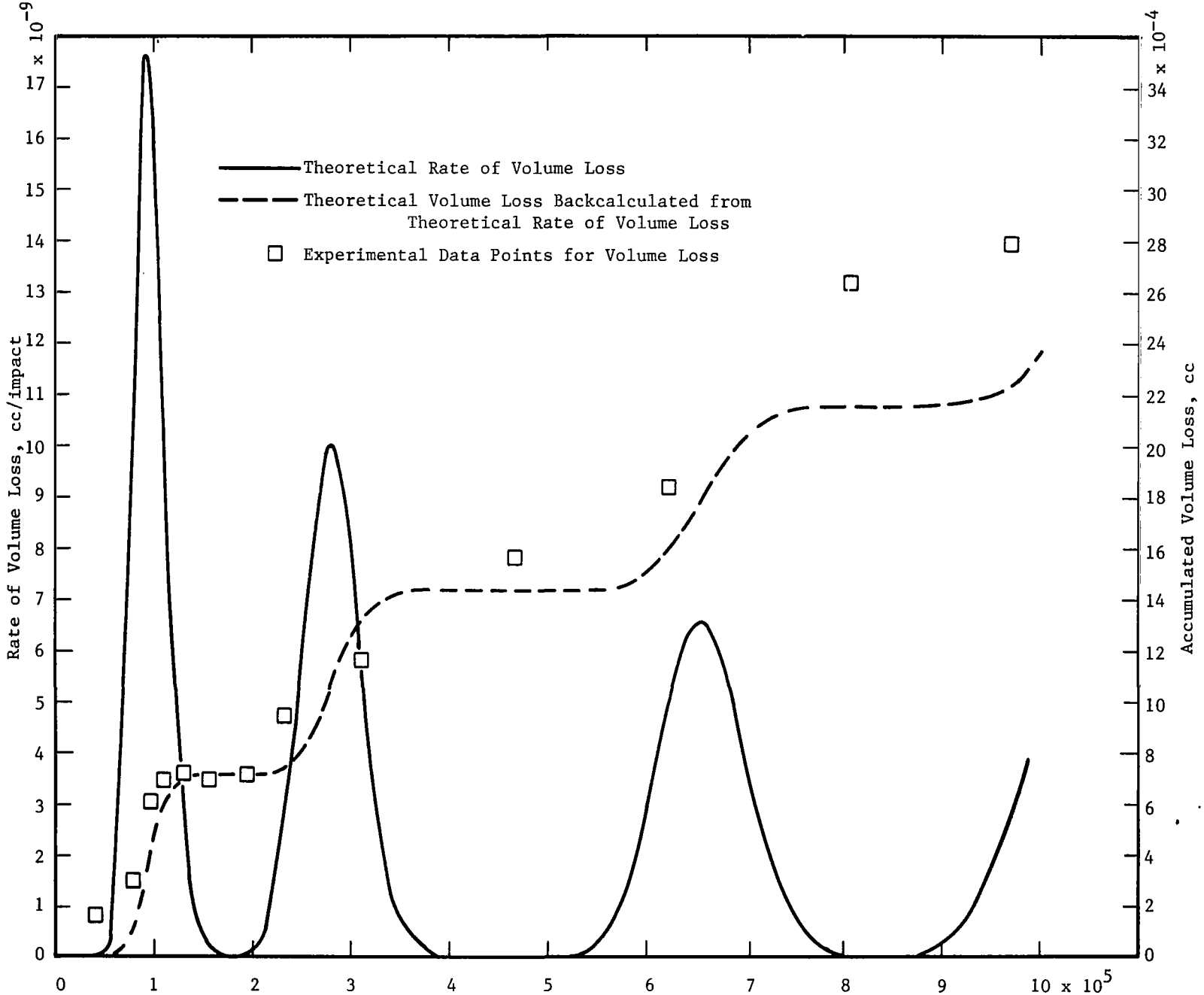

Figure 11. Theoretical Rate-of-Volume-Loss and Accumulated-Volume-Loss Curves for Iron Calculated with Fragments of Equal Volume.

The counting rule, N_i, was expected to pass through the values N_1 = 198.9882 and N_2 = 399.9764 as the angle at which the drops impinge changes from normal incidence to 30 degrees. From inspection of the experimental data, it was concluded that an angle of attack smaller than 30 degrees was reached. Because $N_1 = 2N_o$ and $N_2 = 4N_o$, the value of N_3 was taken to be $8N_o$ or 799.9528.

From Equation 16 and the value of 99.9941 for N_o, the diameter, d, of an eroded nickel fragment was found to be 100 microns. This is roughly double the average grain size of the nickel metal used which was found to be 53 microns with use of the Heyn intercept method. The volume of a tetrahedral fragment is 0.11785 times the cube of the edge length. The calculated value of a tetrahedral fragment for nickel is 1.1785×10^{-7} cm^3. The average volume of an eroded nickel fragment was taken to be 1.49 times the tetrahedral volume or 1.755965×10^{-7} cm^3 because this fragment volume was required in order to bring the first knee of the theoretical volume loss curve into agreement with the first knee formed by the experimental data points.

Both the rate of volume loss and the accumulated volume loss found for nickel with use of the computer program for Equation 7 are shown in Figure 12 along with the experimental data points. It can be seen from Figure 12 that the theoretical volume loss backcalculated from the theoretical rate of volume loss is in relatively good agreement with the experimental data points. The cluster of data points near the origin of this plot suggests that the first sharp rise in accumulated volume loss for nickel should perhaps have been taken to occur at less than 10,000 impacts. This would make the maximum rate of volume loss for nickel larger by nearly a factor of two. However, such a choice would result in a value of N_o which is not compatible with the remaining numbers of the counting rule.

D. Test of the Equations with Experimental Drop-Impact Volume-Loss Data for Tantalum

By inspection of the experimental data, the first sharp rise in accumulated volume loss for tantalum was taken to occur at about n_o = 120,000 impacts. On the basis of this value of n_o, the value of the first number of the counting rule, N_o, was found to be 24.9986 and the

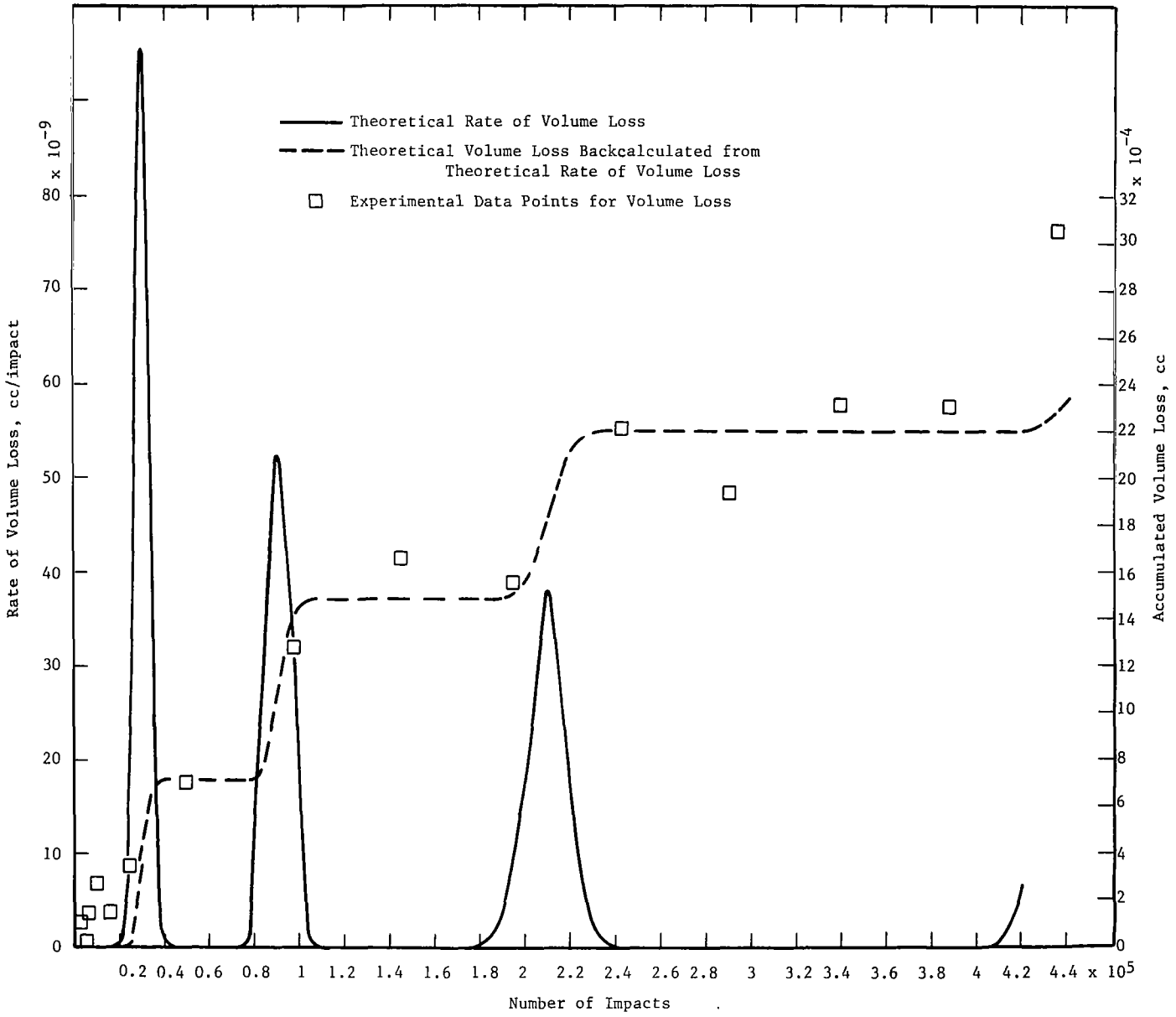

Figure 12. Theoretical Rate-of-Volume-Loss and Accumulated-Volume-Loss Curves for Nickel Calculated with Fragments of Equal Volume.

probability, p, of a hit against the typical cell was found to be 0.000208321. The counting rule, N_i, was expected to pass through N_1 = 49.9970 and N_2 = 99.9940 as the angle at which the drops impinged changed from normal incidence to 30 degrees.

The diameter, d, of an eroded fragment was found to be 24.9986 microns. This is about 1/5 of the average grain size which was found to be 126 microns with use of the Heyn intercept method. The calculated volume of a tetrahedral fragment of tantalum was found to be 1.841097 x 10^{-9} cm^3. It was found necessary to take the average volume of an eroded tantalum fragment to be 1.07 times the tetrahedral volume or 1.969974 x 10^{-9} cm^3 in order to bring the first knee of the theoretical volume loss curve into agreement with the first knee formed by the experimental data points.

The rate of volume loss and the accumulated volume loss found for tantalum with use of the computer program for Equation 7 are shown in Figure 13 along with the experimental data points. From Figure 13 it can be seen that the agreement between the theoretical volume loss back-calculated from the theoretical rate of volume loss is in reasonably good agreement with the experimental data points. In the light of results reported in Section IV, the relatively poor agreement from about 4 x 10^5 to 8 x 10^5 impacts appears to be due to an increase in the volume of an eroded fragment.

E. Test of the Equations with Experimental Drop-Impact Volume-Loss Data for Zinc

The first sharp rise in accumulated volume loss for zinc was taken to be n_o = 10,000 impacts. On the basis of this choice, the first number of the counting rule, N_o, is 300, and the probability, p, of a hit against the typical cell is 0.0300018. The diameter of an eroded zinc fragment is 300 microns. The average grain size of the zinc metal used for the test specimen was found to be just 300 microns. From this it appears that the zinc eroded in units of entire grains.

Inspection of the step structure of the experimental accumulated volume loss data for zinc indicates that there was no change in the angle of attack of the impinging drops, that is, $N_o = N_1 = N_2 \ldots = 300$. There is no obvious answer for the fact that zinc is different from the other

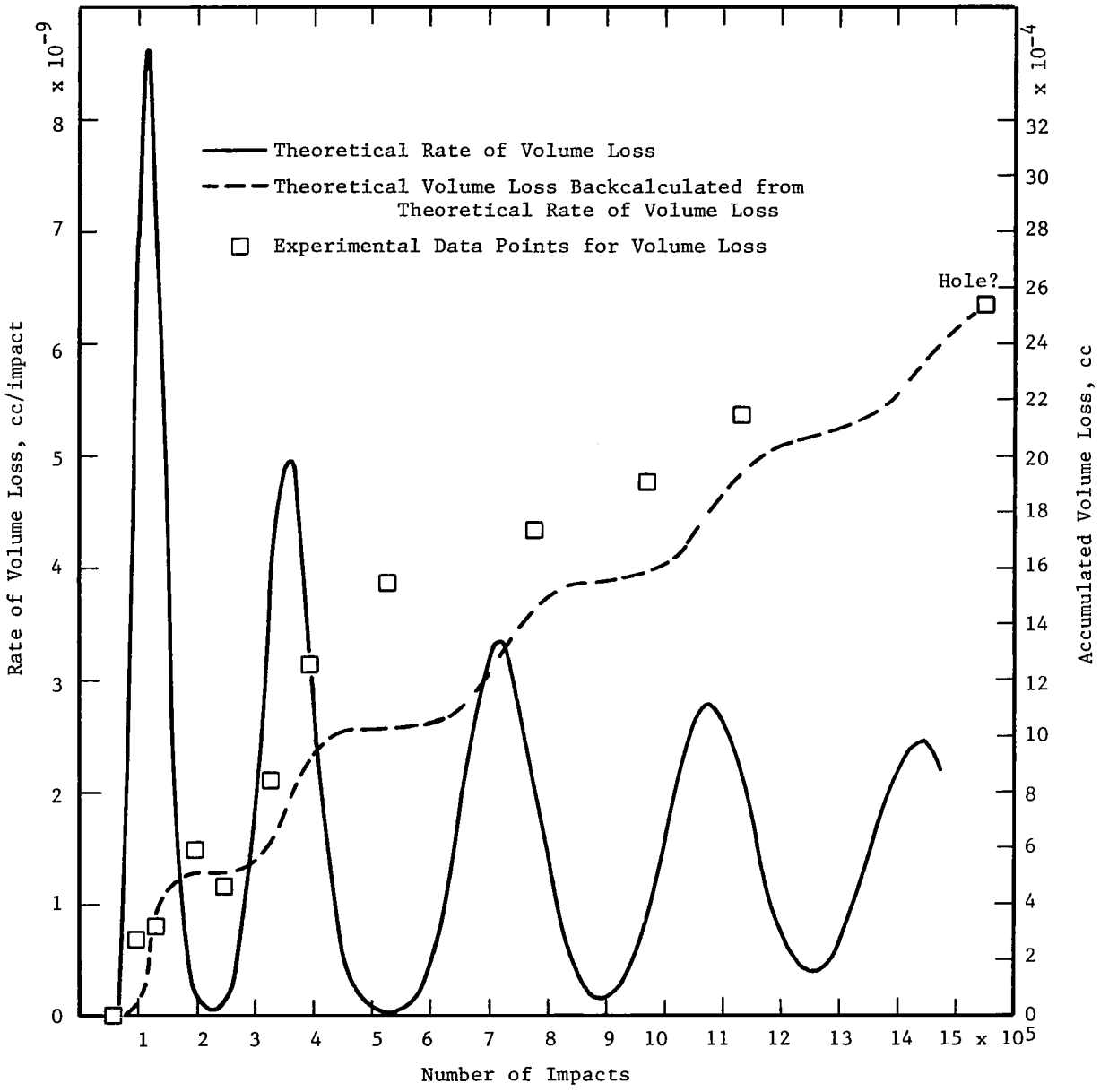

Figure 13. Theoretical Rate-of-Volume-Loss and Accumulated-Volume-Loss Curves for Tantalum Calculated with Fragments of Equal Volume.

metals in this respect. However, the zinc rod was formed by extrusion and an X-ray study of the metal showed that it possessed some orientation; the hexagons of the lattice structure would be seen if the rod were viewed end on. The axis of the test specimen coincided with the axis of the rod stock. The fact that whole grains were broken out of the hexagonal structure that would be seen if a test specimen were viewed end on may account for the fact that there was no change in the angle of attack of the impinging drops.

The rate of volume loss and the accumulated volume loss found for zinc with use of the computer program for Equation 5 are shown in Figure 14 along with the experimental data points. From Figure 14 it can be seen that the agreement between the theoretical curve and the experimental data is good only for the initial section of the plot. In the light of results reported in Section IV the poor agreement found for numbers of impacts greater than 20,000 appears to be caused by a very marked increase in the size of the eroded fragments.

F. Test of the Equations with Experimental Drop-Impact Volume-Loss Data for Aged Udimet 700 Alloy

Udimet 700 is a high-strength alloy. Failure of such a material can be expected to start at weak points (See Section II.A and Figure 1). The statistical model of erosion rate in its present form supposes that, at the start of a test run, all of the σ-cells in the original surface are equivalent. In order to treat high-strength materials successfully, it will be necessary to restrict the number of cells that are subject to crack formation as the result of a drop impact. An attempt was made to apply the present form of the statistical model to aged Udimet 700 alloy; the obstacles that were encountered are described below.

Because of the exceptionally long test times that were required to erode Udimet 700 alloy, it was necessary to collect all of the volume-loss data on one test specimen. This introduced reset errors in the impingement area, A, as a consequence of removing and replacing the test specimen after each increment of test in order to determine the weight loss. The reset error can only be an increase in the impingement area, A. In calculating the probability of a hit, p, the first number of the counting rule, N_o, and the area of a microcell, the impingement area was arbitrarily assumed to have increased from 0.0235606 cm^2 to 0.0352991 cm^2;

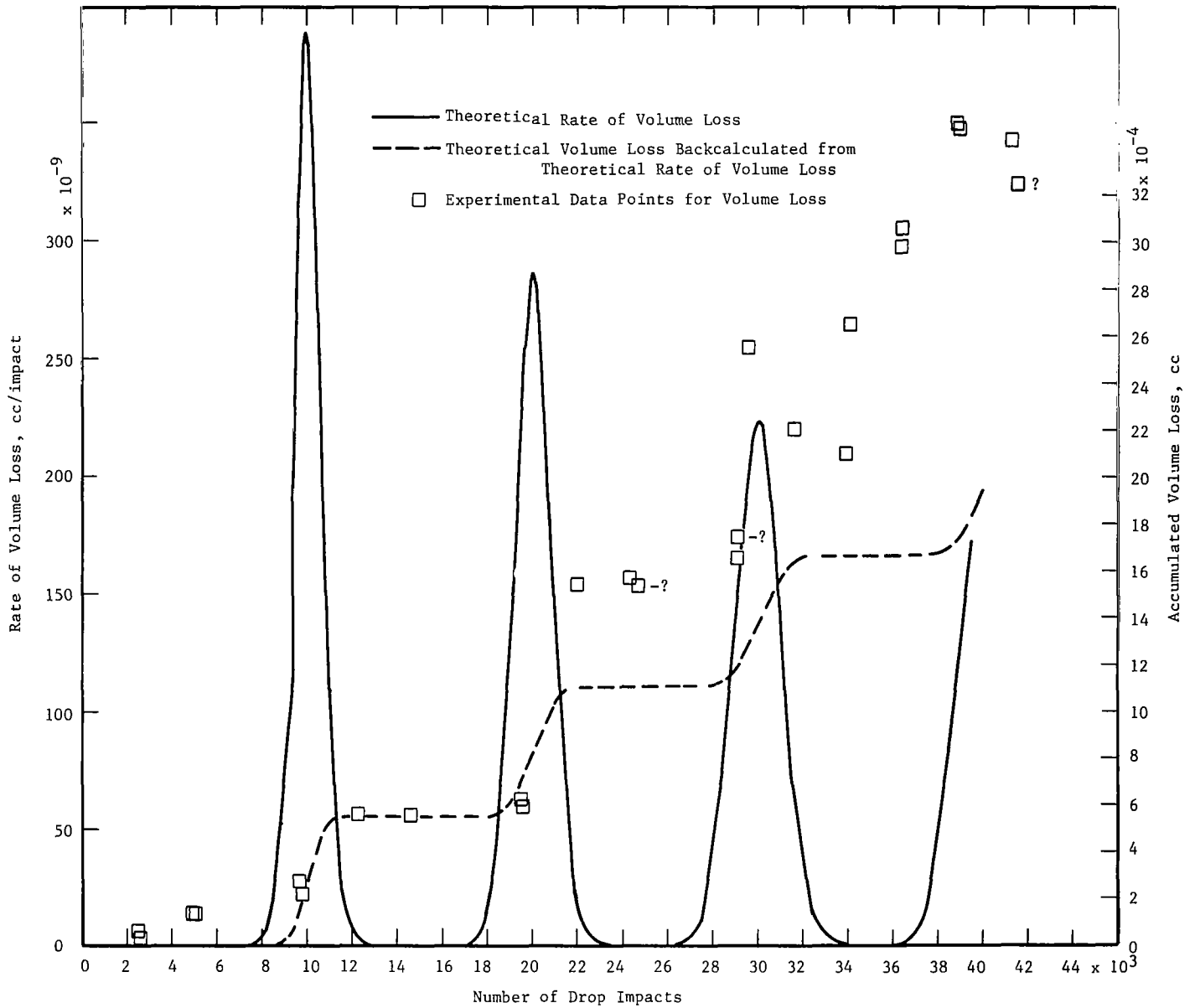

Figure 14. Theoretical Rate-of-Volume-Loss and Accumulated-Volume-Loss Curves for Zinc Calculated with Fragments of Equal Volume.

this is essentially a 50 percent increase. Such an increase in the impingement area has only a small effect on the locus of the theoretical curves. This is shown in Section V.

The experimental volume-loss data for Udimet 700 aged do not show the marked step structure that is apparent in the experimental volume-loss data for iron, nickel, and zinc. Nevertheless, some structure exists; this can be seen by inspection of the aged Udimet 700 volume-loss data shown in Figure 15. From Figure 15 it can be seen that there are sections of the plot that can be fit by straight lines and that these lines gradually change in slope.

From inspection of the experimental data plotted in Figure 15, the first sharp rise in accumulated volume loss was taken to occur at $n_o = 2.2 \times 10^6$ impacts. On the basis of this value of n_o, the probability of a hit against the typical cell was found to be $p = 0.0000011236$ and the first number of the counting rule, N_o, was found to be 2.2472.

The fact that the first number of the counting rule is less than three presents an anomaly because a minimum of three impacts has been accepted as necessary to circumscribe a piece of the solid which then breaks away as an eroded fragment. A number less than three for N_o can only be justified by accepting it as a statistical average and by assuming that residual crack ends contribute to the removal of new fragments.

The diameter of an eroded aged Udimet 700 fragment was found to be 2.2472 microns. This is about 1/70 of the average grain size of the aged Udimet 700 metal used for the test specimen; the average grain size was found to be 160 microns with use of the Heyn intercept method.

The rate of volume loss and the accumulated volume loss found for aged Udimet 700 with use of the computer program for Equation 7 are plotted against number of impacts sustained in Figure 16 along with the experimental data points. From this plot it can be seen that the theoretical rate curve is quite different from that found for the other metals and that the accumulated-volume-loss curve is in agreement with the experimental data only over the range from 2×10^6 to 5×10^6 impacts. Better agreement is found when the change in volume of eroded fragments is taken into account (see Section IV) but the calculated values of the probability, p, and of the first number of the counting rule, N_o, for

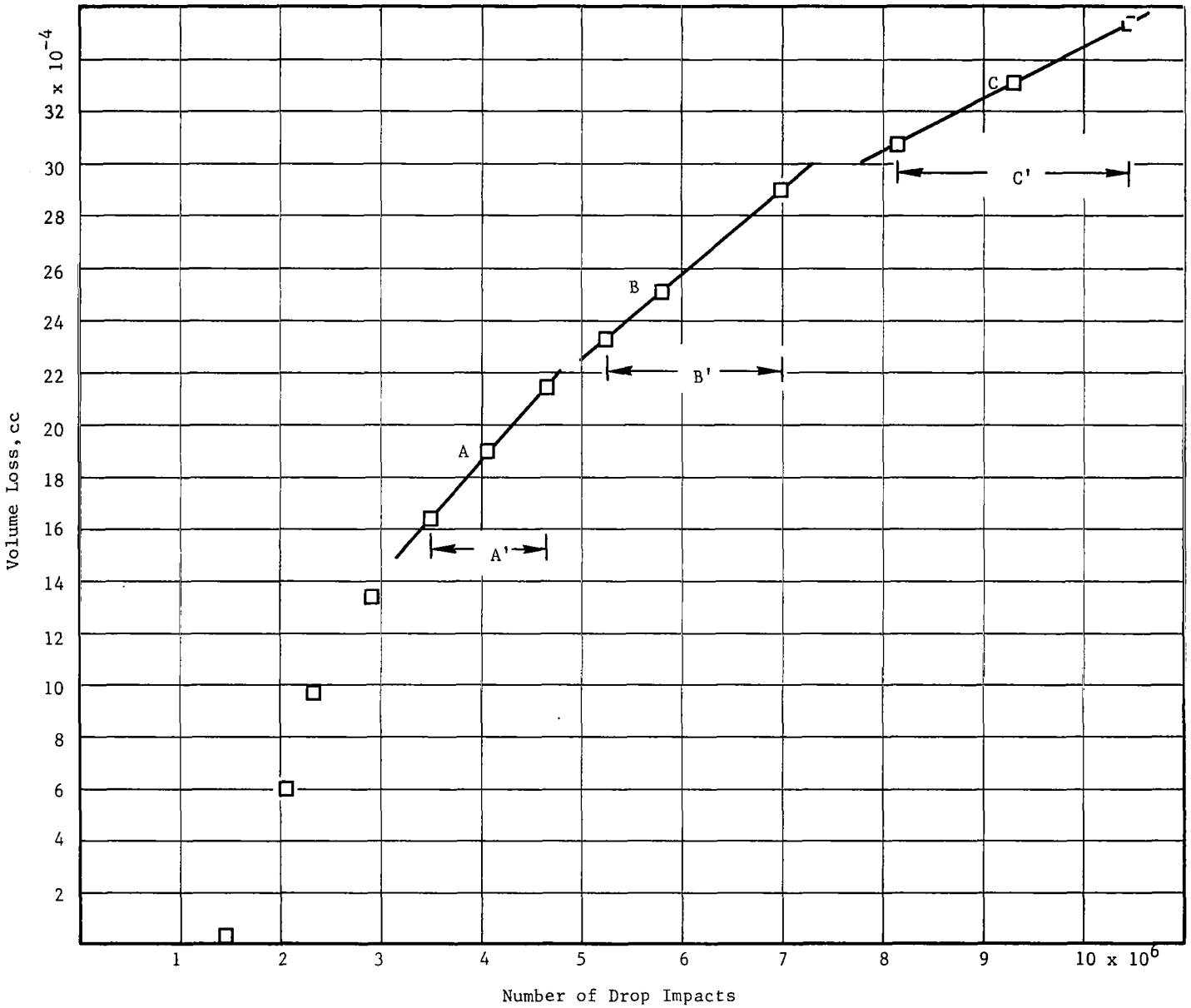

Figure 15. Zones in the Experimental Volume-Loss Data for Aged Udimet 700.

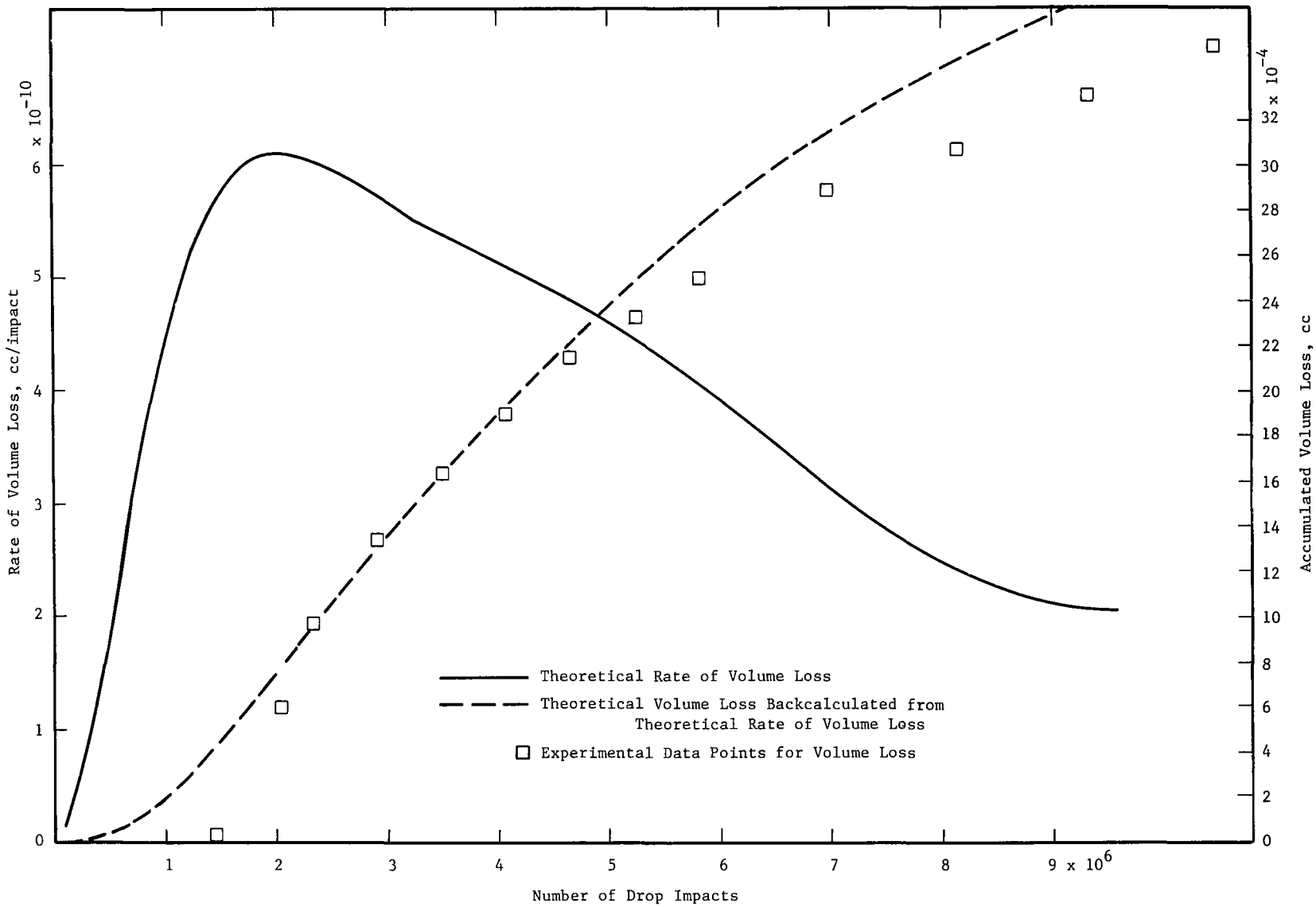

Figure 16. Theoretical Rate-of-Volume-Loss and Accumulated-Volume-Loss Curves for Aged Udimet 700 Calculated with Fragments of Equal Volume.

Udimet 700 aged suggest that this metal is at or beyond the limits of valid use of the cellular model of erosion rate in its present state of development.

G. Features of Rate Curves

As far as drop-impact erosion is concerned, solids may be classified as Class A materials or Class B materials (see Section II.A) depending on whether or not they fail as the result of the radial tensile stresses that are imposed by each drop impact that occurs under an arbitrary set of erosive conditions (relative impact velocity, drop size, and density of drop liquid). The first approach to a cellular model of erosion rate, which has been described in the preceding sections of this report, is directed to Class A solids, that is, to solids that fail under the tensile stresses imposed by each drop impact.

Because of the geometry of fracture (see Section II.B), the erosion of a Class A solid will be characterized by the removal of layers of material. The erosion-rate feature associated with the removal of a layer of material from a solid under drop-impact test is a pulse in which the erosion rate increases to a maximum value and then decays to zero. The calculated rate curves for iron, nickel, and zinc found with use of Equation 7 consist of a series of such pulses; these pulses correspond to the removal of layers of material from the test specimens. The experimental volume-loss data are in agreement with the calculated rate curves because iron, nickel, and zinc are Class A solids with respect to the erosive conditions that were imposed in collecting the experimental volume-loss data.

The statistical model has not yet been developed to include Class B solids which do not fail under the radial tensile stresses imposed by each drop-impact; Class B solids fail only at weak spots after a large number of impacts has been sustained (see Section II.A). It seems reasonable to expect that the calculated erosion-rate curves of Class B solids will not consist of a series of pulses. This expectation is based on the reasoning that Class B solids will only fail after a large number of impacts has been sustained and that the probability distribution for a hit in a σ-cell will spread out as the number of impacts delivered is increased (see Section II.E.1.c). It is inadvisable to say more about the form that the calculated rate curves of Class B solids may have until the statistical model has been developed to include materials of this class.

An attempt to make a partial test of the equations with experimental volume-loss data for Udimet 700 alloy (see F in this Section) has provided evidence which suggests that this alloy is outside the limits of applicability of the statistical model in its present state of development. The very high strength of Udimet 700 alloy in comparison with the strengths of iron, nickel, and zinc strongly suggests that Udimet 700 alloy is a Class B solid with respect to the erosive conditions that were used.

It is important to recognize that whether a solid is in Class A or in Class B depends both on its characteristic strength properties and/or ability to accept energy elastically and on the severity of the erosive conditions that are used in testing it. As in all attempts to separate classes, there will inevitably be an intermediate or transition class. The features of the erosion-rate curve of a given solid will be different depending upon whether it is Class A, Transition Class, or Class B with respect to the severity of the erosive conditions to which it is subjected. The erosion-rate curve found for tantalum (see D in this Section) suggests that tantalum may really be in the Transition Class with respect to the erosive conditions that were used because the pulses in the rate of volume loss do not drop to zero as they do in the case of iron, nickel, and zinc.

H. Correlation Between Quantities N_o and p and Physical Properties of Metals

From the time of the earliest investigations of drop-impact and cavitation erosion it has been found that erosion resistance correlates in general with the tensile strength and hardness of the metal tested. This suggests that correlation should be sought between quantities that appear in Equation 7 and the tensile strength and hardness of the selected metals. The probability of a hit, p, and the first number of the counting rule, N_o, which were found for the selected metals with recourse to the experimental volume-loss data are listed in Table 3 along with the 0.2 percent offset yield strength, the ultimate tensile strength, and the Knoop microhardness number of the particular heat and heat-treatment state of each selected metal.[14]

It can be seen by inspection of the tabulated data that inverse trends exist between the value of the probability, p, and both the 0.2

TABLE 3

A. QUANTITIES THAT APPEAR IN EQ (5) AND PHYSICAL PROPERTIES OF THE SELECTED METALS

Metal	Probability, p	N_o	0.2% Offset Yield Strength	Ultimate Tensile Strength	Knoop Microhardness No.
	- - - -	impacts	dyn/cm^2	dyn/cm^2	- - -
Zinc	0.0300018	300	[a] 4.5×10^8	[a] 1.07×10^9	[a] 32
Nickel	0.00333313	100	[a] 6.3×10^8	[a] 3.54×10^9	[a] 57
Iron	0.00043135	32	[a] 14.8×10^8	[a] 2.76×10^9	[a] 72
Tantalum	0.000208321	25	[a] 15.7×10^8	[a] 2.40×10^9	[a] 104
U-700 Ag.	0.0000011236	2.2	[a] 89.7×10^8	[a] 13.8×10^9	[a] 375

B. OTHER EROSION-RATE QUANTITIES AND STEEL-SPHERE DENTING VELOCITY

Metal	Maximum Rate Volume Loss	Impacts to Reach Maximum Rate Vol. Loss	Eroded Fragment Volume	[b] Average Grain Size	Steel Sphere Denting Velocity
	$cm^3/impact$	impacts	cm^3	micron	cm/sec
Zinc	38.8×10^{-8}	10,000	366×10^{-8}	300	[a] 15.8
Nickel	9.6×10^{-8}	30,000	17.6×10^{-8}	53	[a] 11.2
Iron	1.8×10^{-8}	91,000	0.58×10^{-8}	63	[a] 35.3
Tantalum	0.86×10^{-8}	120,000	0.20×10^{-8}	126	[a] 38.6
U-700 Ag.	0.061×10^{-8}	2,100,000	0.035×10^{-8}	160	[a] 64.2

[a] Values measured for the specific heat and heat-treatment state of the selected metals. See Reference 14.

[b] Values found for average grain size with use of the Heyn intercept method.

percent offset yield strength and Knoop microhardness number; a corresponding trend does not exist through the values of ultimate tensile strength. A plot of negative log p against 0.2 percent offset yield strength is given in Figure 17. In drawing the line shown in this figure, correlation was sought principally for iron, nickel, and zinc, which are Class A metals with respect to the erosive conditions that were used. From Figure 17 it can be seen that tantalum, which may be a Transition-Class metal with respect to the erosive conditions used, also fits on the line. Udimet 700 alloy, which is a Class B metal with respect to the erosive conditions used, does not fit on the line.

An inverse trend exists between the first number of the counting rule, N_o, and both the 0.2 percent offset yield strength and Knoop microhardness number. Plots of log N_o against 0.2 percent offset yield strength and Knoop microhardness number are shown in Figures 18 and 19, respectively. Correlation was sought principally for iron, nickel, and zinc; the difference between tantalum and the purely Class A metals iron, nickel, and zinc shows up in Figure 19. Udimet 700 alloy, which is a Class B metal with respect to the erosive conditions used, shows no correlation with the other metals in either plot.

From Table 3B it can be seen that an inverse trend exists between both the maximum rate of volume loss and the eroded fragment volume and the yield strength of the metals. On the other hand, the number of impacts required to reach the maximum rate of volume loss varies directly with the yield strength of the metals.

I. Experimental Confirmation of the Number of Fragments in an Eroded Layer

An effort was made to obtain experimental confirmation of the intuitive argument that an eroded layer of material contains $\eta\eta'$ fragments by calculating the volume of material lost when the test specimen was punctured by erosion or was near the point of puncture. The numbers of impacts for which this volume loss was calculated for each metal are given in column two of Table 4. The computer print-out of layers removed, which is designated as Z, is given for each of the metals in column three. Values of the product $\eta\eta'$ for the metals are given in column four and the numbers of fragments removed, taken to be the

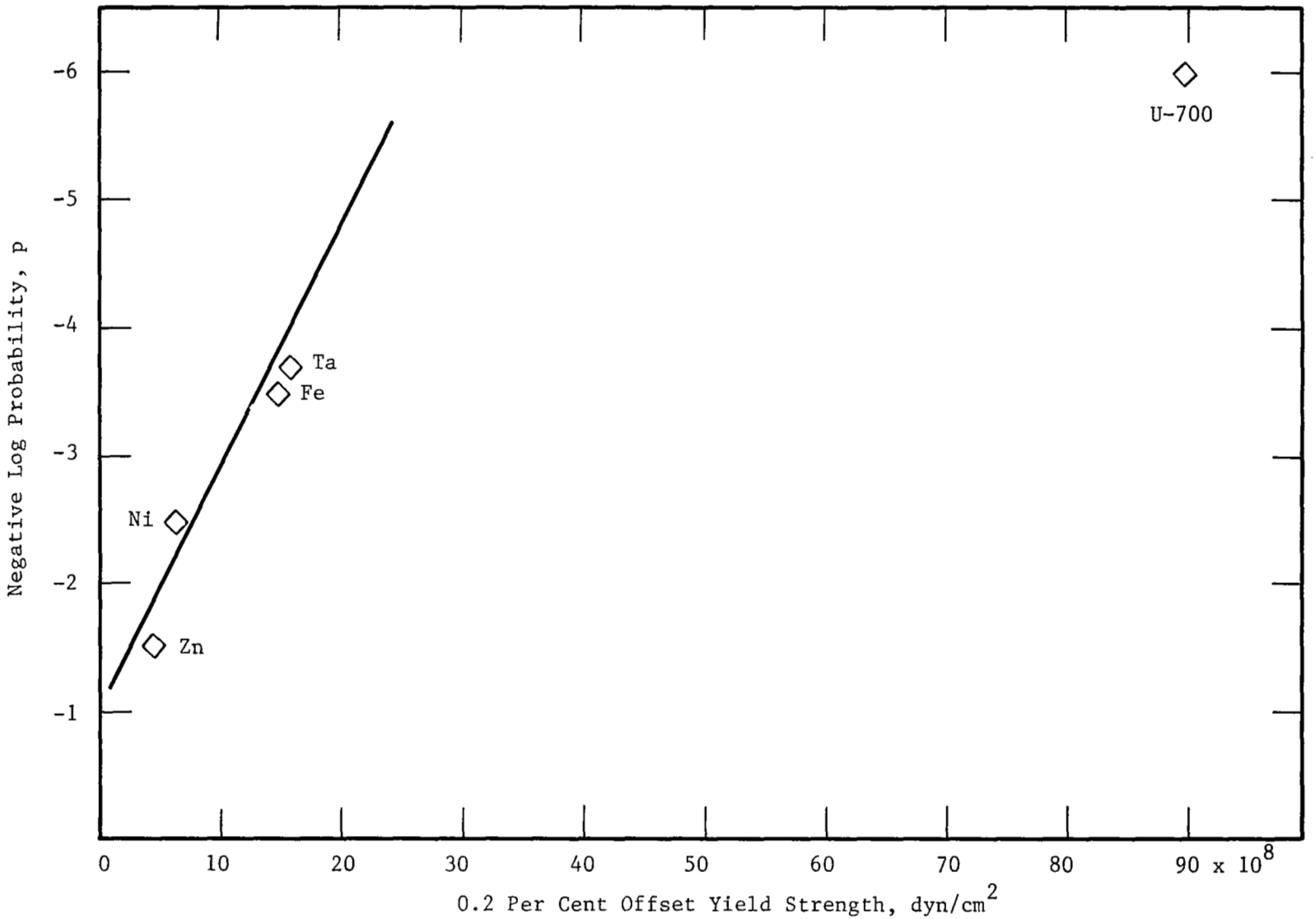

Figure 17. Correlation Between the Probability of a Hit, p, and the 0.2 Per Cent Offset Yield Strength.

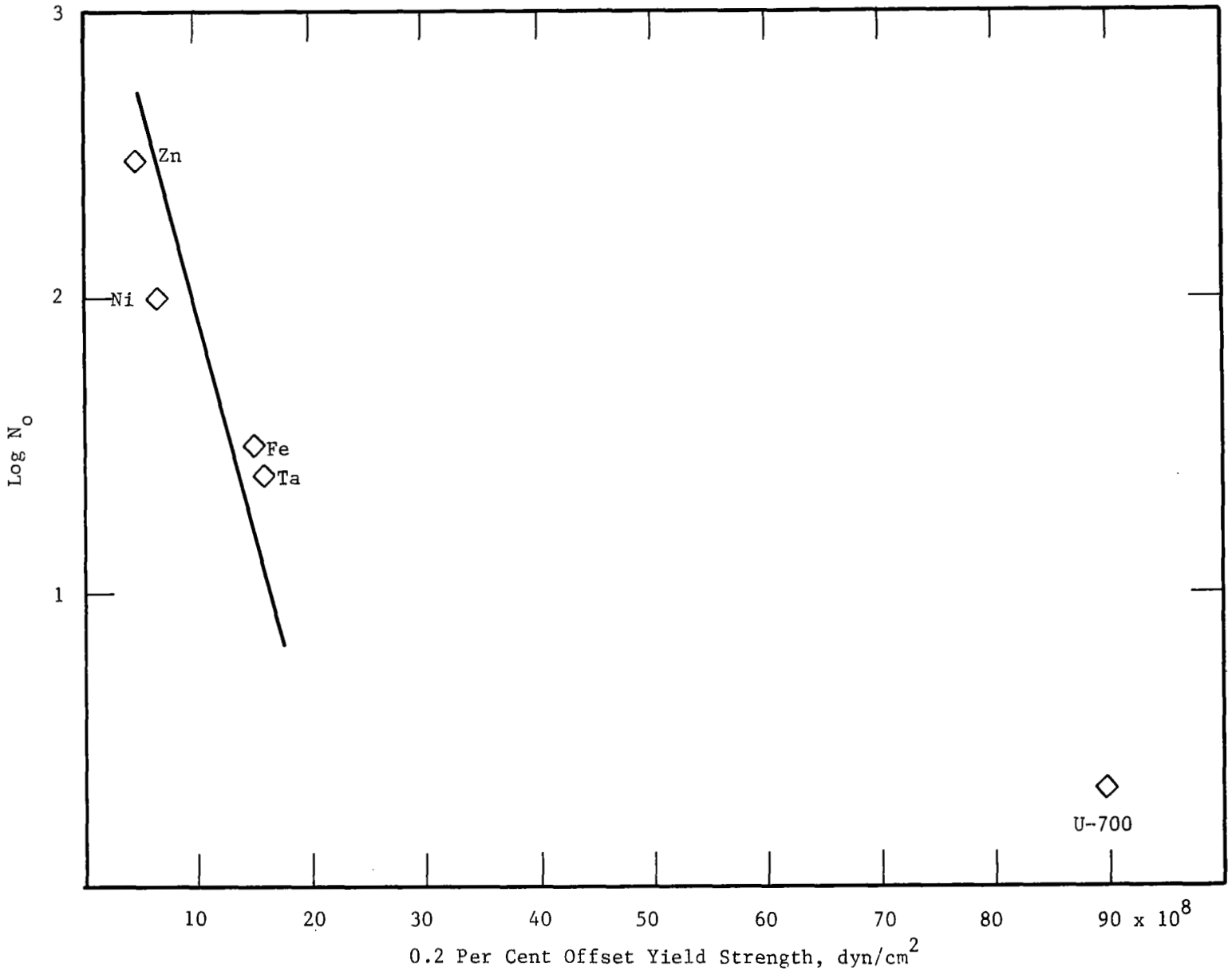

Figure 18. Correlation Between the First Number of the Counting Rule, N_o, and the 0.2 Per Cent Offset Yield Strength.

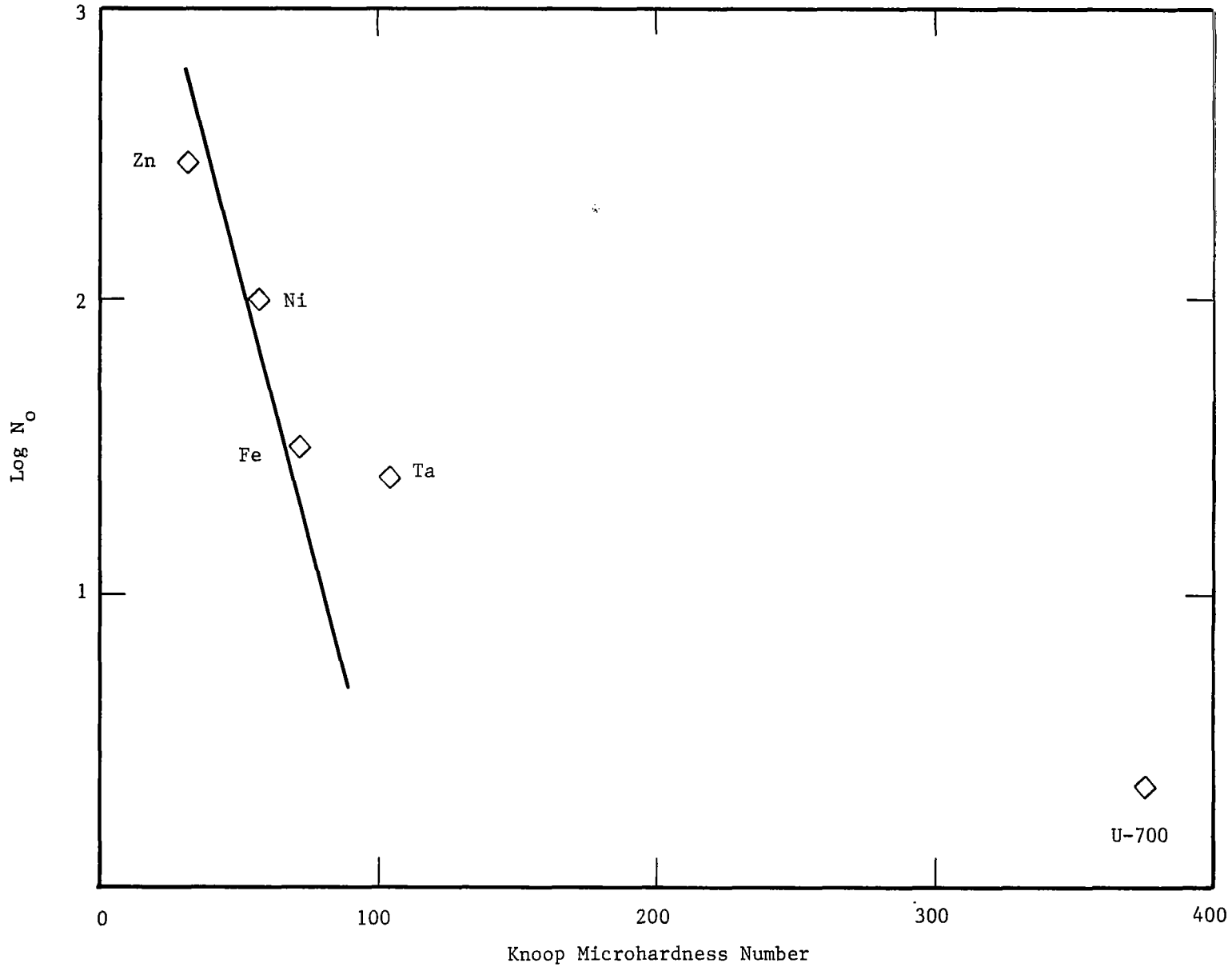

Figure 19. Correlation Between the First Number of the Counting Rule, N_o, and the Knoop Microhardness Number.

TABLE 4

CALCULATED VOLUME OF METAL REMOVED FROM A TEST SPECIMEN BY LIQUID DROP IMPINGEMENT

Metal	Impacts, n	Layers Removed, Z	$\eta\eta'$	Fragments Removed, $\eta\eta' Z$	Volume per Fragment, cc	Volume of Metal Removed, cc	Impacts Actually Sustained by the Test Specimen
Tantalum	15×10^5	4.76766	261209.	1245355.	1.96997×10^{-9}	0.002453	15.5×10^5 Hole Formed
Nickel	4.4×10^5	3.19425	4081.41	13037.1	1.75596×10^{-7}	0.002289	4.36×10^5
Iron	10×10^5	3.28918	124532	409609.	5.79255×10^{-9}	0.002373	9.69×10^5
Zinc	0.4×10^5	3.50484	151.137	529.711	3.65924×10^{-6}	0.001938	0.415×10^5 Hole Formed

product $\eta\eta' Z$, are given in column five. The initial volume of an eroded fragment for each of the metals as found by trial (see Section B through F) is given in column six and the volume of metal removed, taken to be the product of the number of fragments removed multiplied by the volume of a fragment, is given in column seven. The actual number of impacts sustained by a test specimen of each of the metals is given in column eight; for two of the metals (tantalum and zinc) erosion progressed through the thickness of the specimen.

The thickness of the test specimens, as determined by a measurement on one specimen only, was 0.33 cm. The area over which impingement occurred was calculated to be 0.02356 cm^2 on the basis of the observation that the impinging drops struck over an area the radius of which was roughly equal to the drop diameter. The volume of the cylinder of metal that would have been lost had this area been moved through the thickness of the test specimen is 0.00778 cm^3. It can be seen that the calculated volume of metal removed given in column seven of Table 4 is equal to about 30 percent of the quantity 0.00778 cm^3, which is the total possible volume of metal that could have been removed.

On one hand, the total possible volume of metal that could be removed, assessed as 0.00778 cm^3 on the basis of removing a cylinder of metal with a base area equal to the impingement area and a height equal to the thickness of the test specimen, is too high because erosion craters have rounded bottoms (see Figure 20). On the other hand, the calculated volume of metal removed is too low because the volume of eroded fragments increases as tests progress. It is considered that the extent of agreement found is sufficiently good to confirm the use of product $\eta\eta'$ as a multiplying factor to obtain fragments removed from layers removed.

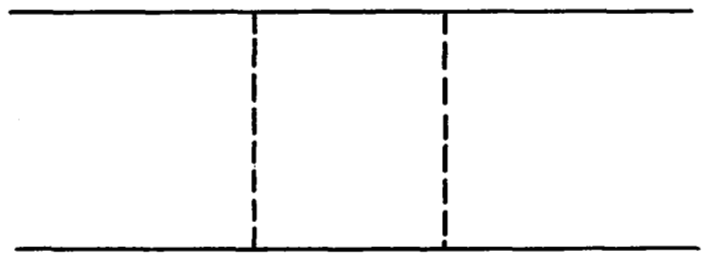

A

Hole through a plate formed by removal of a cylinder of the plate metal

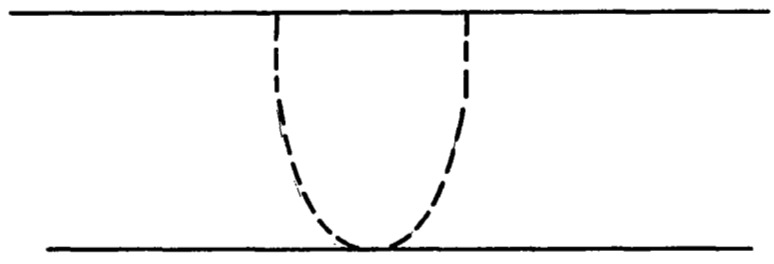

B

Hole through a plate formed by the growth of an erosion crater

Figure 20. Evidence to Show that the Volume of Metal Removed by the Growth of an Erosion Crater is Less Than That Removed by Moving the Area of the Mouth of the Crater Through the Thickness of the Test Specimen.

IV. ACCUMULATED VOLUME LOSS FOUND WITH FRAGMENTS OF CHANGING SIZE

The concept of layers of fragments of constant volume given as integral multiples of $\eta\eta'$ in Equation 7, can be expanded to associate the first layer of eroded fragments with a volume v_1, two layers of eroded fragments with a volume $v_1 + v_2$, and three layers of eroded fragments with a volume $v_1 + v_2 + v_3$. In view of these changes, Equation 7 becomes

$$L(x,n) = v_1 \sum_{x=N_o}^{N_o+N_1-1} P(x,n) + (v_1+v_2) \sum_{x=N_o+N_1}^{N_o+N_1+N_2-1} P(x,n) + (v_1+v_2+v_3) \sum_{x=N_o+N_1+N_2}^{N_o+N_1+N_2+N_3-1} P(x,n) + \ldots \quad (18)$$

where $L(x,n)$ is now the accumulated volume loss found directly for a given number of impacts, n. For the case that $v_1 = v_2 = v_3$, Equation 18 is as well founded as Equation 7. It has the advantage that accumulated volume loss is printed out directly by the computer program; it has the disadvantage that erosion rate is not obtained as an intermediate step in the calculation of accumulated volume loss.

For the case that $v_1 \neq v_2 \neq v_3$, Equation 18 is not as well founded as Equation 7. If the equality between cell size and fragment size is maintained and both the cell size and fragment size are allowed to increase (or decrease) during a calculation, a statistical problem is encountered; a corresponding change in the probability of a hit must be made. On the other hand, if the cell size and, consequently, the probability of a hit are maintained constant throughout a calculation but the volume of a fragment or of a layer of fragments is allowed to change, then a physical problem is encountered; the radius of the circle of

fracture is fixed because it is determined by the drop size and it is not clear how a change in average fragment size can be accounted for (see Figure 4) if the fragment dimensions are increased (or decreased) equally. If, however, it is assumed that the fragments increase (or decrease) in volume because the depth at which the cracks intersect to release a fragment becomes greater (or less), no problem is encountered. With recourse to this argument, the statistical model and the computer program in the state of development in which they now exist can be used to make calculations in which the volume of a fragment changes.

Equation 18 was used to calculate accumulated-volume-loss curves of the selected metals for the case that the volume of a layer of fragments changes. For each metal, the same probability, p, of a hit against the typical cell and the same counting rule, N_i, were used as were used in obtaining the calculated curves of Section III. The value of v_1 was assessed directly from plots of experimental volume loss of the metals plotted against number of impacts sustained. It was taken to be the volume loss reached at the first knee in these plots. Values of the succeeding v_i were also assessed approximately from inspection of the experimental volume-loss plots; they were expressed in terms of v_1 for each of the metals. The direct printout of the accumulated volume loss for each of the five selected metals was plotted against the numbers of impacts sustained. The plots obtained are shown in Figures 21, 22, 23, 24 and 25. Comparison of Figures 21-25 with Figures 11-14 and 16 shows that in almost every case the correction for increasing fragment size is all that is needed to establish good agreement between the theoretical curves and the experimental data.

The volume of the first layer, v_1, and the nature of the percentage layer-volume change for the selected metals is given in Table 5. It can be seen that in the case of aged Udimet 700, and eventually in the case of tantalum, the change in layer volume is a <u>decrease</u>. Because Udimet 700 is a Class B metal and because tantalum may be Transition-Class metal with respect to the erosive conditions that were used, this observation suggests that Class B metals may be characterized by a decrease in eroded fragment size. The 0.2 percent offset yield strength and the ultimate tensile strength of each metal is also given in Table 5. There appears to be no correlation between the 0.2 percent offset yield strength and

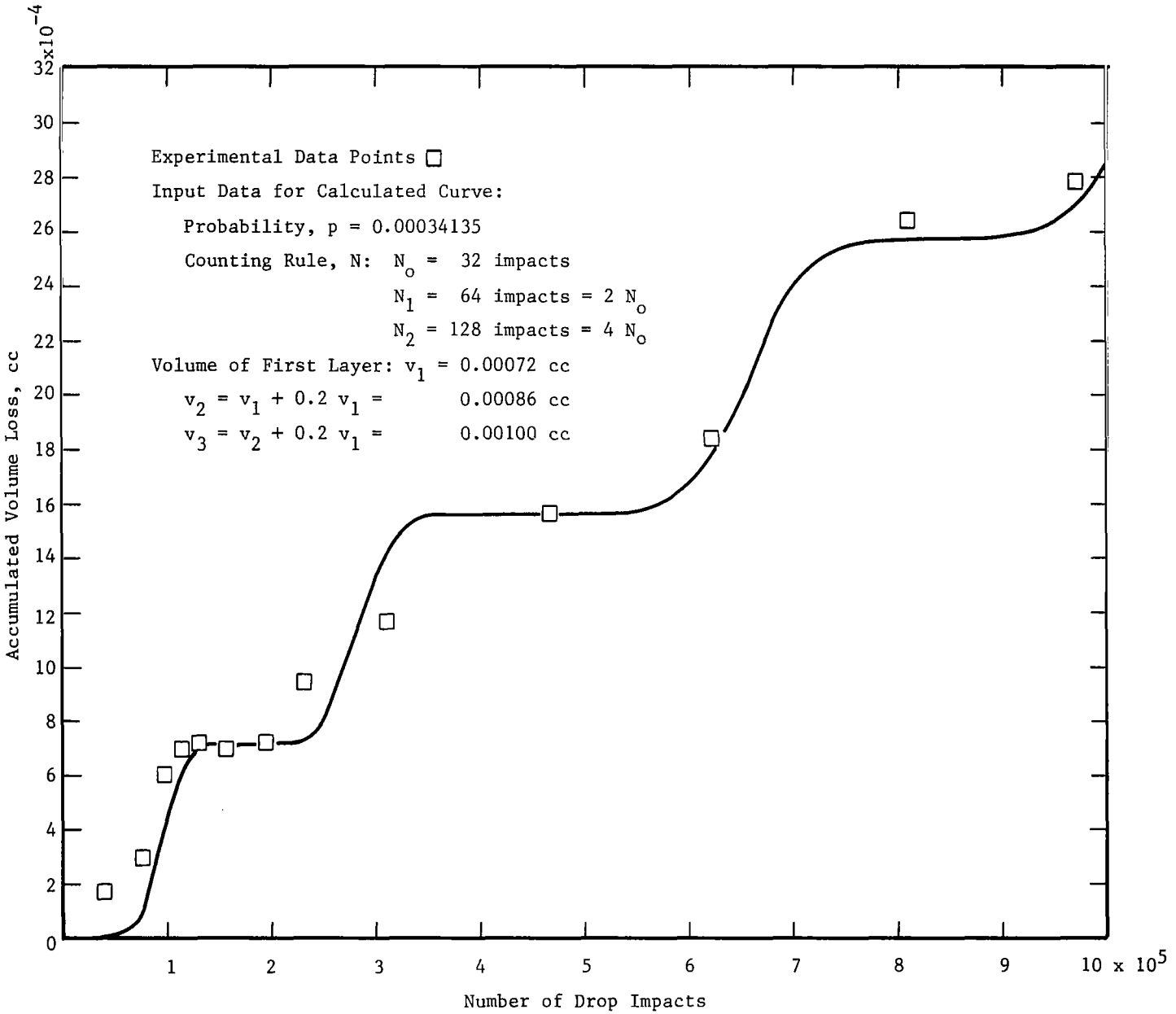

Figure 21. Calculated Accumulated-Volume-Loss Curve for Iron with Fragments of Increasing Volume.

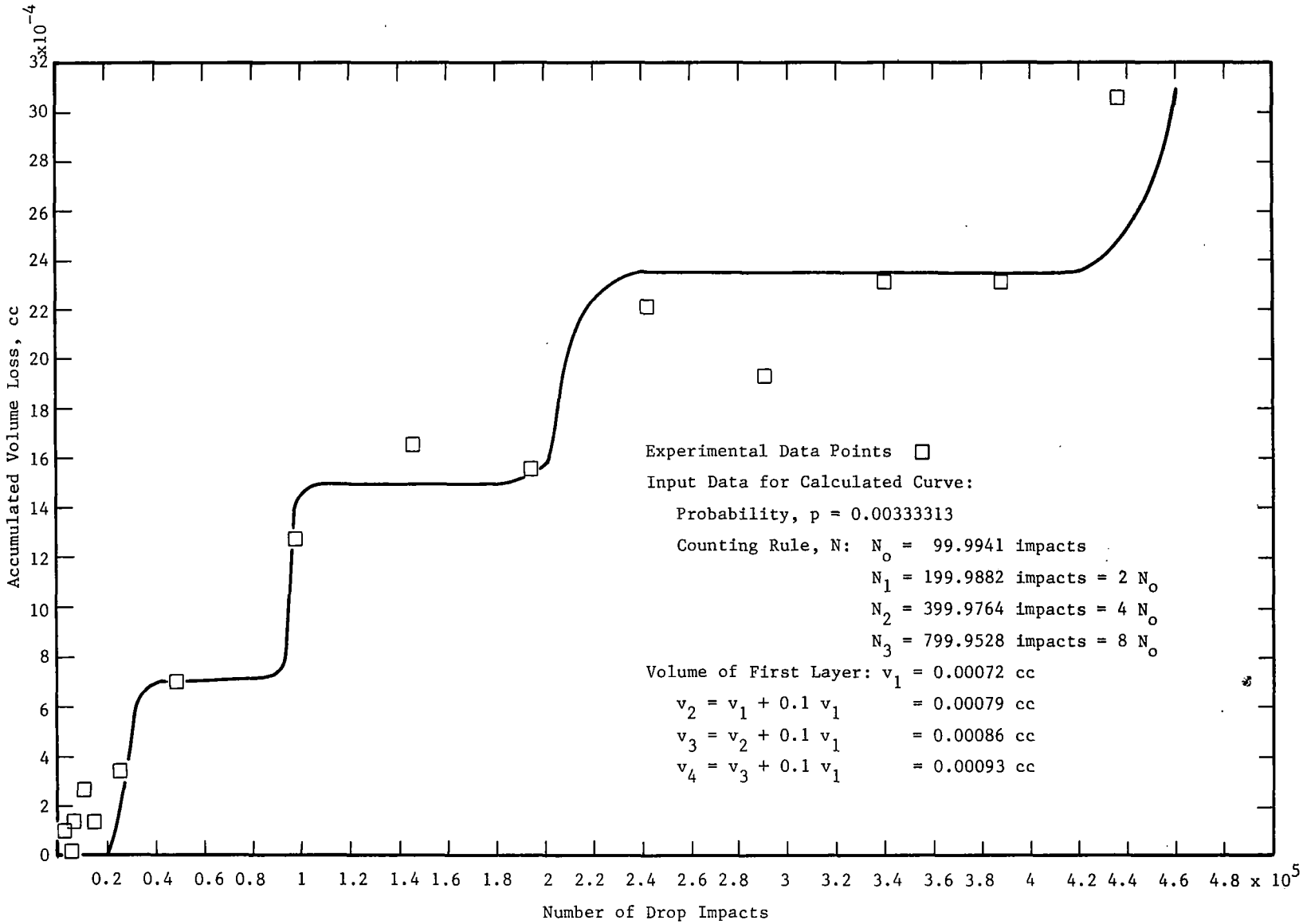

Figure 22. Calculated Accumulated-Volume-Loss Curve for Nickel with Fragments of Increasing Volume.

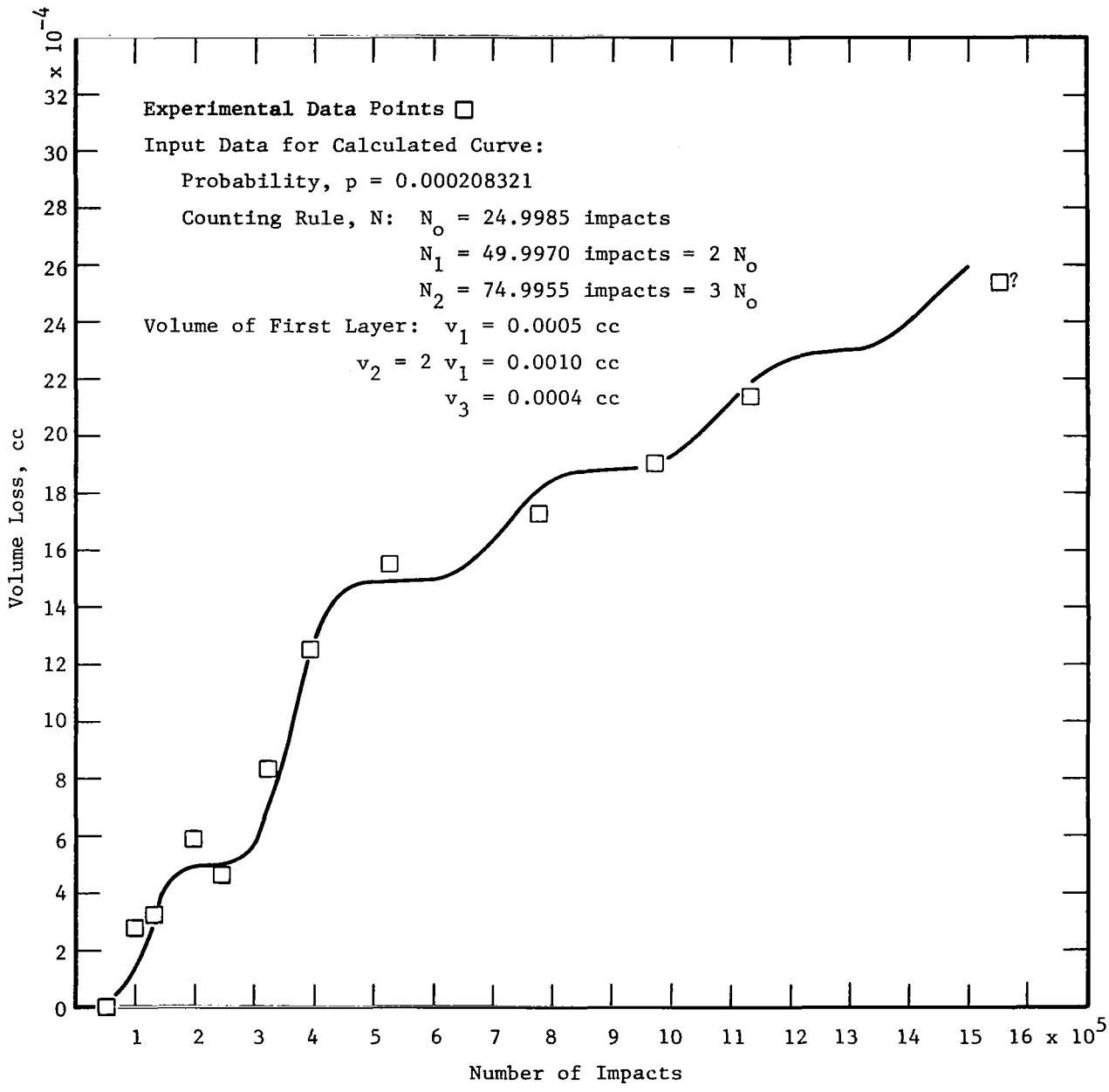

Figure 23. Calculated Accumulated-Volume-Loss Curve for Tantalum with Fragments of Increasing Volume.

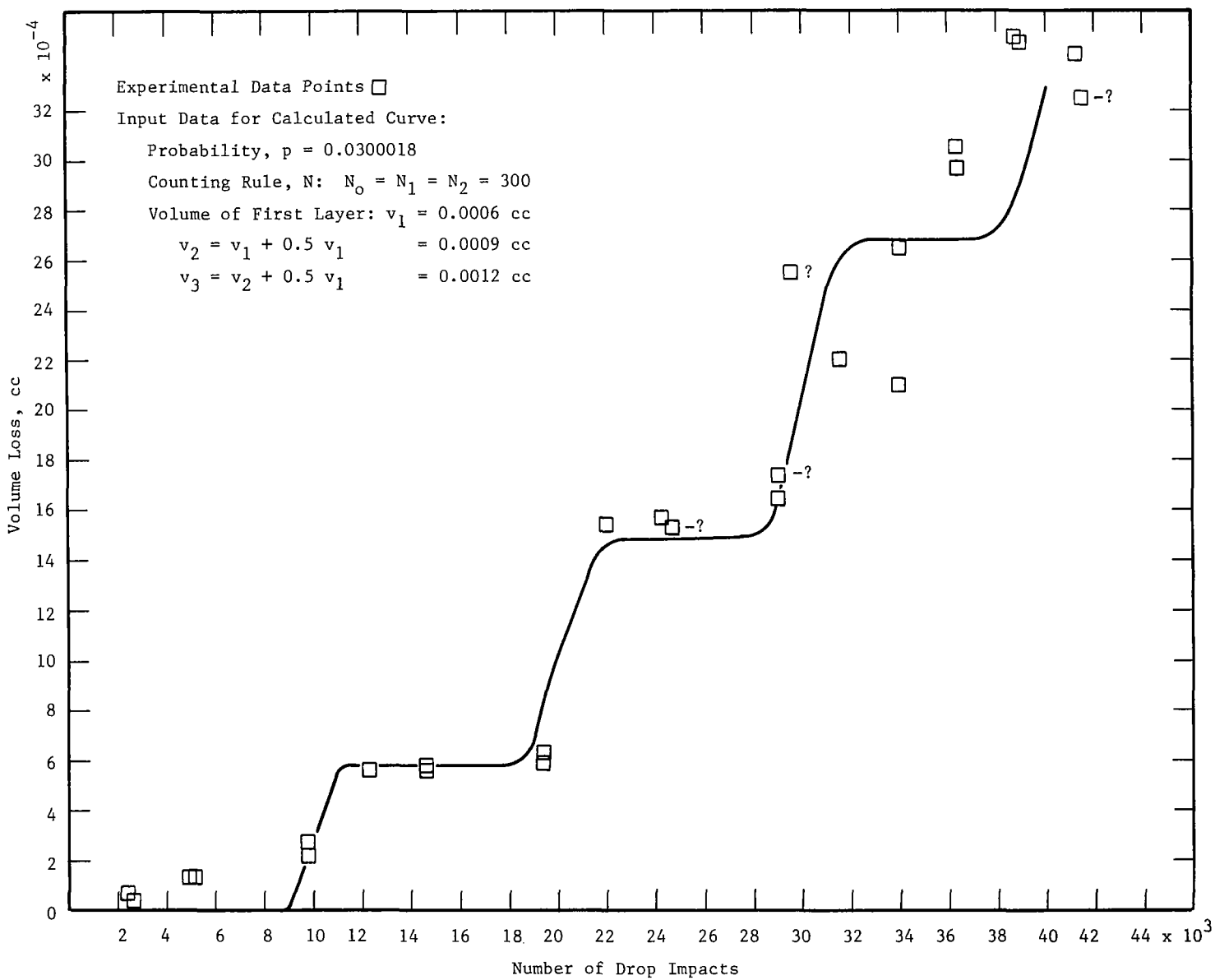

Figure 24. Calculated Accumulated-Volume-Loss Curve for Zinc with Fragments of Increasing Volume.

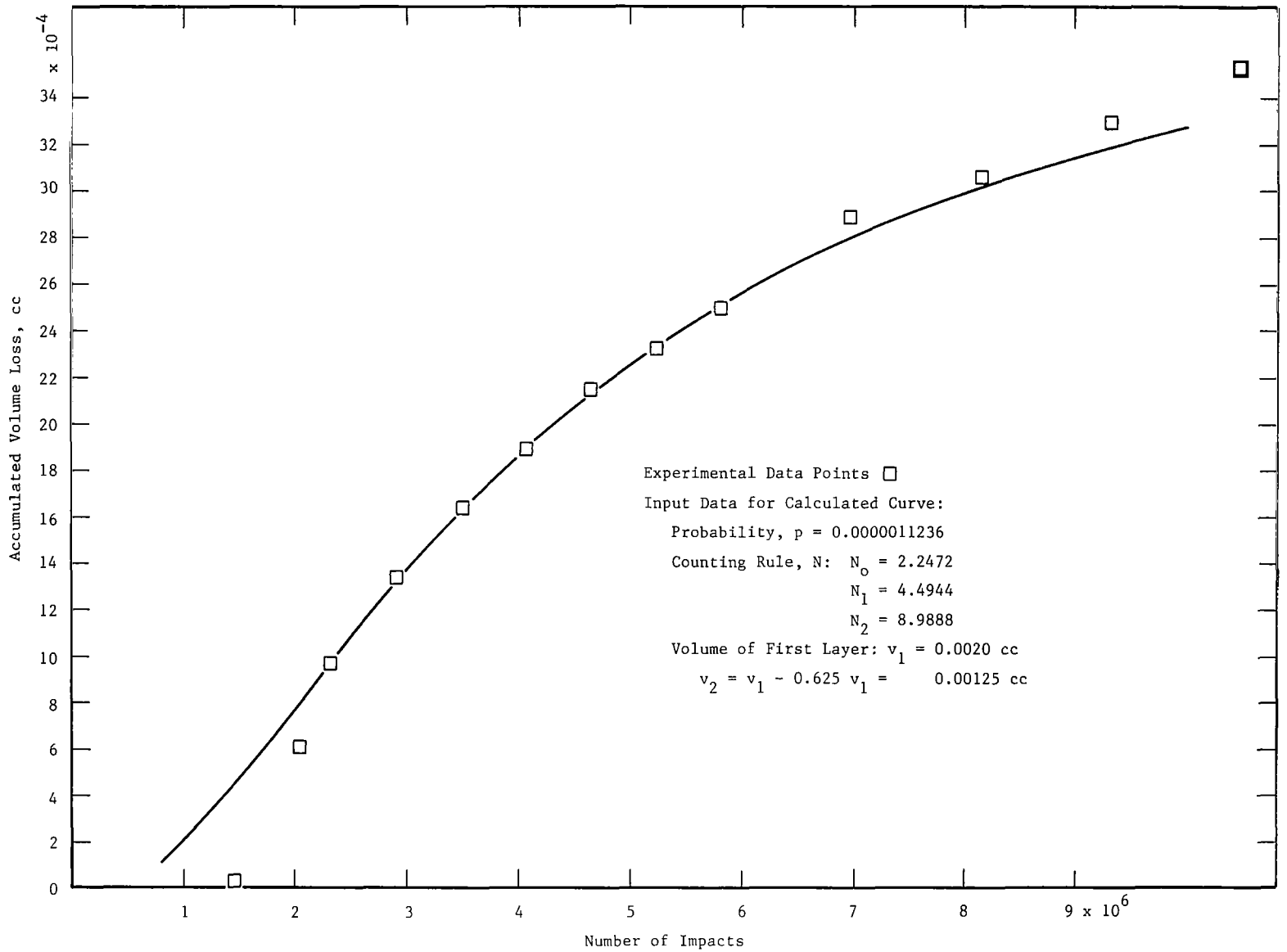

Figure 25. Calculated Accumulated-Volume-Loss Curve for Aged Udimet 700 with Fragments of Increasing Volume.

TABLE 5

LAYER VOLUME AND PERCENTAGE CHANGE IN LAYER VOLUME

Metal	Layer Volume, v_1	Percentage Change in Layer Volume	0.2% Offset Yield Strength	Ultimate Tensile Strength
	cm^3		psi	psi
Udimet 700	0.0020	62.5% Decrease	130,000	201,000
Nickel	0.00072	10% Increase	9,000	51,000
Iron	0.00072	20% Increase	21,000	43,000
Tantalum	0.0005	100% Increase then 20% Decrease	23,000	35,000
Zinc	0.0006	50% Increase	7,000	15,000

the layer volume, v_1, or the percentage change in layer volume. However, the ultimate tensile strength appears to correlate directly with the layer volume, v_1, and inversely with the percentage change in layer volume (see Figures 26 and 27).

In Figures 26 and 27 the volume of the first layer, v_1, and the percentage change in layer volume in terms of v_1 are plotted, respectively, against the ultimate tensile strength. Correlation was sought principally for iron, nickel, and zinc, which are Class A metals with respect to the erosive conditions that were used. The slight divergence of tantalum and the wide divergence of Udimet 700 alloy are evident in these plots. These divergences reflect the fact that Udimet 700 is a Class B metal and that tantalum may be a Transition-Class metal with respect to the erosive conditions that were used.

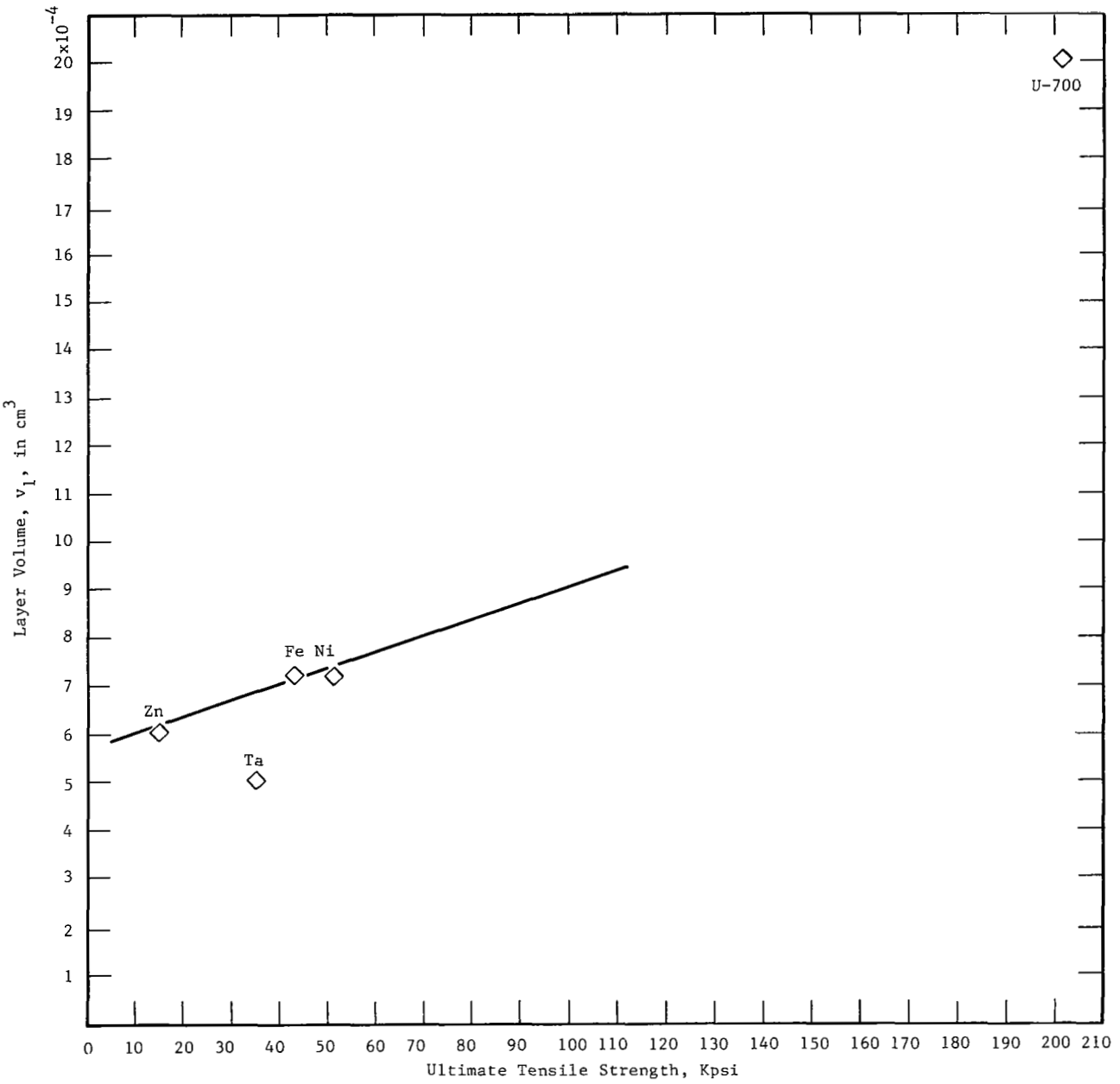

Figure 26. Plot of Layer Volume Against Ultimate Tensile Strength.

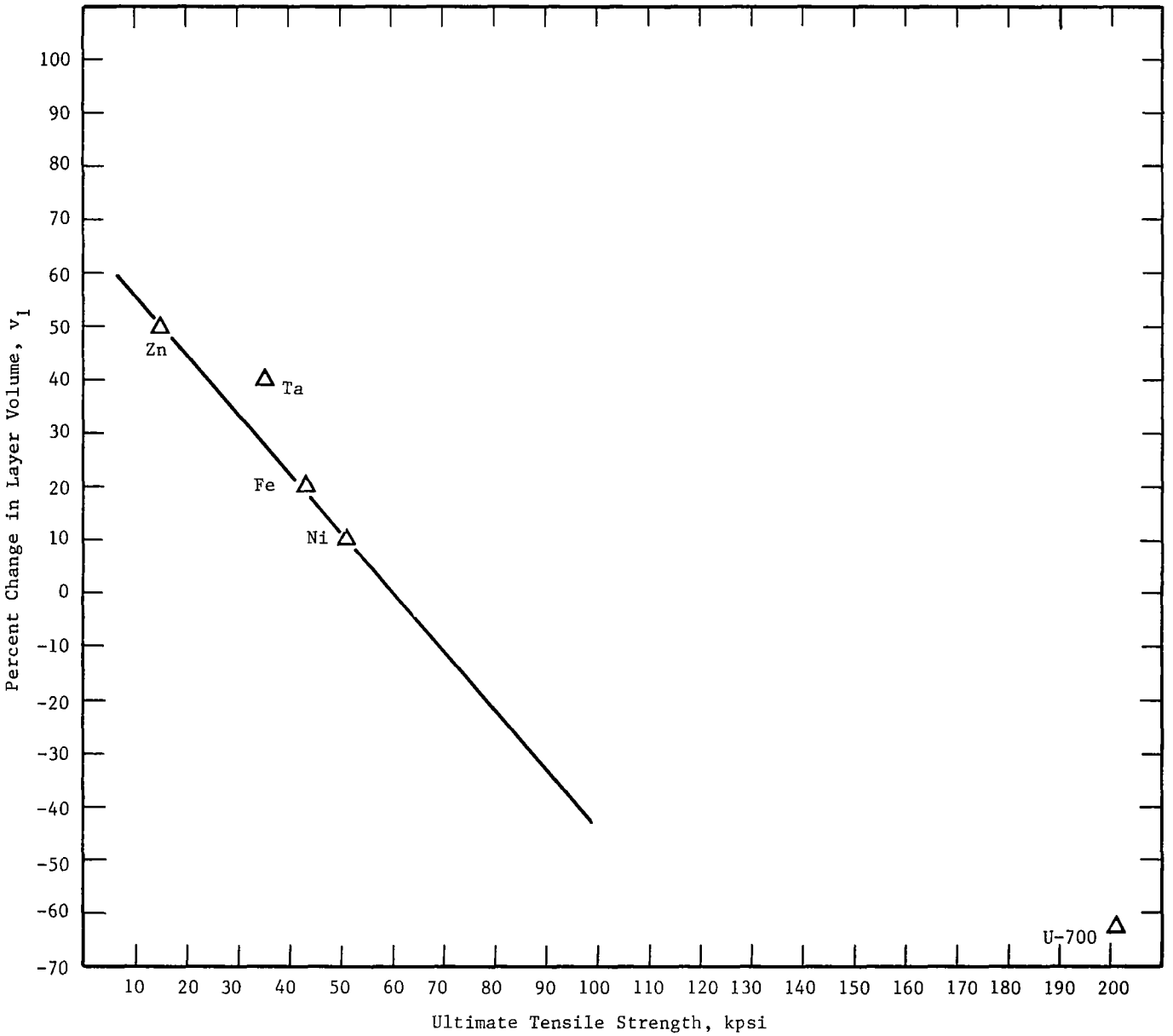

Figure 27. Plot of Change in Layer Volume Against Ultimate Tensile Strength.

V. EFFECT OF A CHANGE IN SIZE OF THE IMPINGEMENT AREA, A

To what extent a change in size of impingement area, A, may affect the locus of the accumulated-volume-loss curve is an important consideration. In collecting drop-impact volume-loss data, area A was assessed visually by watching drops impinge and comparing the diameter of the area over which impingement occurred with the diameter of a drop. The value of area A assessed in this way is not known with a high degree of reliability. It is, therefore, important to know to what extent agreement between the theoretical accumulated-volume-loss curve and the experimental data may be affected by a change in the value of area A. An additional reason for determining the importance of a change in the value of area A on the theoretical accumulated-volume-loss curve is that in collection of cavitation erosion data with use of a magnetostrictive device the eroded area tends to increase in size during a test run.

The accumulated-volume-loss curve for iron was calculated with an approximately 50 percent increase and 50 percent decrease in the size of area A. The calculation was carried out with use of Equation 18 of Section IV. The calculated curves are plotted along with the experimental accumulated-volume-loss data for iron in Figure 28. The curve for an impingement area A equal to 0.0235606 in Figure 28 is the same curve as that given for iron in Figure 21.

Two conclusions can be drawn on the basis of the curves shown in Figure 28. The first conclusion is that changing the size of the impingement area by a factor of three is not important as far as the fit of calculated curves with experimental data points is concerned for metals with an erosion resistance comparable to that of iron. There is reason to suppose that this effect may be more important for metals that are highly erosion resistant. The second conclusion is that the step-structure of the calculated accumulated-volume-loss curve is sharper and better delineated for large than for small values of the probability, p, and of the counting rule, N_1. (See data inset in Figure 28). On the basis of the relation given by Equation 6, an increase in size of area A should have the effect of smoothing out the step structure of a calculated curve.

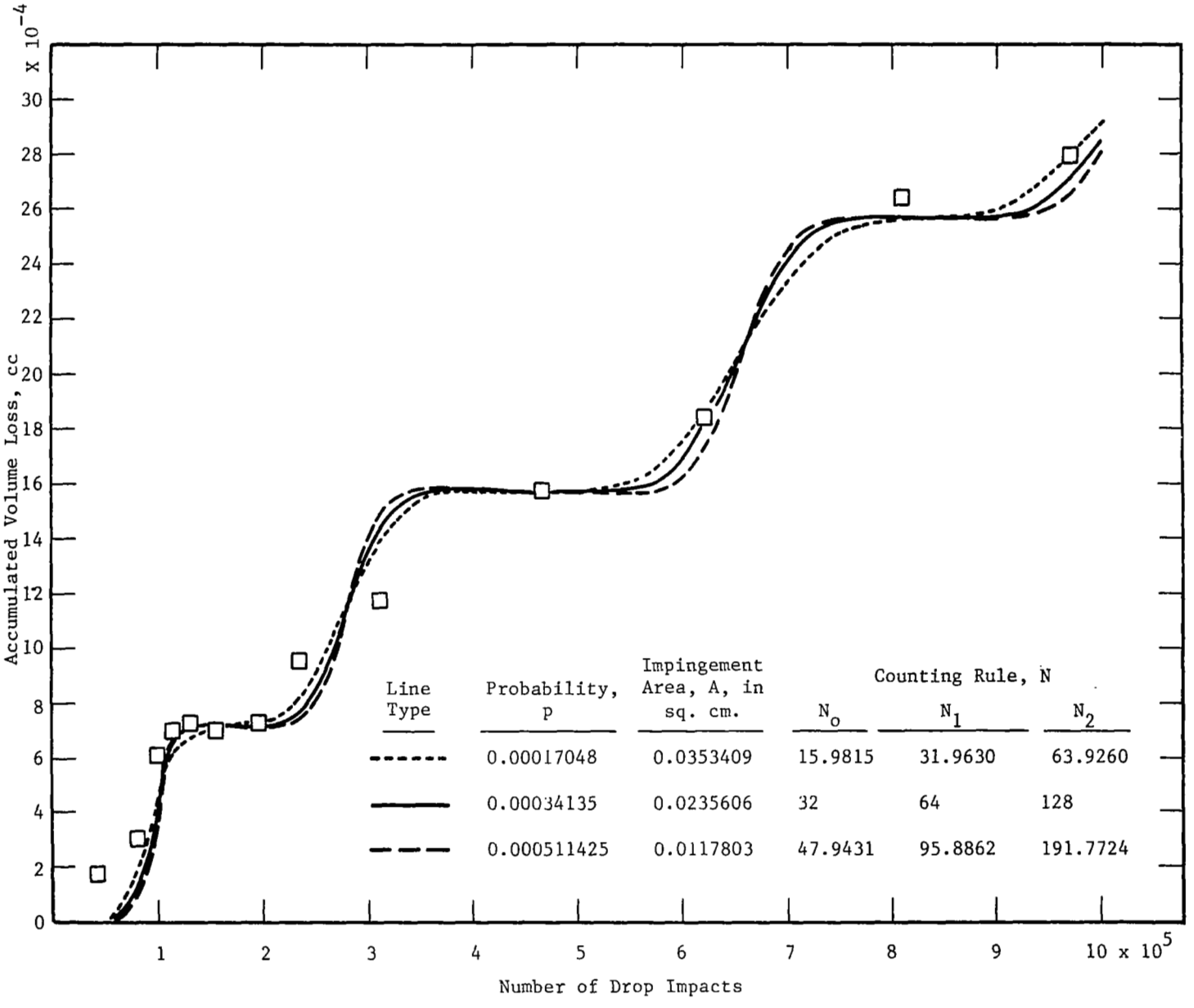

Figure 28. Effect of an Increase in the Area Over Which Impingement Is Occurring.

VI. CONCLUDING NOTE

The work on a statistical model of erosion rate described in this report is by no means finished. Two quantities, namely, n_o, the number of impacts that must occur against area A before the first sharp rise in volume loss occurs, and v, the volume of an eroded fragment, can at present only be assessed by recourse to experimental data for volume loss with elapsed time or number of impacts sustained. Although the relation between impact energy and velocity and the volume of an eroded fragment has been established for two shapes of fragments, no work has as yet been done to determine the dependence of the volume of an eroded fragment on the strength of the solid material against which impingement occurs.

In addition to completing the statistical model for Class A brittle materials which fail under each drop impact, the model needs to be developed further to include the Class B brittle materials whose ability to accept energy is large in comparison with the impact energy delivered by each drop blow. Finally, the model should also be extended to include materials that are permanently ductile or plastic and even rubbery materials such as neoprene. What has been presented in this report is really only a beginning.

VII. REFERENCES

1. Naude, C. F. and Ellis, A. T., Trans. A.S.M.E. 83, 648, 1961.

2. Thiruvengadam, A. Preiser, H. S., Journal of Ship Research 8, 39, 1964.

3. Hammitt, F. G.; Robinson, M. J.; Seibert, C. A.; and Aydinmakine, F. A.; University of Michigan Report 03424-14-T (NASA Grant No. NsG-39-60), 1964.

4. Heymann, F. J., Symposium on Erosion and Cavitation, A.S.T.M. Special Technical Publication No. 408, 1967.

5. Mok, C. H., Mechanics Section TM #068-11, General Electric Company Space Sciences Laboratory, Philadelphia, Pennsylvania, 1968.

6. Hammitt, F. G.; Huang, Y. C.; Kling, C. L.; Mitchel, T. M.; and Solomon, L. P.; University of Michigan College of Engineering Report No. 02643-2-PR, 1969.

7. Hoff, G.; Langbein, G.; and Rieger, H.; Symposium on Erosion and Cavitation, A.S.T.M. Special Technical Publication No. 408, 1967.

8. Engel, O. G., Discussion of a Paper given by F. J. Heymann, A.S.T.M. Special Technical Publication No. 408, 1967.

9. Gould, G. C., Proceedings of the A.S.T.M. Symposium on Characterization and Determination of Erosion Resistance, Atlantic City, N.J., 1969.

10. Schwarz, M. v. and Mantel, W., Zeit. des Vereines Deutscher Ingenieure 80, 863, 1936.

11. Baker, D. W. C.; Jolliffe, K. H.; and Pearson, D.; Phil. Trans. Roy. Soc. 260A, 193, 1966.

12. Engel, O. G., National Bureau of Standards Jour. of Research 64A, 499, 1960.

13. Engel, O. G., Wright Air Development Center, TR 53-192 Part III, 1953.

14. Engel, O. G., General Electric Company, Report GESP-253 (Contract NASW 1481), 1969.

15. Engel, O. G., Wright Air Development Center, TR 53-192 Part VII, 1957.

16. See, for example, Engel, O. G., National Bureau of Standards Jour. of Research, 54, 51 (1955) and Brunton, J. H., A.S.T.M. Special Technical Publication No. 307, 1961.

17. Auleytner, J., X-Ray Methods in the Study of Defects in Single Crystals, Pergamon Press, New York, 1967.

REFERENCES (Cont'd)

18. Barrett, C. S., Structure of Metals, McGraw-Hill Book Co., Inc., New York, 1943.

19. Friedel, J., Dislocations, Addison-Wesley Publishing Co., Inc. Reading, Massachusetts, 1964.

20. Bragg, W. L., Proc. Phys. Soc. 52, 54, 1940.

21. Burgers, J. M., Proc. Phys. Soc. 52, 23, 1940.

22. Brandenberger, E. and DeHaller, P., Schweiz. Arch. 10, 331 and 379, 1944.

23. Hoff, G. and Langbein, G., Proc. Second Meersburg Conference on Rain Erosion and Allied Phenomena, Vol. 2, Ministry of Technology, Royal Aircraft Establishment, Farnborough, Hants, England, 1967.

24. DeHaller, P., Schweizerische Bauzeitung 101, 243 and 260, 1933.

25. See, for example, Kern, W. F. and Bland, J. R., Solid Mensuration, 2nd Ed., John Wiley and Sons, Inc., New York, 1938. See page 51.

26. Griffith, A. A., Phil. Trans. Roy. Soc. 221A, 163, 1920-21.

27. Adamson, A. W., Physical Chemistry of Surfaces, Interscience Publishers, Inc., New York, 1960.

28. Ripken, J. F., A.S.T.M. Special Technical Publication No. 408, 1967.

VIII. LIST OF PRINCIPAL SYMBOLS

A = area over which impingement is occurring

σ = area of a single cell in the array of cells covering area A

r = radius of the drops that impinge

η = A/σ = number of cells in area A

η' = number of cells that develop cracks when a single drop impact occurs

d = diameter of a cell and also distance across an eroded fragment

N_i = numbers of the counting rule

N_o = first number of the counting rule or number of impacts required to remove a layer of fragments from the original surface

V = impact velocity

M = drop mass

θ = angle of attack measured from the surface of the test specimen

R = rate of volume loss

J = average rate of ejection of fragments from area A

v = average volume of an eroded fragment

n = some arbitrary number of impacts against area A

p = σ/A = probability of a hit against any one of the cells in area A

$P(x,n)$ = probability of x impacts on cell area, σ, when n impacts have occurred on area A

$F(x,n)$ = number of fragments ejected from area A after n impacts have occurred on area A

Q = incremental volume loss

L = accumulated volume loss

n_o = ηN_o = number of impacts that must occur against area A before the first sharp rise in volume loss occurs

v_c = minimal volume of an eroded fragment

v_p = volume of a prismatic eroded fragment

v_t = volume of a tetrahedral eroded fragment

LIST OF PRINCIPAL SYMBOLS (Cont'd)

E = the part of the impact energy invested in crack formation

E_c = amount of energy needed to form a crack of smallest size or the minimal value of E

V_c = impact velocity for which the energy invested in crack formation is E_c

A_c = area of an eroded platelet of smallest possible size

t_σ = thickness of an eroded platelet

T = surface tension

Y = Young's modulus of elasticity

ν = Poisson's ratio

c = half length of a Griffith crack

S_y = 0.2 percent offset yield strength

S = strength of a solid

APPENDIX A

POSSIBILITY OF IMPACT IONIZATION OF WATER

The heat of neutralization of water at infinite dilution is 13.4 Kcals/mole, that is,

$$H^+(liq) + OH^-(liq) \rightleftharpoons H_2O(liq) \qquad \Delta H = 13.4 \text{ Kcals/mole.}$$

The volume of a 0.2-cm drop is (4/3)(3.1416)(0.001) or 4.2×10^{-3} cm^3. For water, this drop volume is equivalent to 4.2×10^{-3} grams. Because one mole of water is 18 grams, the heat of neutralization per drop is found to be $(4.2 \times 10^{-3}/18)[13.4]$ or 3.1×10^{-3} Kcals.

If the relative collision velocity is 880 ft/sec (26,822 cm/sec), the kinetic energy of the impact is $(1/2)(4.2 \times 10^{-3})(2.682 \times 10^4)^2$ or 3.6×10^{-5} Kcals. This is about 0.01 of the heat of neutralization per drop, which was found to be 3.1×10^{-3} Kcals. In terms of this result it is reasonable to expect that some ionization will occur. At relative collision velocities higher than 880 ft/sec, ionization will become more probable.

APPENDIX B

COLLECTION OF DROP-IMPACT-EROSION DATA

by John A. Almo

I. EXPERIMENTAL APPARATUS

The basic facility consists of a 24 inch diameter rotor with a test specimen attached at the periphery, rotating in a horizontal plane. A vertical stream of water drops is generated and made to fall into the path of the rotating test specimen. Photoelectric cells triggered by a slotted disk connected to the rotor provide signals for synchronized drop generation and for stroboscopic observation of the rotor and falling drop stream. Additional electronic apparatus is used to provide constant-speed operation at any target velocity from 400 ft/sec to 1250 ft/sec, to count the number of drop impacts and to control the relative position of the drop stream and the rotating specimen. (Figures 1 and 2 show the rotor assembly with a 1/4-inch diameter test specimen mounted in the rotor tip.)

The rotor is enclosed in a protective steel chamber fitted with thick plastic viewing windows. The chamber is evacuated during operation to reduce power requirements and eliminate windage disturbance of the drop stream. (Figure 3 shows the test rig with the protective chamber closed. A view of the test rig with the chamber opened to permit inspection or change of the test specimen is shown in Figure 4.)

The rotor system, essentially patterned after those used in ultra-centrifuges, provides extremely stable high-velocity operation. The test apparatus can be operated continuously for up to four hours during which time water drops strike the target with dispersion no greater than two drop diameters.

II. APPARATUS CHARACTERISTICS AND TEST PROCEDURES

The following are descriptions of several apparatus characteristics and test procedures which have a bearing on the reliability and interpretation of the test data obtained.

A. Water Drops

Degassed, distilled water was used throughout the test program. The water drops (generated by a vibrating capillary tube) experienced oscillatory shape changes immediately after formation. These oscillations were rapidly damped out in the vertical fall from the drop generator to the impact target, however, and drop shape at the time of impact was observed to be essentially spherical.

Drop volume was derived from measurements of flow rate to the drop generator and of drop generation rate. This method of measurement gave a value of drop volume accurate to ±1%. Drop diameter was then calculated assuming a spherical drop of the measured volume.

B. Target Velocity

Target velocity was calculated from measurements of the rotor diameter and rotation rate. The rotation rate was monitored continuously throughout the test period and the impact process was interrupted if the target velocity drifted outside the limits ±1 ft/sec.

C. Drop Alignment and Impact Count

Drop generation was initiated after stabilization of the rotor speed. Alignment of the drop stream and the target specimen was indirectly accomplished with the drop stream descending clear of the rotor tip. Once good alignment was obtained externally, the drop stream was electrostatically deflected into the path of the target. Simultaneously, an electronic counter was connected to the deflection circuit to measure the total number of deflected, and thus impacted, drops. The synchronization of the drop generator, deflection circuit and rotor was such that an impact with a deflected drop occurred for every rotor revolution.

The operator continuously observed the target specimen through a telescope and allowed the count to proceed unless he observed excessive drift in the impact location. If this occurred, he could interrupt the drop deflection and realign the drop impact point. Once realigned, the deflection was reestablished and the impact count continued.

For run times exceeding five minutes the elapsed time on the target, rather then the number of impacts, was measured. For convenience, all

data are listed in elapsed time, but may easily be converted to number of impacts using the known impact rate.

D. Impinged Area

At the 1000 ft/sec operating speed used in these tests, windage effects from the remaining air in the test chamber produced a random impingement location circumscribed by a circle of diameter equal to two drop diameters. All tests, with two exceptions to be noted later, were carried out under these dispersion conditions.

E. Drop Splash

Observations of the conical spray pattern produced at impact suggest that the initial lateral liquid flow following impact does not occur in a purely radial direction, but possesses an additional component normal to the specimen face. No quantitative measurements of this flow were made.

F. Ambient Test Pressure

Throughout the test program the ambient pressure was maintained at 0.02 atmospheres. No evidence of drop instability (indicative of boiling) was observed. At pressures greater than 0.02 atmospheres, the windage disturbance of the drop streams increased, resulting in an increased dispersion of the impact location. At pressures lower than 0.02 atmospheres, drop stability was adversely affected.

G. Ambient Test Temperature

The temperature on all walls of the test chamber was kept at $10^{o}F$ to condense water vapor formed by the impact process. The drop generator expelled drops at essentially room temperature, but the drop and target temperatures at the time of impact are unknown. Tests conducted at speeds below 500 ft/sec in an earlier program showed an ice formation around the target area. At 1000 ft/sec no ice formation was evident, but radial forces were probably too great to allow ice formation.

H. Specimen Handling

All targets were initially inspected for obvious surface chips, dents, or other mechanical irregularities and individually washed in methyl ethyl ketone to remove machine oil and grease. After the MEK wash, the targets were handled only with forceps or surgical gloves to avoid further oil contamination. The targets were then thoroughly washed

in distilled water, dried for one hour in a hot air stream, and stored in a desiccator jar in individual specimen envelopes.

After 24 hours in the desiccator, the targets were weighed on a laboratory balance (accuracy ± 0.05 milligram) and returned to storage in the desiccator. As a precaution, the targets were weighed again just prior to testing and any discrepancies with the first measurement were resolved by additional weighings before the targets were mounted on the rotor arm for testing. Immediately after testing the targets were gently washed in distilled water, dried in the hot air stream, and returned to the desiccator. The final weights were then recorded after 24 hours in the desiccator. Again as a precaution each target was weighed at least twice.

I. Test Methods

The weight-loss-versus-exposure-time data for zinc, iron, tantalum, and nickel were obtained by a single-test-point-per-sample method. Each data point represents a different sample of the material tested for the indicated time. This method of testing was chosen so that individual specimens representing the various exposure times could be retained for physical examination. The Udimet materials were tested in the usual cumulative-weight-loss-on-a-single-sample manner for reasons to be explained later.

III. RESULTS

Six materials were tested: zinc, iron, tantalum, nickel, Udimet 700 (aged), and Udimet 700 (solutioned). A discussion of the tabulations of weight loss versus exposure time for each material is presented below.

A. Zinc (see Table 1)

Little or no "incubation" time was observed for the zinc samples under the conditions of testing. The shortest exposure time taken, Sample 2, showed a very distinct crater after 15.2 sec of exposure.

Distinct ridges around the impact crater are probably indicative of plastic deformation. These were observed on Samples 2, 4, 5, 10, 12, A, and C. Samples 14 and 18 are not reliable, since a hole was punched through the target during the test run and the time at which the

punch-through occurred could not be observed. During the test run on Sample 13 the impact location drifted vertically approximately 5 drop diameters; Sample 13 is therefore also unreliable.

Sample 15 was hit at two separate locations. At one a small crater formed after 11.9 sec and at the other a much larger crater formed after 180 sec of impact time. The final weight figure shown for this sample is the sum of the losses for the two craters; the weight loss for the 11.9 sec exposure crater alone was 0.2 milligram.

B. Iron (See Table 2)

The distinct ridge around the crater evident in many of the zinc samples was present only on Sample 1 of the iron series. The additional column labeled "initial damage" lists the exposure time at which the operator first observed damage on the test specimen face. Although the test procedure from sample to sample was unchanged, a wide variation in initial damage time was observed.

C. Nickel (See Table 3)

Samples 1, 8, and 12 of the nickel series had distinct ridges surrounding the impact crater. The nickel tests were conducted early in the program before it became apparent that initial damage time might vary significantly from sample to sample. For this reason only four values of initial damage time were recorded.

Unlike the other materials tested, most of the nickel samples showed clear evidence of some form of secondary impact damage. With the exception of Samples 1 and 2, which had the lowest exposure times, the nickel targets were characterized by the appearance of small dents distributed over the face of the target after an impact erosion crater had formed. The dents did not have the same shape as the primary crater formed at the impact point, but rather appeared to be small material deformations with little or no actual material loss. Possibly these indentations were formed by the impact of the target with small material fragments removed from the drop impact crater. Since only the nickel specimens exhibited the secondary impact damage, the secondary impact of the target with the liquid spray cone formed at the drop impact point (which occurred for all materials tested) is probably not the damage mechanism.

D. Tantalum (See Table 4)

Samples 1, 3, and 8 had distinct ridges surrounding the impact crater. Sample 2 was inadvertently run at a pressure of 0.04 atmospheres, resulting in an impact area 3 drop diameters wide. Sample 9 was punched through sometime during the test run and is therefore unreliable. The initial damage times observed had large variations, again with no variations in test procedure from sample to sample.

E. Udimet 700 (See Tables 5 and 6)

The U-700 materials proved to be very resistant to damage and were therefore tested for cumulative weight loss on a single sample. If the single-test-point-per-sample method used with the other materials had been used on the U-700 series, over 100 hours of testing time would have been necessary to gather sufficient data for a well defined weight loss curve.

Sample 1, aged U-700, was tested for a total of 1080 minutes, as shown in Table 5. The sample was removed from the apparatus, washed, dried, and weighed at the time intervals shown. The weight column lists the sample weight at the end of any test interval; the time column is cumulative. The sample was not weighed at the initial damage time.

Samples 2 and 3 of the solutioned U-700 material were tested to initial damage time only. Sample 4, solutioned U-700, was tested for a total of 960 minutes, as shown in Table 6.

REFERENCE

1. Ripken, J. F., "A Test Rig for Studying Impingement and Cavitation Damage," Erosion by Cavitation or Impingement, ASTM Technical Publication No. 408, 1967.

TABLE 1

ZINC

Sample	V (ft/sec)	Drop Diam. (mm)	Impact Exposure T. (sec)	Impact Rate drop/sec	Initial Wt. (gms)	Final Wt. (gms)	Comments
A [1]	1000	.866	195.1	161.5	.9379	.9222	Crater Ridge [2]
B	1000	.866	135.8	161.5	.9490	.9380	
C	1000	.866	75.7	161.5	.9641	.9600	Crater Ridge
2	1000	.866	15.2	161.5	.9663	.9660	Crater Ridge
4	1000	.866	30.1	161.5	.9724	.9713	Crater Ridge
5	1000	.866	60.3	161.5	1.0144	1.0128	Crater Ridge
7	1000	.866	120.4	161.5	.9844	.9801	
10	1000	.866	240.2	161.5	1.0148	.9899	Crater Ridge
12	1000	.866	90.0	161.5	.9816	.9775	Crater Ridge
13	1000	.866	152.5	161.5	.9731	.9621	Drop Drift
14	1000	.866	182.7	161.5	.9696	.9514	No. 14 Hit Off Center Hole Through Target
15	1000	.866	180.0	161.5	.9938	.9814	No. 15 Two Holes, One 180 Sec. One 11.9 Sec.
16	1000	.866	210.5	161.5	.9701	.9512	
17	1000	.866	225.1	161.5	.9603	.9391	
18	1000	.866	257.1	161.5	.9620	.9388	Drill Through

[1] Specimens A, B, And C were thicker than the other specimens.

[2] A ridge of metal formed around the crater; eroded particles appeared to detach from this ridge.

TABLE 2

IRON

Sample	V (ft/sec)	Drop Diam. (mm)	Impact Exposure T. (sec)	Impact Rate drop/sec	Initial Wt. (gms)	Final Wt. (gms)	Initial Damage T. (sec)	Comments
1	1000	.866	240.1	161.5	1.0645	1.0631	170	Crater Ridge[1]
2	1000	.866	480.1	161.5	1.0664	1.0640	210	
3	1000	.866	960.1	161.5	1.0376	1.0321	180	
4	1000	.866	1920.1	161.5	1.0625	1.0533	190	
5	1000	.866	3840.1	161.5	1.0424	1.0279	170	
6	1000	.866	1440.0	161.5	1.0515	1.0440	185	
7	1000	.866	2880.2	161.5	1.0738	1.0614	297	
8	1000	.866	6000.1	161.5	1.0634	1.0414	197	
10	1000	.866	600.2	161.5	1.0604	1.0556	121	
11	1000	.866	802.1	161.5	1.0482	1.0425	157	
12	1000	.866	1207.2	161.5	1.0566	1.0509	200	
13	1000	.866	5000.0	161.5	1.0362	1.0154	245	
15	1000	.866	701.1	161.5	1.0432	1.0377	75	

[1] A ridge of metal formed around the crater.

TABLE 3

NICKEL

Sample	V (ft/sec)	Drop Diam. (mm)	Impact Exposure T. (sec)	Impact Rate drop/sec	Initial Wt. (gms)	Final Wt. (gms)	Initial Damage (sec)	Comments
1	1000	.866	14.6	161.5	1.2242	1.2233	10	Crater Ridge[1]
2	1000	.866	30.4	161.5	1.2050	1.2048	25	
3	1000	.866	90.1	161.5	1.2087	1.2074	40	
4	1000	.866	36.0	161.5	1.2172	1.2159	15	
5	1000	.866	61.9	161.5	1.2135	1.2111		
6	1000	.866	150.2	161.5	1.2400	1.2369		
7	1000	.866	302.3	161.5	1.2404	1.2341		
8	1000	.866	600.2	161.5	1.2533	1.2419		Crater Ridge
9	1000	.866	900.0	161.5	1.2457	1.2309		
10	1000	.866	1500.0	161.5	1.1957	1.1760		
11	1000	.866	1200.2	161.5	1.2530	1.2391		
12	1000	.866	1800.0	161.5	1.2448	1.2275		Crater Ridge
13	1000	.866	2100.2	161.5	1.2524	1.2318		
14	1000	.866	2400.0	161.5	1.2413	1.2207		
15	1000	.866	2700.7	161.5	1.2064	1.1792		Footnote 2

[1] A ridge of metal formed around the crater.

[2] The eroded hole was oblong which suggests that there was some drift in the point of impact of the drop.

TABLE 4

TANTALUM

Sample	V (ft/sec)	Drop Diam. (mm)	Impact Exposure T. (sec)	Impact Rate drop/sec	Initial Wt. (gms)	Final Wt. (gms)	Initial Damage (sec)	Comments
1	1000	.866	348.7	161.5	2.3510	2.3510	320	Crater Ridge
2	1000	.866	6900.0	161.5	2.2779	2.2286	270	Drop Scatter 3 Drop Diam.
3	1000	.866	1206.3	161.5	2.3154	2.3055	230	Crater Ridge
4	1000	.866	6000.2	161.5	2.2502	2.2186	250	
5	1000	.866	2419.6	161.5	2.2475	2.2267	170	
6	1000	.866	4799.2	161.5	2.2710	2.2423	230	
8	1000	.866	600.3	161.5	2.3456	2.3410	277	Crater Ridge
9	1000	.866	9600.0	161.5	2.2915	2.2493	230	Hole Thru Target
11	1000	.866	3250.1	161.5	2.2068	2.1810	250	
12	1000	.866	2000.2	161.5	2.1901	2.1762	320	
13	1000	.866	7000.6	161.5	2.2161	2.1805	-	
14	1000	.866	1500.0	161.5	2.2761	2.2684	400	
15	1000	.866	800.2	161.5	2.2090	2.2036	200	

TABLE 5

AGED UDIMET 700

Sample No. 1	V (ft/sec)	Drop Diam. (mm)	Impact Exposure T. (sec)	Impact Rate drop/sec	Weight (gms)	Comments
			00000	-	1.1004	
	1000	.866	8100.0	161.5		Initial Damage (Approximate)
	1000	.866	9000.0	161.5	1.1001	
	1000	.866	12616.5	161.5	1.0956	
	1000	.866	14416.5	161.5	1.0927	
	1000	.866	18016.5	161.5	1.0898	
	1000	.866	21616.5	161.5	1.0874	
	1000	.866	25216.5	161.5	1.0854	
	1000	.866	28816.5	161.5	1.0834	
	1000	.866	32416.6	161.5	1.0820	
	1000	.866	35999.9	161.5	1.0806	
	1000	.866	43200.0	161.5	1.0775	
	1000	.866	50400.0	161.5	1.0761	
	1000	.866	57600.2	161.5	1.0742	
	1000	.866	64800.0	161.5	1.0724	Hole Thru Target

TABLE 6

SOLUTIONED UDIMET 700

Sample	V (ft/sec)	Drop Diam. (mm)	Impact Exposure T. (sec)	Initial Wt. (gms)	Final Wt. (gms)	Comments
2	1000	.866	3661.2	1.1626	1.1623	
3	1000	.866	7200.0	1.1515	1.1513	

Sample No. 4	V (ft/sec)	Drop Diam. (mm)	Impact Exposure T. (sec)	Impact Rate drop/sec	Weight (gms)	Comments
			0000.0	-	1.0731	
	1000	.866	7265.0	161.5		Initial Damage
	1000	.866	9065.8	161.5	1.0707	
	1000	.866	10866.2	161.5	1.0669	
	1000	.866	12666.2	161.5	1.0658	
	1000	.866	16266.2	161.5	1.0632	
	1000	.866	19866.3	161.5	1.0617	
	1000	.866	27066.4	161.5	1.0586	
	1000	.866	33553.2	161.5	1.0544	
	1000	.866	41405.7	161.5	1.0500	
	1000	.866	49605.7	161.5	1.0466	
	1000	.866	57602.9	161.5	1.0454	Hole Thru Target

APPENDIX C

A. DESCRIPTION OF THE REQUIRED COMPUTER PROGRAM

by Dr. J. K. Casey, Applied Mathematician,
Computations Operation, General Electric Company, Evendale, Ohio

The required program is for the function

$$T(n) = \sum_{x=o}^{n} v(x)P(x,n)$$

where

$$P(x,n) = \frac{n!}{(n-x)!\ x!}\ p^x\ (1-p)^{n-x}$$

and

$$\begin{aligned}
v(x) &= 0 && \text{for } 0 && \leq x < N_o \\
&= R_1 && \text{for } N_o && \leq x < N_o + N_1 \\
&= R_1 + R_2 && \text{for } N_o + N_1 && \leq x < N_o + N_1 + N_2 \\
&= R_1 + R_2 + R_3 && \text{for } N_o + N_1 + N_2 && \leq x < N_o + N_1 + N_2 + N_3 \\
&= R_1 + R_2 + R_3 + R_4 && \text{for } N_o + N_1 + N_2 + N_3 && \leq x < N_o + N_1 + N_2 + N_3 + N_4
\end{aligned}$$

etc.

The function v(x) is a step function; the N_i quantities are the length of the treads and the R_i are heights of the risers.

The graph of v(x) should, therefore, have the appearance indicated below.

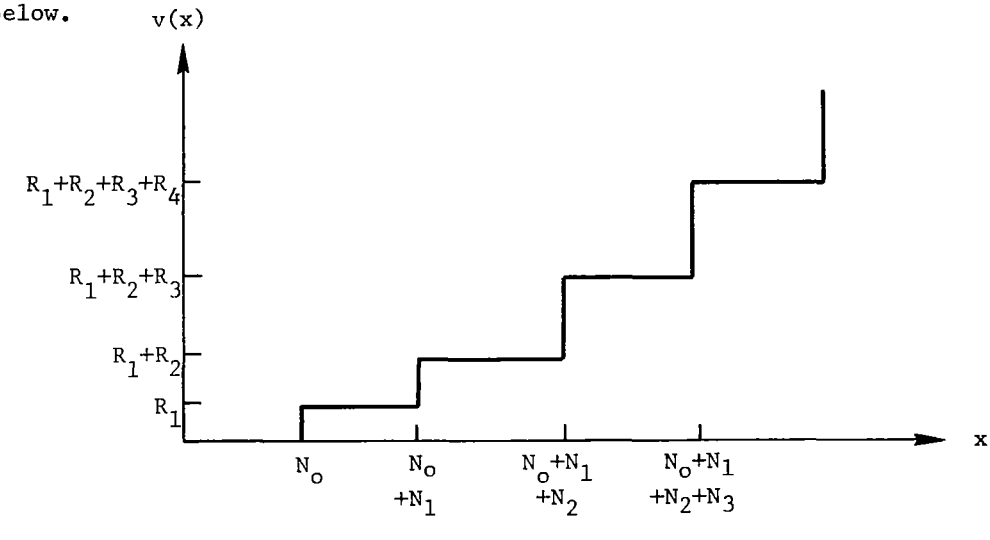

Tread lengths and riser heights beyond those specified in input are assumed to equal the last values that were input. Thus if N_0, ... N_4 and R_1, ... R_4 were input, then N_5, N_6, ... are taken equal to N_4 and R_5, R_6, ... are taken equal to R_4. Provision should be made for at least 7 tread lengths and 6 riser heights to be supplied in the input.

B. COMPUTER PROGRAM

by M. A. Cummings, Manager, Mathematical Applications
Computations Operation, General Electric Company, Evendale, Ohio

A computer program for the function T(n) was written in double precision Fortran IV. The program was based on an earlier version in the basic language by Lars H. Sjodahl. A printout of the program is given below.

The input data for the program are:

probability, p
counting rule, N_0, N_1, N_2, N_3, N_4, etc.
volumes, --, R_1, R_2, R_3, R_4, etc.
number of impacts, n = ____ to n = ____ Step n = ____

If the program is run with $R_1 = R_2 = R_3 = \text{etc.} = 1$, the printout is in layers of fragments removed at the specified values of impacts, n. If the program is run with the specified values of the R_i, the printout is accumulated volume loss at the specified values of impacts, n.

Runs with use of this program can be obtained by applying to Mr. M. A. Cummings, Mail Stop H8, General Electric Company, Evendale, Ohio.

```
      DIMENSION NN(201),RR(200)
      DOUBLE PRECISION P0,N,P1,D,L,X,R1,R2,T,S,P,X0,X1,P,DI,R,
     2 NDELTA,NMAX,NN,RR,BOUND1,BOUND2
      DOUBLE PRECISION XX
      NAMELIST/IN/P0,N,NN,RR,NDELTA,NMAX
      WRITE (6,10)
   10 FORMAT (1H1,5X,2HP0,10X,1HN,20X,9HFRAGMENTS//)
    5 CALL FLGEOF(5,IEOF)
      READ (5,IN)
      IF (IEOF .NE. 0) GO TO 990
      P1=P0/(1.-P0)
  100 T=0.
      S=0.
      INUM=1
      SBOUND=NN(1)
      PSTAR=0.
      D=-1.
      L=N*P0
      IF (NN(1) .GE. L) L=NN(1)
      X1=RR(INUM)
      BOUND1=NN(INUM)
      BOUND2=NN(INUM)+NN(INUM+1)
      IL=IFIX(L)
      X=IL
      R1=X*  DLOG(P0)
      R2=(N-X)*  DLOG(1.-P0)
      R=0.
      DO 200 I=1,IL
      XI=FLOAT(I)
  200 R=R+  DLOG((N 1.-XI)/XI)
      R=DEXP(R+(N-X)*DLOG(1.-P0)+X*DLOG(P0))
      P=R
  420 IF (X.LT.BOUND1.AND.BOUND1.GT.NN(1)) GO TO 440
      XX=DABS(BOUND1-NN(1))
      IF (XX .LT. (.000001) .AND. X .LT. BOUND1) GO TO 435
  430 IF (X.GE. BOUND1 .AND. X.LT. BOUND2) GO TO 445
      IF (INUM .NE. 200) GO TO 433
      WRITE (6,432)
  432 FORMAT (17H PARTIAL SOLUTION)
      XX=X1*P
      WRITE (6,434) P0,N,S,XX
  434 FORMAT (F12.9,F11.0,2F16.9)
      GO TO 660
  433 INUM=INUM+1
      BOUND1=BOUND2
      BOUND2=BOUND2+NN(INUM+1)
      X1=X1+RR(INUM)
      GO TO 430
  435 D=1.
      GO TO 600
  440 BOUND2=BOUND1
      INUM=INUM-1
      BOUND1=BOUND1-NN(INUM+1)
      X1=X1-RR(INUM+1)
  445 S=S+P*X1
      PSTAR=PSTAR+P
  480  IF (D .LT. (0.)) GO TO 500
      P=P*(N-X)/(X+1.)*P1
```

```
    GO TO 510
500 P=P*X/(N-X+1.)/P1
510  X=X+D
    IF ((P*X1) .GE. (.000001)) GO TO 420
590 IF (D .EQ. (-1.0)) SBOUND=X
    IF (D.EQ.1.0) UBOUND=X
    D=D+2.0
600 IF (S.EQ.0.0) GO TO 610
    T=T+S
    S=0.
610 IF (D.NE.1.0) GO TO 620
     IX=IFIX(L+1.)
    X=FLOAT(IX)
    IL=IFIX(L)
    P=R*(N-FLOAT(IL))/(FLOAT(IL)+1.)*P0/(1.-P0)
    GO TO 430
620 WRITE (6,650) P0,N,SBOUND,UBOUND,T
650 FORMAT (F12.9,F11.0,F6.0,F5.0,F16.9)
660 IF (N .GE. NMAX) GO TO 5
    N=N+NDELTA
    GO TO 100
990 STOP
    END
```